10:23:46 OCA PAD INITIATION - PROJECT HEADER INFORMATION 05/25/88

Active

Project #: G-33-646 Cost share #: Rev #: 0
Center # : Q5456-0A0 Center shr #: OCA file #:
Work type : RES
Contract#: 1 S10 RR04001-01 Mod #: Document : GRANT
Prime #: Contract entity: GIT

Subprojects ? : N
Main project #:

Project unit: CHEM Unit code: 02.010.136
Project director(s):
PIEROTTI R A CHEM

Sponsor/division names: DHHS/PHS/NIH / NATL INSTITUTES OF HEALTH
Sponsor/division codes: 108 / 001

Award period: 880516 to 890515 (performance) 890815 (reports)

Sponsor amount	New this change	Total to date
Contract value	133,000.00	133,000.00
Funded	133,000.00	133,000.00
Cost sharing amount		0.00

Does subcontracting plan apply ?: N

Title: SHARED-USE FTIR SPECTROMETER - DRR-BRS SHARED INSTRUMENTATION GRANT

PROJECT ADMINISTRATION DATA

OCA contact: E. Faith Gleason 894-4820

Sponsor technical contact

MARJORIE A. TINGLE, PH.D., DIRECTOR
(301)496-6743
BIOMEDICAL RESEARCH SUPPORT PROGRAM
NATIONAL INSTITUTES OF HEALTH
BETHESDA, MD 20892

Sponsor issuing office

IVAN HERNANDEZ, GRANTS MGT OFFICE
(301)496-9840
DIVISION OF RESEARCH RESOURCES
NATIONAL INSTITUTES OF HEALTH
BETHESDA, MD 20892

Security class (U,C,S,TS) :
Defense priority rating :
Equipment title vests with: Sponsor GIT X

ONR resident rep. is ACO (Y/N): N
supplemental sheet

RESTRICTED TO BASIC INSTRUMENTATION AS APPROVED. ANY DEVIATION REQ PRIOR APPR
*EQUIPMENT SHOULD BE PURCHASED WITHIN THE 1ST 6 MONTHS OF THE GRANT

Administrative comments -
INITIATION.

GEORGIA INSTITUTE OF TECHNOLOGY
OFFICE OF CONTRACT ADMINISTRATION

NOTICE OF PROJECT CLOSEOUT

Date July 18, 1989

ject No. G-33-646 Center No. Q5456-0A0

ject Director R. A. Pierotti School/Lab Chemistry

nsor DHHS/PHS/NIH

tract/Grant No. 1 S10 RR04001-01 GTRC ___ GIT XX

me Contract No. N/A

le Shared-Use FTIR Spectrometer - DRR-BRS Shared Instrumentation Grant

ective Completion Date 5/15/89 (Performance) 8/15/89 (Reports)

seout Actions Required:

- None
- Final Invoice or Copy of Last Invoice - SF269
- Final Report of Inventions and/or Subcontracts - Already submitted.
- Government Property Inventory & Related Certificate
- Classified Material Certificate
- Release and Assignment
- Other ___

ludes Subproject No(s). ___

roject Under Main Project No. ___

inues Project No. ___ Continued by Project No. ___

ribution:

Project Director	X Reports Coordinator (OCA)
Administrative Network	___ GTRC
Accounting	X Project File
Procurement/GTRI Supply Services	2 Contract Support Division (OCA)
Research Property Management	___ Other ___
Research Security Services	

G-35-646

Six Month Interim Report on the Subject Grant

"Diagnostic Studies of the H_xO_y-N_xO_y-O_3 Photochemical System

Using Data from NASA GTE Field Expeditions"

NASA Grant NAG-1-786

PI: William L. Chameides

School of Geophysical Sciences

Georgia Institute of Technology

Atlanta, Georgia 30332

During the first six months of the three-year granting period the major focus of the research effort funded by NASA has been on the analysis of data gathered during the Spring, 1984 GTE CITE-1 field expedition. Data from the field exercise was obtained from a GTE Data Archive Tape. Chemical and supporting meteorological data taken over the Pacific Ocean was statistically and diagnostically analyzed to identify the key processes affecting the concentrations of ozone and its chemical precursors in the region. The analysis has been completed and a paper has been submitted to the Journal of Geophysical Research. Reviews for the paper have been recently received and we are now making our final revisions to the paper.

Having completed our analysis of the Spring CITE-1 data, the P.I. in collaboration with Dr. D. D. Davis and other GTE scientists has begun analysis of the GTE CITE-2 data. Initial results of our analysis were presented at the Fall meeting of the American Geophysical Union in San Francisco.

In addition to the work described above, three other papers have been completed with partial support from the subject grant. Titles of all papers completed with funds from NASA during the granting period are:

1. Acid Dew and the Role of Chemistry in the Dry Deposition of Reactive Gases to Wetted Surfaces, W.L. Chameides, J. Geophys. Res., 92, 11,895-11,908, 1987.

2. Absorption Cross Sections and Kinetic Considerations of the IO Species as Determined by Laser Flash Photolysis/Laser-Absorption Spectroscopy, R.E. Stickel, A.J. Hynes, J.D. Bradshaw, W.L. Chameides and D.D. Davis, J. Phys. Chem., in press, 1988.

3. High Ozone Events in Atlanta, Georgia in 1983 and 1984, R.W. Lindsay, W.L. Chameides, Environmental Science and Technology, in press, 1988.

4. Ozone Precursors and Ozone Photochemistry Over the Eastern North Pacific Ocean During the Spring of 984 Based on the NASA/CITE 1 Airborne Observations, W.L. Chameides and D.D. Davis, J. Geophys. Res., in review, 1988.

Copies of the four papers listed above are included in this report as an appendix.

Plans for research during the next 12 to 18 months of the granting period include:1. Completion of our analysis of the GTE CITE-2 data. Two major studies on this data are envisioned: a comparison of measured and theoretically calculated NO/NO_2 ratios and a diagnostic analysis of ozone photochemistry implied by the observations. The latter study will include a comprehensive propagation of error analysis to determine the accuracy and precision with which we are able to calculate ozone photochemical tendencies from a set of state-of-the-art chemical measurements.

2. An initial study of the data obtained during the GTE ABLE-2A and 2B experiments aimed at determining to what extent long-range transport of pollutants can affect oxidant levels in remote Brazilian locations.

3. Preparation of a paper in collaboration with Dr. D.D. Davis and other GTE scientists comparing measured and model-calculated OH levels from the spring CITE 1 mission.

Twelve Month Interim Report on the Subject Grant

"Diagnostic Studies of the H_xO_y-N_xO_y-O_3 Photochemical System

Using Data from NASA GTE Field Expeditions"

NASA Grant NAG-1-786

PI: William L. Chameides

School of Geophysical Sciences

Georgia Institute of Technology

Atlanta, GA 30332

During the first year of the three-year granting period the major focus of the research effort funded by NASA has been on the analysis of data gathered during the Spring, 1984 GTE CITE-1 and the Summer, 1986 GTE CITE-2 field expeditions.

In the case of the Spring CITE-1 flights data from the field exercise was obtained from a GTE Data Archive Tape. Chemical and supporting meteorological data taken over the Pacific Ocean was statistically and diagnostically analyzed to identify the key processes affecting the concentrations of ozone and its chemical precursors in the region. The analysis has been completed and a paper has been submitted to the Journal of Geophysical Research. Reviews for the paper have been recently received and we are now making our final revisions to the paper.

Our analysis of the GTE CITE-2 data is being carried out in collaboration with Dr. D.D. Davis and other GTE scientists. Initial results of our analysis were presented at the Fall meeting of the American Geophysical Union in San Francisco and we have begun work on a paper describing our results. This paper should be completed and submitted to the Journal of Geophysical Research by the end of the summer.

In addition to the work described above, six other papers have been completed with partial support from the subject grant. Titles of all papers completed with funds from NASA during the granting period are:

1. Acid dew and the role of chemistry in the dry deposition of reactive gases to wetted surfaces, W.L. Chameides, *J. Geophys. Res., 92*, 11,895-11,908, 1987.

2. Absorption cross sections and kinetic considerations of the IO species as determined by laser flash photolysis/laser-absorption spectroscopy, R.E. Stickel, A.J. Hynes, J.D. Bradshaw, W.L. Chameides and D.D. Davis, *J. Phys. Chem.*, in press, 1988.

3. High ozone events in Atlanta, Georgia, in 1983 and 1984, R.W. Lindsay and W.L. Chameides, *Environ. Sci. Technol., 22, No. 4*, 426-431, 1988.

4. Ozone precursors and ozone photochemistry over the eastern North Pacific Ocean during the spring of 1984 based on the NASA/CITE 1 airborne observations, W.L. Chameides and D.D. Davis, *J. Geophys. Res.*, in revision, 1988.

5. Ozone trends in Atlanta, Georgia: Have emission controls been effective? R.W. Lindsay, J.L. Richardson, W.L. Chameides, submitted to *JAPCA*, in review, 1988.

6. The biochemistry of ozone deposition to plant leaves: The role of ascorbic acid, W.L. Chameides, submitted to *Environmental Science and Technology,* in review, 1988.

7. The role of biogenic hydrocarbons in urban photochemical smog: Atlanta as a case study, W.L. Chameides, R.W. Lindsay, J.L. Richardson and C.S. Kiang, submitted to *Science,* in review, 1988.

Copies of papers 1, 2, 3, and 4 listed above have already been forwarded to NASA in our six month Interim Report. Copies of papers 5, 6, and 7 are included in this report as an appendix.

Plans for research during the next 12 months of the granting period include:

1. Completion of our analysis of the GTE CITE-2 data. Two major studies on this data are envisioned: a comparison of measured and theoretically calculated NO/NO_2 ratios and a diagnostic analysis of ozone photochemistry implied by the observations. The latter study will include a comprehensive propagation of error analysis to determine the accuracy and precision with which we are able to calculate ozone photochemical tendencies from a set of state-of-the-art chemical

measurements.

2. An initial study of the data obtained during the GTE ABLE-2A and 2B experiments aimed at determining to what extent long-range transport of pollutants can affect oxidant levels in remote Brazilian locations.

3. Preparation of a paper in collaboration with Dr. D.D. Davis and other GTE scientists comparing measured and model-calculated OH levels from the Spring CITE 1 mission.

Reprinted from ENVIRONMENTAL SCIENCE & TECHNOLOGY, Vol. 22, Page 426, April 1988

High-Ozone Events in Atlanta, Georgia, in 1983 and 1984

Ronald W. Lindsay and William L. Chameides*

School of Geophysical Sciences, Georgia Institute of Technology, Atlanta, Georgia 30332

■ Measurements of ozone levels and meterological parameters were analyzed to determine the relative importance of transport-related processes and photochemical production in causing high-ozone events in and around the Atlanta metropolitan area. Back-trajectories calculated by the Branching Air Trajectory Model indicate that the air associated with high-ozone events had often traveled a significant distance within the previous 3 days: for days with ozone levels above 100 ppbv, half of the calculated trajectories showed that the air had traveled over 600 km, with half of those coming from the northwest quadrant. Six-hour vector-averaged winds were used to find that the concentrations of ozone in the air leaving the metropolitan area averaged 20–40 ppbv more than that entering the area.

Introduction

The southeastern United States is one of the fastest growing areas of the country. In large part as a result of this growth, major population and industrial centers in the Southeast have begun to experience air quality degradation similar to that which has for many years plagued urban areas in the northern and western United States. This study examines the surface ozone concentrations in and around the Atlanta area in order to determine what proportion of the ozone concentration measured during high-concentration days can be attributed to (a) local photochemical production within the metropolitan area, (b) long-range transport of ozone and its precursors from distant sources, and (c) natural sources. We investigate the nature of regional ozone events, the origin and chemical character of air entering the metropolitan area during such events, and the net effect of the metropolitan area on the air as it passes over the city.

The Atlanta area is different from many other cities afflicted with high-ozone concentrations in that it is free of confining topographical barriers and is relatively isolated from other large cities. Often during the summer months there is significant instability in the lower atmosphere that helps to ventilate the mixed layer. High-ozone events occur when a high-pressure system dominates the region and suppresses convection. The summertime winds are usually light, but stagnant air from distant source regions such as the Midwest or the Northeast can sometimes be brought into the airshed.

There is ample evidence for the importance of long-range transport in causing regional ozone events in the eastern United States. Vukovich et al. (*1*) showed that high levels of ozone over the Northeast occur on the backsides of transitory anticyclones, in air that has resided over populated areas for several days. Wight et al. (*2*) also showed how clean air enters the Midwest as an anticyclone from western Canada and accumulates pollution as it moves slowly across the Northeast, with the worst ozone concentrations found, again, on the backside of the anticyclone. Vukovich and Fishman (*3*) presented a climatology of summertime ozone levels from rural stations in the eastern United States and showed that wide areas with monthly averages above 70 ppbv are not uncommon, compared to levels of 40–50 ppbv in the west and near the southern coast. They showed that when the paths of major migratory high-pressure systems remained in the northern portion of the country, the Southeast was largely spared from high-ozone concentrations; but when the migratory high-pressure systems passed through the central or southern portion of the country, the centers of high ozone shifted into the South. They drew an important distinction between these migratory anticyclones and the quasi-stationary Bermuda High that is centered off the East Coast in the summer months and dominates the mean-pressure analyses but is not necessarily associated with high-ozone events. The climatological study of Zishka and Smith (*4*) showed that July anticyclones commonly originated in western Canada and traversed the northeastern portion of the United States along the 40th parallel. Rarely were they seen to drop below the 35th parallel, so that the South is largely spared from the migratory anticyclones that Vukovich and Fishman (*3*) associate with regional high-ozone events.

 0013-936X/88/0922-0426$01.50/0

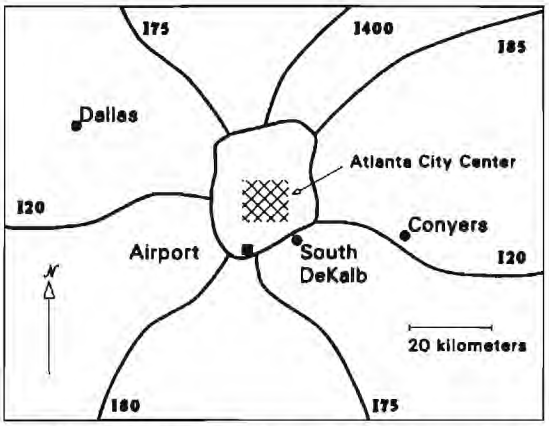

Figure 1. Map of the Atlanta metropolitan area showing the locations of the ozone-monitoring stations Dallas, South DeKalb, and Conyers and the National Weather Service observing station at Hartsfield Atlanta International Airport.

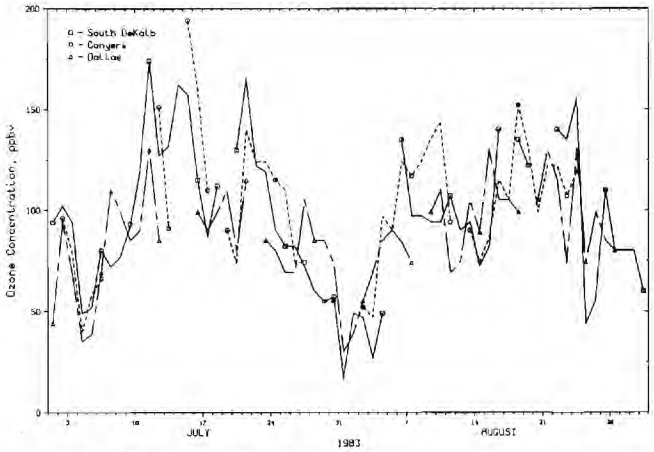

Figure 2. Maximum daily ozone concentrations for three stations: South DeKalb, Conyers, and Dallas; July and August 1983.

Our study focuses both on the back-trajectories of high-ozone days and on the analysis of the surface wind observations. We address four key questions: Where has the air of high-ozone episodes in Atlanta come from? How do the back-trajectories for high-ozone days differ from those of low-ozone days? What is the ozone concentration of the air entering the city on episode days, and what is it as the air leaves? And what is the typical ozone budget for episode days, i.e., what proportion can be attributed to (a) local production, (b) long-range transport, and (c) natural sources?

Ozone Data

The hourly averaged ozone concentrations from the three urban and suburban monitoring stations in the Atlanta area were obtained from the Georgia Department of Natural Resources for the period of May through November, 1983 and 1984. These stations are South DeKalb Community College, located just southeast of the center of the metropolitan area; Conyers, 25 km to the east of DeKalb; and Dallas, 60 km to the northwest. Figure 1 shows the location of the three stations, the perimeter freeway that encircles much of the metropolitan area, the major freeways that enter the area, and Hartsfield Atlanta International Airport, from which we obtained the surface winds. Suburban communities extend beyond the perimeter but are in general closer to the perimeter than the two suburban ozone-monitoring stations. The stations are well situated to monitor the effect of the metropolitan area on ozone concentrations for the dominant northwest and east winds but poorly placed for south or north winds.

The maximum daily ozone concentrations between the hours of 9 a.m. and 8 p.m. were extracted from the time series, excluding days in which the maximum was at the beginning or at the end of a break in the data. As an example of the time series, the daily maxima for the three Atlanta area stations during July and August of 1983 are plotted in Figure 2. We see that there were two extended episodes of high-ozones concentrations, one in mid-July and the other in mid-August. These two months contributed 22 of the 32 days in 1983 and 1984 on which the ozone concentrations exceeded the National Ambient Air Quality Standard (NAAQS) of 120 ppbv. 1983 was the worst year for violations of the NAAQS in the 7-year period of 1979–1986 for which we have records: over the course of that year, there were 24 days above 120 ppbv. In the 14 months of the record (428 days) there were 154 days (36%) on which the concentration at one of the three stations was greater than or equal to 80 ppbv and 70 days (16%) on which it was greater than or equal to 100 ppbv.

BAT Model

The Branching Air Trajectory (BAT) model was obtained from the National Climatic Data Center along with 1983 and 1984 radiosonde data for North America. The model is described by Heffter (*5*). It uses the conventional National Weather Service (NWS) radiosonde network for input data, restricts the tracked air mass to the mixed layer and below 3000 m, and allows each trajectory to branch into as many as three different layers, thereby reflecting the isolation of the high layers from the surface during the night. Up to 20 different branches are tracked simultaneously. The BAT model was modified to produce back-trajectories for one parcel a day, tracing its progress backwards for 3 days starting at 1700 EST. Only radisondes within the map area shown in Figures 3–6 were used as input data; any branches that left the map area were dropped. Lost branches were of particular importance to the south, where the boundary of the model area was chosen to be just off the coast since there were no observations south of it. Branches were also dropped if they contained less than 5% of the original mass of the air parcel.

It should be noted that significant uncertainties are associated with back-trajectory calculations from conventional meteorological data. For example, Kahl and Samson (*6*) found that boundary-layer trajectories calculated with the current NWS network of radiosondes with 12-h resolution have a 50% chance of exceeding horizontal displacement errors of 200 km after 24 h, 280 km after 48 h, and 350 km after 72 h of travel time. However, while the uncertainty of any one trajectory calculation is large, we believe that by determining a large number of back-trajectories some insight into the typical past history of air over the Atlanta area during event and nonevent days can be obtained.

The maximum daily ozone concentration of the three stations near Atlanta was used to rank the days in decreasing order. The back-trajectories for the 10 days with the highest ozone concentrations are shown in Figure 3. The three points plotted for each day represent the position of the center of mass of the trajectory after 1, 2, and 3 days. All of the trajectories converge, of course, on Atlanta, which is indicated with a circle. In the lower right corner of the figure are the date (YYMMDD), the maximum ozone concentration (ppbv), and the percent of mass remaining for each trajectory at the end of each day.

The two worst days are examples of two extreme varieties of trajectories. July 15, 1983, saw ozone concentra-

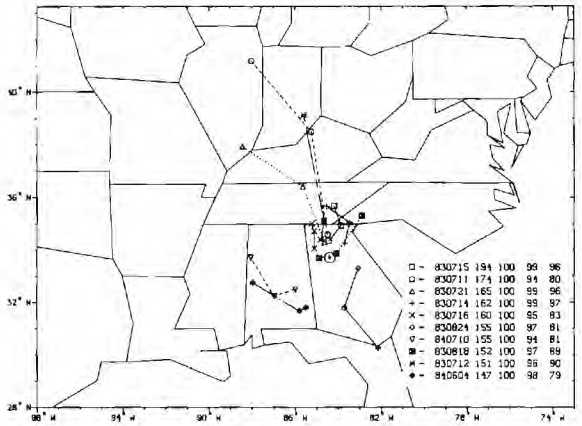

Figure 3. Positions of the center of mass of the trajectory branches at the end of 1, 2, and 3 days for the top 10 days in ozone concentration. The date (YYMMDD), maximum ozone concentration (ppbv), and the remaining mass (%) for each of the 3 days are listed in the corner.

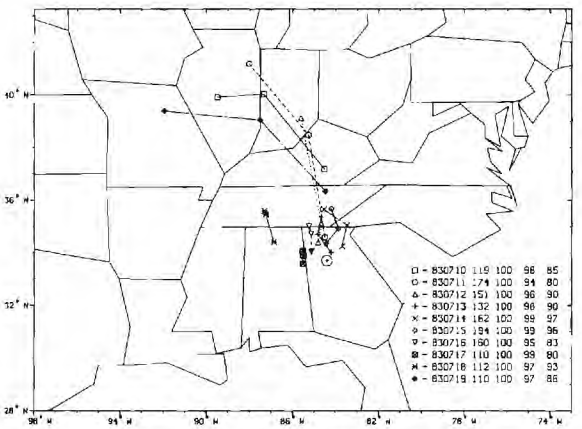

Figure 4. Positions of the center of mass of the trajectory branches at the end of 1, 2, and 3 days for 10 consecutive days in July 1983 with ozone concentrations above 100 ppbv. The date (YYMMDD), maximum ozone concentration (ppbv), and the remaining mass (%) for each of the 3 days are listed in the corner.

tions peak at 194 ppbv, and the air showed very little movement over the previous 3 days. In contrast, July 11, 1983, with 174 ppbv ozone, showed little movement over the previous day but moderately strong motion during the 2 days before; this movement brought air into the Atlanta area from the population and industrial centers of the Midwest and the Ohio Valley near the beginning of the 19-day episode of high-ozone levels seen in July.

The episode in July 1983 was one of the worst in several years and is a good illustration of how a mix of transport and stagnation can contribute to such episodes. Figure 4 shows the 3-day back-trajectories for the first 10 consecutive days of a 16-day period in mid-July with maximum ozone concentrations above 100 ppbv. Some days, such as the 15th, showed significant movement over the previous 3 days, while the bulk of the trajectories showed little net motion. Most of the trajectories moved in a southerly or southeasterly direction, reflecting the presence of the center of an anticyclone to the west. The surface weather maps for this period show a persistent high-pressure center that moved slowly from the Northeast, stalled west of Atlanta for 5 days when the highest concentrations were registered, and then drifted to the South, and again stalled south of Louisiana. This is in contrast to the findings of Vukovich et al. (*1*) and Wight et al. (*2*) that the strongest pollution episodes in the Northeast occur on the backside, or western side, of anticyclones; in this

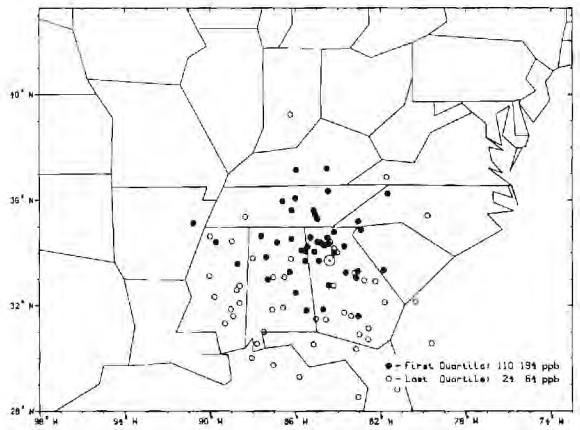

Figure 5. Positions of the center of mass of the trajectory branches for the first and last quartiles of ozone concentration at the end of the first day.

case we find that the worst episode occurred on the eastern flank of the system. The relatively uncommon episodes of prolonged high-ozone concentrations in Atlanta reflect the rare occurrence of a migratory high-pressure center to the west of the Atlanta metropolitan area (*4*). More commonly the area is dominated in the summer by the Bermuda High, usually found to the east and bringing air into the area from the south. This air from the south tends to be relatively pollution-free as well as moist; the moisture contributes to convective storms that help to ventilate the mixed layer.

In order to compare the typical movement of air on event and nonevent days, 3-day back-trajectories were calculated for all of the days in the 3 summer months (June, July, and August) for both 1983 and 1984, a total of 184 days. The days were divided into quartiles on the basis of their rank in ozone concentration. The first quartile is the 25% of the days with the highest ozone concentrations (110–194 ppbv), and the last quartile is the 25% with the lowest concentrations (24–64 ppbv). There were 46 points in each quartile. In Figure 5, the position of the center of mass of all branches of each back-trajectory is plotted after 1 day for both the first and the last quartiles. Note that the high-ozone days are clustered nearer to Atlanta, reflecting the generally light winds associated with high-ozone measurements. The high-ozone days also come predominantly from the north and west, although no direction is completely excluded. The low-ozone days show much larger travel distances, and the air comes predominantly from the south.

Figure 6 shows the positions of the center of mass of each back-trajectory for all days in which the maximum-ozone concentration was greater than 100 ppbv after 1, 2, and 3 days. The median distance traveled after 1 day was 200 km, after 2 days it was 400 km, and after 3 days it was 600 km. Of the 22 trajectories that had traveled 600 km in 3 days, 11 had come from the northwest quadrant, 5 from the northeast, 4 from the southwest, and 2 from the southeast. This dominance of trajectories originating in the Midwest is apparent in Figure 6c where we see a concentration of points indicating air coming from the Ohio Valley region. The inventories of hydrocarbons and NO_x of both Benkovitz (*8*) and Clark (*9*) indicate that this region is in fact a strong source area for these ozone precursors. The studies of Wight et al. (*2*) and Wolff et al. (*7*) also show evidence of the Ohio Valley being an important source area for regional high-ozone episodes in the entire eastern United States.

The BAT back-trajectories indicate that about half of the days with high-ozone concentrations were characterized

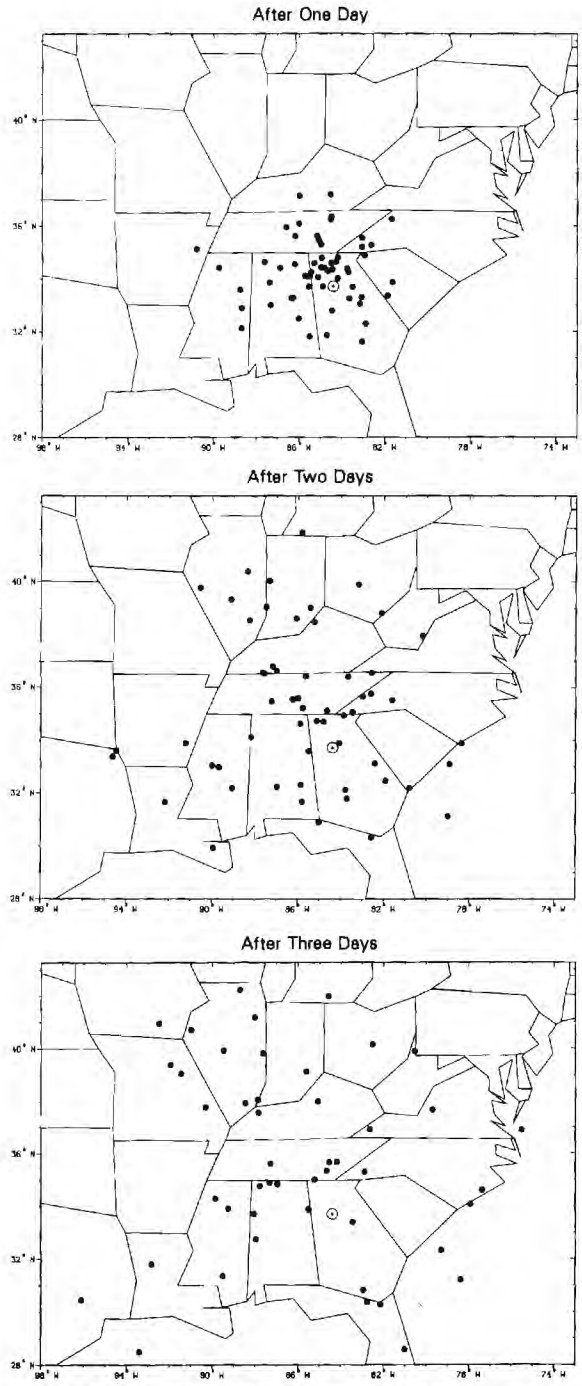

Figure 6. Positions of the center of mass of the trajectory branches for all days with ozone concentrations greater than 100 ppbv after 1, 2, and 3 days.

by air that had moved a substantial distance over the previous 3 days; of those, about half had come from the northwest. Days with low concentrations of ozone are generally characterized by much greater air movement than the high-ozone days, and the air more often appears to have come from the south. The fact that the air of many high-ozone days originated in the Midwest is a strong indication that on occasion long-range transport of ozone and ozone precursors is contributing to the ozone concentrations seen in Atlanta.

Surface Wind and Ozone Relations

Because of the uncertainties in the trajectory calculations and the large distance to the nearest radiosonde station (Athens, GA, 100 km to the east), the surface winds from Hartsfield Atlanta International Airport were used

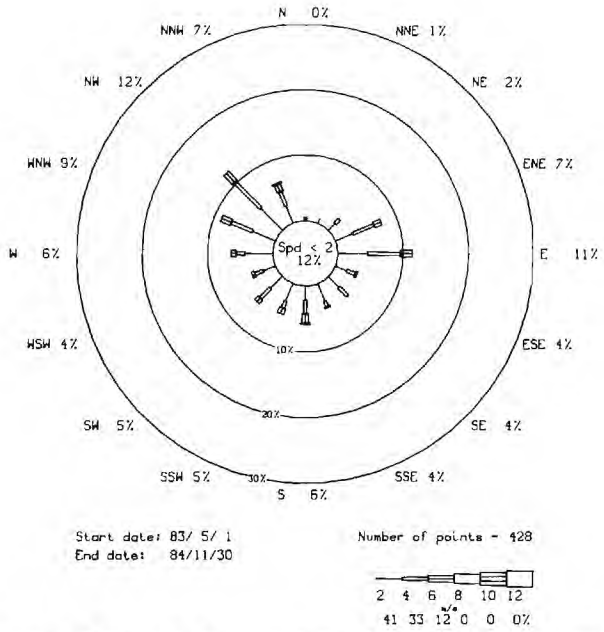

Figure 7. Windrose of afternoon (1200–1700 EST) vector-averaged winds for 1983 and 1984, 8 months each year.

to further define the nature of ozone events in the Atlanta area. Figure 7 shows a windrose of the 6-h vector averaged afternoon (1200–1700 EST) surface winds from the airport for the period during which the ozone measurements were made (May–November, 1983 and 1984). There is a predominance of northwest winds with a secondary peak for east winds. Figure 8 summarizes the afternoon winds of days in which the ozone concentrations at Dallas and Conyers exceeded 100 ppbv. We can see that the two suburban stations are directly affected by the urban plume. In Dallas, which is northwest of the city, concentrations were in excess of 100 ppbv mostly for days with calm winds and winds from the east; in Conyers, which is southeast of the city, ozone concentrations were in excess of 100 ppbv predominantly for days with winds from the west and northwest. There were also a number of days with high-ozone concentrations in Dallas when winds were from the west and northwest. These days included occasions when the BAT calculations show that the air had come from distant source regions as well as occasions when the air had reentered the city after a period of near calm or after a wind reversal.

Other studies have provided direct measurements of the urban plume downwind of Atlanta. In a 1981 field study for the EPA, Westberg and Lamb (*10*) found that a well-defined plume was often observed 50–75 km downwind from the city center. Ozone levels of 130–160 ppbv were commonly observed at heights of 500–800 m above the ground on 10 different afternoon flights. For example, on one day the plume at 40 km from the city center was some 50 km wide with surface winds about 3 m s^{-1} from the north-northwest.

Lying outside the metropolitan area, Dallas and Conyers are well situated to provide a comparison between the incoming and the outgoing air for the predominant northwest and east winds. Figure 9 shows the difference in ozone levels at Conyers and Dallas for each wind direction sector and for three different layers of ozone concentrations: both stations less than 80 ppbv, at least one station greater than 80 ppbv, and at least one station greater than 100 ppbv. At the bottom of the figure are listed the number of observations in each sector, the mean differences, and the standard deviations of the differences.

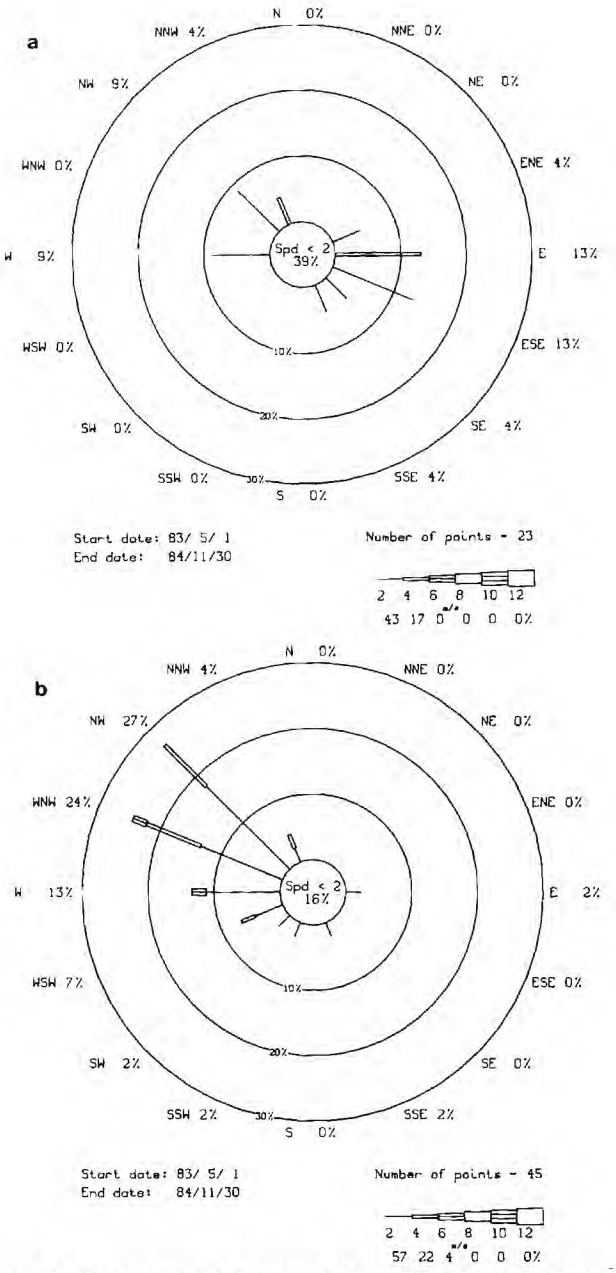

Figure 8. (a) Windrose of afternoon (1200–1700 EST) winds for days with ozone concentrations greater than 100 ppbv at Dallas. (b) Windrose of afternoon (1200–1700 EST) winds for days with ozone concentrations greater than 100 ppbv at Conyers.

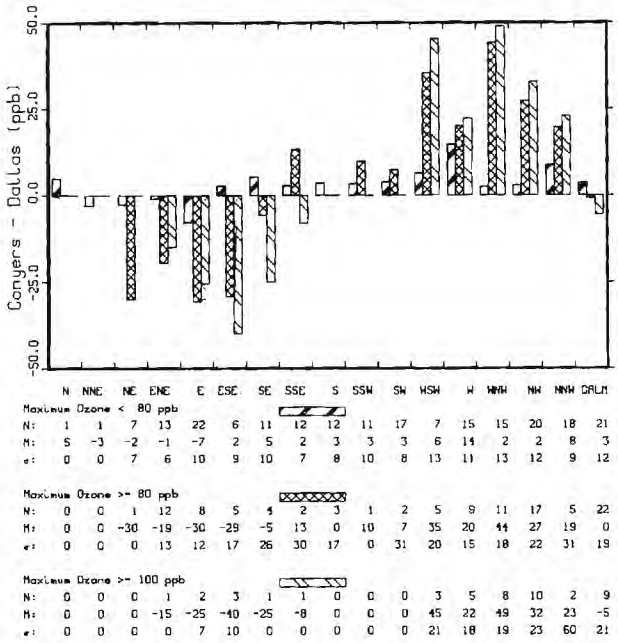

Figure 9. Bar graph of the mean Conyers – Dallas ozone concentration difference for each wind direction sector and for the maximum ozone level of the two stations <80, >80, and >100 ppbv. The number of observations, the mean difference, and the standard deviation of the difference is given for each direction and concentration class.

Table I. Conyers and Dallas Ozone Levels for East and West Winds and Different Wind Speeds[a]

	ozone <80 ppbv		ozone >80 ppbv		ozone <100 ppbv	
	west	east	west	east	west	east
	Calm: SPD < 2 m s^{-1}					
N	9	10	9	10	5	3
CN	54	62	95	84	105	90
DL	42	61	89	94	104	113
CN – DL	12	1	6	−10	1	−23
	SPD ≥ 2 m s^{-1}					
N	101	74	48	32	27	8
CN	50	47	108	69	124	81
DL	44	51	78	89	86	108
CN – DL	6	−3	30	−20	38	−27

[a] *N* = number of observations; CN = Conyers; DL = Dallas; SPD = wind speed at Hartsfield Airport, concentrations in ppbv.

We see that the northwest winds bring ozone levels 20–45 ppbv higher at Conyers than at Dallas during episode days (>100 ppbv), and east winds bring similar differences in the opposite senses. However, on nonepisode days (<80 ppbv) there is little average difference between the two stations for all wind directions.

This change in the ozone concentration with wind direction is further summarized in Table I, where the wind is divided into east and west components and stratified by wind speed. We see that for near calm winds there is little difference between the two stations. But with winds greater than 2 m s^{-1} and ozone levels above 80 ppbv at one of the two stations, the downwind station is 20–40 ppbv higher than the upwind station. Further stratification of the results by wind speed did not reveal any significant trend with wind speed for winds greater than 2 m s^{-1}. For all speeds greater than 2 m s^{-1} and ozone levels above 80 ppbv, there is 30 ppbv more ozone measured at Conyers than at Dallas for west winds and 20 ppbv more at Dallas than at Conyers for east winds. These values rise to 38 ppbv and 27 ppbv, respectively, for days with ozone levels above 100 ppbv. Also of interest are the relatively high values of the ozone concentration at the upwind station: 78 ppbv at Dallas for west winds and 90 ppbv at Conyers for east winds on moderate (>80 ppbv) days, and 86 ppbv and 81 ppbv, respectively, on the high-concentration (>100 ppbv) days. These levels indicate that high-ozone air is entering the area either (a) from long-range transport of pollution from other urban and industrial centers, (b) from local air already burdened with ozone reentering the city after a reversal in wind direction, and/or (c) from ozone produced rurally in conditions favorable to photochemical production. Progressive vector diagrams of the surface winds indicate that some of the cases in which ozone concentrations at the upwind station were high or actually exceeded those at the downwind station did indeed occur on days following wind reversals. Moreover, such wind reversals are not uncommon.

In order to better characterize the source of the apparent excess ozone entering Atlanta on high-ozone days, we have

also examined ozone measurements obtained at Leslie, a rural ozone-monitoring station in southwestern Georgia 125 km south of Atlanta. On days when one of the three Atlanta-area stations was above 100 ppbv and the winds were out of the west greater than 2 m s^{-1}, the ozone concentration at Leslie averaged 65 ppbv. This compares to the average of 85 ppbv measured at Dallas on similar days, implying that Dallas was some 20 ppbv greater than the rural background level. Moreover, the 65 ppbv measured at Leslie on these days is about 20 ppbv above the 2-year mean for this rural station. Thus, we find that there was a 20 ppbv enhancement of the ozone concentration in the rural parts of the region during ozone episodes in Atlanta, and the air entering the Atlanta metropolitan area was another 20 ppbv above this level. The addition of almost 40 ppbv as the air crossed over the city, as discussed above, brought the ozone concentrations in excess of the National Ambient Air Quality Standard (see Table I) during these episodes.

Conclusions

Both the trajectory analysis and the surface winds indicate that days of high-ozone concentrations are often characterized by low winds. Though the wind speeds are not great, rarely exceeding 5 m s^{-1}, back-trajectory calculations indicate that there is sometimes significant transport of air over the preceding 3 days. Half of the trajectories for days over 100 ppbv had moved over 600 km in the 3 days before; of these, half had come from the northwest quadrant. The movement appears to be bringing high levels of ozone and/or ozone precursors into the region. On those days in which there was more than 100 ppbv ozone in Atlanta and the air had traveled over 600 km from the northwest, we find that the average ozone concentration at the rural station of Leslie was 82 ppbv (n = 8) versus 65 ppbv (n = 47) for all days over 100 ppbv in Atlanta. This suggests that sometimes the air coming from the northwest is indeed bringing with it enhanced levels of ozone and ozone precursors and affecting a large portion of the state.

An approximate ozone budget for the Atlanta metropolitan area during the summers of 1983 and 1984 is as follows: the rural background level for all wind directions during episode days (greater than 100 ppbv at one of the Atlanta-area stations) is near 65 ppbv, well above the mean rural level of about 45 ppbv due to the photochemical production of ozone from natural sources, from sources in small towns and cities, and from distant large sources; the upwind station measured 15–20 ppbv more than the rural background due to the recycling of metropolitan air after previous calm conditions, from wind reversals or from long-range transport, bringing the concentration up to 80 or 85 ppbv; during the passage over the city, the ozone concentration is further increased by 30–40 ppbv, bringing the total to 110–125 ppbv. Thus, it appears that the 1-day production of ozone from the precursors emitted in the metropolitan area is insufficient to raise the ozone concentrations all the way from the rural level (about 65 ppbv on ozone event days) to the NAAQS level of 120 ppbv; instead, the air entering the city must already be elevated in ozone in order for the air in Atlanta and/or leaving Atlanta to exceed the NAAQS for ozone.

The 30–40 ppbv increase in the ozone concentration as the air passes over the city is similar to a value cited for Detroit. In a 1981 study of the Detroit area, Kelly et al. (*11*) looked at the days in the first (highest) quartile of the daily maximum hourly ozone levels measured at 16 sites. The site with the maximum mean (of the first quartile days, 104 ppbv) was 57 ppbv more than that of midmorning air at the site with the lowest concentrations (47 ppbv), and this value was attributed to the photochemical production of ozone in the Detroit plume. The midmorning value was considered representative of the boundary-layer air before significant photochemical production could occur. If the first quartile mean daily maximum of the low-concentration station (73 ppbv) was used instead of the midmorning mean, an increment due to the city of only 31 ppbv would have been found. This lower value would be the additional ozone formed during the day due to the presence of the city and is more comparable to the calculation we have made, both in the way it is done and in the magnitude.

The elevated ozone levels of the air entering the city on high-ozone days can result from a variety of causes that may vary considerably from one year to the next, with little or no correlation to the photochemical activity of the city itself. For this reason we do not believe that a reliable indication of photochemical smog production from Atlanta-based sources can be obtained by simply monitoring the number of days per year that O_3 in and around the Atlanta area exceeds the NAAQS. A far more reliable indication may possibly be obtained by monitoring the difference between the ozone level in air leaving Atlanta from that entering Atlanta. In the summers of 1983 and 1984, our study indicated that for high-ozone days the air leaving the city had an ozone concentration some 30–40 ppbv greater than the air entering the city. We believe this increment is a good indication of the impact of the metropolitan area on air quality. Monitoring the variation of this increment from year to year may provide a useful and accurate means of determining the efficacy of air pollution control efforts within this area.

Acknowledgments

We express our gratitude to Robert H. Collom, Jr., and William Estes of the Georgia Department of Natural Resources for their helpful discussions and for providing us with the ozone data from Georgia.

Registry No. O_3, 10028-15-6.

Literature Cited

(1) Vukovich, F. M.; Bach, W. D., Jr.; Crissman, B. W.; King, W. J. *Atmos. Environ.* **1977**, *11*, 967–983.
(2) Wight, G. D.; Wolff, G. T.; Lioy, P. J.; Meyers, R. E.; Cederwall, R. T. *ASTM Spec. Tech. Publ.* **1978**, *No. 653*, 445–457.
(3) Vukovich, F. M.; Fishman, *Atmos. Environ.* **1986**, *12*, 2423–2433.
(4) Zishka, K. M.; Smith, P. J. *Mon. Weather Rev.* **1980**, *108*, 387–401.
(5) Heffter, J. L. *NOAA Technical Memorandum ERL ARL-121*; National Oceanic and Atmospheric Administration: Rockville, MD, 1983, 16 p.
(6) Kahl, J. D.; Samson, P. J. *J. Clim. Appl. Meteorol.* **1987**, *25*, 1816–1831.
(7) Wolff, G. T.; Kelly, N. A.; Ferman, M. A. *Water, Air, Soil Pollut.* **1982**, *18*, 65–81.
(8) Benkovitz, C. M. *Atmos. Environ.* **1982**, *16*, 1551–1563.
(9) Clark, T. L. *Atmos. Environ.* **1980**, *14*, 961–970.
(10) Westberg, H.; Lamb, B. "Unpublished Report to EPA from the Laboratory of Atmospheric Research"; Washington State University: Pullman, Washington, 1985.
(11) Kelly, N. A.; Ferman, M. A.; Wolff, G. T. *J. Air. Pollut. Control Assoc.* **1986**, *36*, 150–158.

Received for review May 22, 1987. Accepted August 22, 1987. This work was supported in part by funds from the National Science Foundation under Grant ATM-8600888.

Ozone Trends in Atlanta, Georgia: Have Emission Controls Been Effective?

Ronald W. Lindsay

Jennifer L. Richardson

William L. Chameides

School of Geophysical Sciences

Georgia Institute of Technology

Atlanta, GA 30332

The authors are associated with the School of Geophysical Sciences at the Georgia Institute of Technology, Atlanta, GA 30332. Ronald Lindsay, who has an MS from the University of Washington, is a Research Scientist, Jennifer Richardson is a Graduate Student, and William Chameides, who has a Ph.D. from Yale University, is a Professor of Geophysical Sciences.

April 6, 1988

Abstract: Nine years of summertime ozone data from the Atlanta Metropolitan Area are analyzed and compared to local emissions of volatile organic carbon and nitrogen oxides. Trends from 1979 to 1987 were studied for the number of days per year ozone exceeded the NAAQS standard, the second-highest ozone level observed per year, and the first quartile summertime average ozone observed, as well as the mean difference between the ozone level observed downwind and upwind of the city. Because this last parameter is sensitive to chemical factors but relatively insensitive to meteorological variations its trend may provide a better indication of how effective emission controls have been in reducing O_3 in the Atlanta area. In spite of sizeable reductions reported for volatile organic carbon emissions over the past several years the data give no indication that ozone levels have decreased and in fact imply that summertime ozone production may have increased. The results suggest the need for a reevaluation of our nation's strategy for O_3 abatement in Atlanta and comparable cities.

I. Introduction

In 1952 Haagen-Smit first used the term "photochemical smog" to describe the mix of air pollutants that arise in the Los Angeles area from the oxidation of volatile organic carbon (VOC) and nitrogen oxides (NO_x) in the presence of sunlight and water vapor.[1,2] Photochemical smog is now recognized to be responsible for the high O_3 levels ($[O_3]$) typically found in all areas with large VOC and NO_x emissions and adequate sunlight. In an effort to prevent $[O_3]$ from exceeding the 120 ppbv National Ambient Air Quality Standard (NAAQS), the U.S. Environmental Protection Agency (EPA) in conjunction with state and municipal agencies have mandated reductions in anthropogenic VOC and NO_x emissions. Because O_3 production in most American cities is believed to be limited by VOC rather than NO_x, EPA has focussed primarily on VOC reductions.[3] It is estimated that nationwide from 1976 to 1985, VOC emissions have been reduced by 19% and NO_x emissions by only 1%.[4]

To determine if emission controls have successfully reduced $[O_3]$, data from numerous American cities have been analyzed. While some investigators have found evidence for a downward trend in $[O_3]$, others have concluded that $[O_3]$ has either remained constant or increased slightly.[4,5,6] One possible reason for these conflicting results is that meteorological factors have a major impact on $[O_3]$; the meteorological fluctuations that a city typically experiences can cause large year-to-year variations in $[O_3]$ and these variations can obscure the presence of a small secular $[O_3]$ trend due to changes in VOC.[7,8]

In this work we analyze O_3 data gathered from 1979 to 1987 in Atlanta, Georgia, a city in the southeastern U.S. characterized by frequent O_3

episodes. Our analysis is unique in that we have been able to determine the trend in a parameter which we believe to be sensitive to O_3 chemistry but relatively insensitive to meteorological factors. This parameter can therefore be used with less ambiguity to determine if emission controls enforced over the last several years have been effective.

II. VOC and NO_x Emissions

Figure 1a shows the total (point and area sources) annual VOC and NO_x emission rates as a function of year for the eleven county Atlanta metropolitan area as obtained from the National Emissions Data System (NEDS) maintained by EPA. The data indicate that VOC declined steadily from 1979 to 1982, increased by 25% from 1982 to 1983, and then returned to a decline. The large increase in VOC from 1982 to 1983 is not reflected in the raw fuel usage for the area which increased by only 3% and appears to be an artifact caused by a change EPA made in 1983 to the algorithm used to calculate VOC emissions from gasoline-powered motor vehicles; for the same fuel consumption rates the new algorithm calculates significantly more VOC emissions than the old algorithm.[9] To correct for this artifact and obtain a consistent trend, the VOC emission factor from gasoline-powered vehicles was increased by 0.05 tons/gallon for the years 1979 to 1982. This "adjusted" VOC trend is also illustrated in Figure 1a.

VOC emissions appear to have been reduced significantly in the Atlanta metropolitan area. From 1979 to 1985, VOC emissions dropped by 37% (22% before adjustment) in the eleven county area. In Fulton County, the most populous and centrally located of the eleven counties, VOC emissions dropped by 55% (44% before adjustment) reflecting its slower growth rate compared to

the suburban counties. Changes in NO_x emissions have been more modest: a 4% increase in the eleven counties and a 16% decrease in Fulton county. If VOC-emissions are the limiting chemical factor in O_3 production in Atlanta, then these sizeable VOC reductions should have caused a significant reduction in O_3. Whether or not this has been the case is addressed below.

III. O_3 Concentrations and Trends

Our O_3 analyses for the Atlanta area are based on hourly-averaged $[O_3]$ observed by the Georgia Department of Natural Resources (DNR) from three stations in the Atlanta area (South Dekalb, Conyers, and Dallas) during the months of June, July, and August from 1979 to 1987. Figure 2 shows the locations of the three stations and of Hartsfield Atlanta International Airport where the surface winds used in our analysis were measured. (Note that in 1979 observations to the northwest of the city were actually made at New Hope, a location relatively close to Dallas. Furthermore, in 1980 the Conyers station was down for much of the year, causing a small gap in our data.) All O_3 measurements were made using the photoluminescence method, with calibration by UV photometry.

Figure 1b illustrates the annual variations in one of the parameters EPA uses to follow ozone trends: the number of days each year that the daily maximum $[O_3]$ exceeds the NAAQS. The year-to-year variations in this parameter are fairly large but a slightly significant upward trend is discernible; the slope is 14 ± 12%/yr. The years 1983, 1986, and 1987 appear to have been high in O_3, while 1982, 1984, and 1985 were low; interestingly EPA obtained a similar pattern for the nation as a whole with a high number of exceedances in 1983.[4]

Another parameter followed by EPA is the second highest daily maximum (SHDM) [O_3] observed at a location for the year. Although not illustrated in Figure 1, the pattern of year-to-year variations in the SHDM [O_3] in Atlanta is quite similar to that obtained for the number of NAAQS exceedances in Atlanta: a maximum in 1983 and minima in 1982 and 1984/85. There is no evidence of a secular trend; the slope is 0.2 ± 1%/yr.

Figure 1c illustrates the variations in the summertime average of the first-quartile in daily [O_3] maxima from the three stations; since the parameter is less sensitive to outliers that the two discussed above it is a more robust statistic.[5] The pattern of variations in the first-quartile average is also quite similar to that of the number of NAAQS exceedances; however there is no evidence for a significant secular trend. Slopes of 1.7 ± 1.6, 0.3 ± 1.5 and 0 ± 1.9%/yr were calculated for South Dekalb, Conyers and Dallas, respectively.

The lack of a significant downward trend in any of the above parameters would appear to imply that reductions in VOC emissions have not been effective in reducing O_3. However some caution should be exercised in interpreting these results since variations in the above parameters can be unrelated to chemical factors. For instance note that each of the above parameters is strongly affected by meteorological variations. In Atlanta, as in most cities, the days with the highest [O_3] often have stagnant winds, so summers with long periods of near-calm winds and warm temperatures tend to have higher average [O_3] and a higher number of NAAQS exceedances[10] regardless of how ozone-precursor emissions varied for the year.

Furthermore [O_3] in an urban area is a function of the amount of O_3 that is advected into the city; we have found for instance that in 1983 and 1984

air entering Atlanta during an O_3 episode day contained, on average, about 85 ppbv O_3.[10] Given the magnitude of this value, it is not inconceivable that yearly variations in average $[O_3]$ maxima in the city could be simply due to changes in the $[O_3]$ being advected into the city and have nothing to do with local emissions.

In order to unambigiously determine if emission controls have effectively limited ozone production in a location, one must study the trend in a parameter which is directly linked to the local ozone production rate. An analysis of a parameter having these properties is presented below.

IV. $\Delta(O_3)$ Trend

In a previous study[10] based on Atlanta O_3 data from 1983 and 1984, we found that $[O_3]$ measured at Conyers and Dallas could be used to indicate the intensity of O_3 production in the Atlanta area. Note in Figure 2 that when the winds are out of the northwest, Conyers lies downwind of the city and Dallas lies upwind of the city. On the other hand when the winds are out of southeast, Dallas is downwind while Conyers is upwind. Thus $\Delta(O_3)$, defined as the difference between the daily maximum $[O_3]$ measured at Conyers and at Dallas, should reflect the increment of O_3 added to an air mass as it advects over the city.

In Figure 3 $\Delta(O_3)$ is plotted as a function of the six-hour (1200-1700) vector-averaged wind direction for summer days from 1979 to 1987. Because our focus is on those processes that cause O_3 episodes, only days during which at least one of the two stations recorded a daily maximum $[O_3]$ above 80 ppbv are included in the figure. Furthermore, because the use of $\Delta(O_3)$ as an indicator of photochemical activity can only be valid when there is a

significant flow of air over the city, all days with winds less than 2 m/s were excluded from the figure. The overall trend in $\Delta(O_3)$ as a function of wind direction is easily discernible in Figure 3; $\Delta(O_3)$ is most positive when the winds are out of the northwest and most negative when the winds are out of the east-southeast. However, not all days follow this trend; there are some days when $\Delta(O_3)$ has the opposite sign - negative for west winds and positive for east winds - implying that O_3 was actually consumed as it passed over the city. In general these days appear to have occurred when there was significant cloud cover over the city and therefore little photochemical activity or when there were wind reversals so that air already polluted by the metropolitan area was brought back into the city. In the trend analysis described below we have excluded these days from our calculation.

In Figure 1d the annually averaged values for $\Delta(O_3)$ for west winds (i.e., winds having directions from 260-320°) and for east winds (i.e. winds having directions of 70-130°) are plotted for the years from 1979 to 1987. Because the individual points in Figure 1d are not functions of the number of O_3 events per year and because they were calculated for days with specific meteorological conditions (i.e., a specific wind direction and minimum wind velocity), the year-to-year meteorological variations that determine how many O_3 episodes a city experiences each year are factored out of the trend. The fact that the year-to-year variability in $\Delta(O_3)$ is much smaller than and different from the variability in the parameters plotted in Figures 1b and 1c tends to support this contention. For this reason we believe that $\Delta(O_3)$ represents a more accurate indication of the secular trend in ozone production in Atlanta and of how effective VOC-emission reductions have been in reducing O_3 in the urban area.

The slopes of the $\Delta(O_3)$ trends in Figure 4 are +3.9 ± 2 and +2.1 ± 2.2%/yr for west and east winds, respectively, indicating a slight upward trend in ozone production in Atlanta over the eight year period. The possibility that $\Delta(O_3)$ has decreased over the period can be excluded at the 90% and 80% confidence levels for west and east winds, (N = 8, R = .58 and .36). While we do not understand why a larger and more significant slope was obtained for west winds than for east winds, it should be noted that the west-wind analysis included almost three times as many data points (145 days) as that of the east-wind analysis (58 days) and is therefore more robust.

V. Conclusion

An analysis of eight years of ozone data gathered in the Atlanta metropolitan area indicate that the sizeable VOC-emission reductions reported by NEDS for the area have not been accompanied by a significant reduction in O_3. While VOC emissions appear to have decreased significantly over the last several years, summertime $[O_3]$ has not decreased and there are indications that O_3 photochemical production in the area during O_3 episodes has actually increased. For each 10^5 ton reduction in VOC emissions in the eleven county metropolitan area, ozone production over the five years of overlapping data is calculated to have increased by 12 ± 8 and 1 ± 8 ppbv for west and east winds, respectively. While we do not mean to imply a causal relationship between the VOC decrease and O_3 increase with this statistic, it does serve to illustrate the fact that our strategy for reducing O_3 in Atlanta appears to have been largely ineffective

Why has O_3 production not decreased over the last nine years? One possibility is that the NEDS VOC inventories are incorrect and VOC emissions

in the Atlanta area have not decreased significantly since 1979. If, on the other hand, VOC emissions have decreased significantly then it would appear that, contrary to the results of numerical and smog chamber simulations,[3] O_3 in the Atlanta area is relatively insensitive to VOC levels.

In light of the above result it is interesting to note that while natural emissions of VOC (primarily isoprene and terpene) from trees can be quite large[11], these sources have been largely ignored in the development of our current O_3 abatement strategies.[12] In fact, in the Atlanta area biogenic emissions of VOC appear to be comparable in magnitude to the NEDS estimate of VOC emissions from anthropogenic sources. Using 1976 LANDSAT photographs obtained from Dr. N. Faust of the Georgia Tech Engineering Experiment Station and urban growth rates supplied by the Atlanta Regional Commission, we estimate that approximately 60% of the 11 county Atlanta metropolitan area was covered by forest in 1985, roughly 20% each by deciduous, coniferous, and mixed forests. Combining these results with measured daytime and nighttime emission factors for isoprene, α-pinene and β-pinene from each forest type[11], we calculated a total summertime biogenic VOC source for the area of about 400 tons C/day, a result consistent with measurements made in a 1981 Atlanta area field study.[13] The NEDS estimated anthropogenic VOC source for 1985 is also about 400 tons C/day (see Figure 1). This result suggests that natural VOC compounds may play a significant role in the formation of O_3 in the Atlanta area. The fact that natural VOC measured levels in the Atlanta area tend to be much lower than anthropogenic VOC's does not necessarily mean that natural VOC can be neglected since they tend to be more reactive. The size of the natural VOC source suggests that the supply to the area may be very much larger than has been previously assumed;[12] perhaps large enough to make

NO_x rather than VOC the limiting chemical precursor to O_3 production. If this were the case, NO_x emission controls would be more effective in reducing $[O_3]$ than VOC.[14]

Our results indicate that efforts to limit VOC emissions in Atlanta have not been effective in reducing summertime O_3 photochemical production. Trend studies by other investigators suggest similar results for other locations.[5] We believe that a careful reevaluation of the nation's strategy for reducing O_3 is needed. This reevaluation should perhaps include a more careful assessment of VOC emission trends, of the relative importance of VOC and NO_x in limiting O_3 production, and of what role, if any, natural hydrocarbons play in urban and regional O_3 episodes.

VI. Acknowledgement: This work was supported in part by funds from Grant ATM 8600888 from the National Science Foundation and Grant NAG-1-786 from the National Aeronautics and Space Administration. In addition the authors would like to thank R. Collum, W. Estes, and D. Kemmerick of the Georgia Department of Natural Resources for the use of their data and their helpful comments, N. Faust of the Georgia Tech Research Institute for his help with the LANDSAT photographs, and Dr. C.S. Kiang of the Georgia Institute of Technology, School of Geophysical Sciences for his advice and encouragement.

VII References

1. A.J. Haagen-Smit, "Chemistry and physiology of Los Angeles smog," *Ind. Eng. Chem.*, 44: 1342 (1952).

2. A.J. Haagen-Smit and M. Fox, "Ozone formation in photochemical oxidation of organic substances," *Ind. Eng. Chem.*, 48: 1484 (1956).

3. M.C. Dodge, "Combined use of modelling techniques and smog chamber data to derive ozone-precursor relationships," in *Proceedings of the International Conference on Photochemical Oxidant Pollution and its Control.* EPA-600/3-77-001b, U.S. EPA, Research Triangle Park, pp. 881-889, 1977.

4. *National Air Quality and Emission Trends Report,* 1985. EPA-450/4-87-001, U.S. EPA, OAQPS, Research Triangle Park, NC 1987.

5. H.M. Walker, "Ten-year ozone trends in California and Texas," *JAPCA, 35: 903 (1985).*

6. *Air Quality Trends in the South Coast Air Basin through 1979,* California Air Resources Board Technical Services Division, 1980.

7. A. Davidson, "Comment on 'Ten-year ozone trends in California and Texas'," *JAPCA,* 36: 597 (1986).

8. H.M. Walker, "Author's reply," *JAPCA,* 36: 600 (1986).

9. *Compilation of Air Pollutant Emission Factors, Volume II: Mobile Sources* AP-42, EPA Motor Vehicle Emissions Laboratory, Ann Arbor, 1985.

10. R.W. Lindsay, W.L. Chameides, "High ozone events in Atlanta, Georgia in 1983 and 1984," *Env. Sci. Techn.*, in press, (1988).

11. P.R. Zimmerman, *Determination of emission rates of hydrocarbons from indigenous species of vegetation in the Tampa/St. Petersburg, Florida area.* EPA 904/9-77-028, U.S. EPA, Atlanta, GA February 1979.

12. A.P. Altshuller, "Review: natural volatile organic substances and their effect on air quality in the United States," *Atmos. Environ.*, 17: 2131 (1983).

13. H. Westberg, B. Lamb, "Ozone production and transport in the Atlanta, Georgia region," EPA/600/S3-85/013, U.S. EPA, Research Triangle Park, NC April 1985.

14. M. Trainer, E.J. Williams, D.D. Parrish, M.P. Buhr, E.J. Allwine, H.H. Westberg, S.C. Liu, "Models and observations of the impact of natural hydrocarbons on rural ozone," *Nature*, 329 705 (1987).

Figure Captions

Figure 1., a) Annual VOC and NO_x emissions from NEDS and the adjusted VOC emissions, b) number of days any of the three stations measured ozone concentrations above 120 ppbv, c) annual top quartile of ozone concentrations for each of the three stations, and d) $\Delta(O_3)$ for west and east winds as shown in Figure 3.

Figure 2., Map of Atlanta area showing the locations of the three ozone monitoring stations and that of the Atlanta Hartsfield International Airport where the winds were measured. Also shown is the outline of the city's urbanized area.[4]

Figure 3., The difference between the maximum ozone concentrations at Conyers and and Dallas ($\Delta(O_3)$) versus wind direction. Only days when one of the two stations recorded over 80 ppbv are shown. The winds were six-hour vector-averaged (1200-1700 EST) and must have averaged over 2 m/s. The boxes enclose the data points that were used for the analysis illustrated in Figure 1d. West winds, 206° - 320°, included 145 days and east winds, 70°-130°, 58 days, both over eight years.

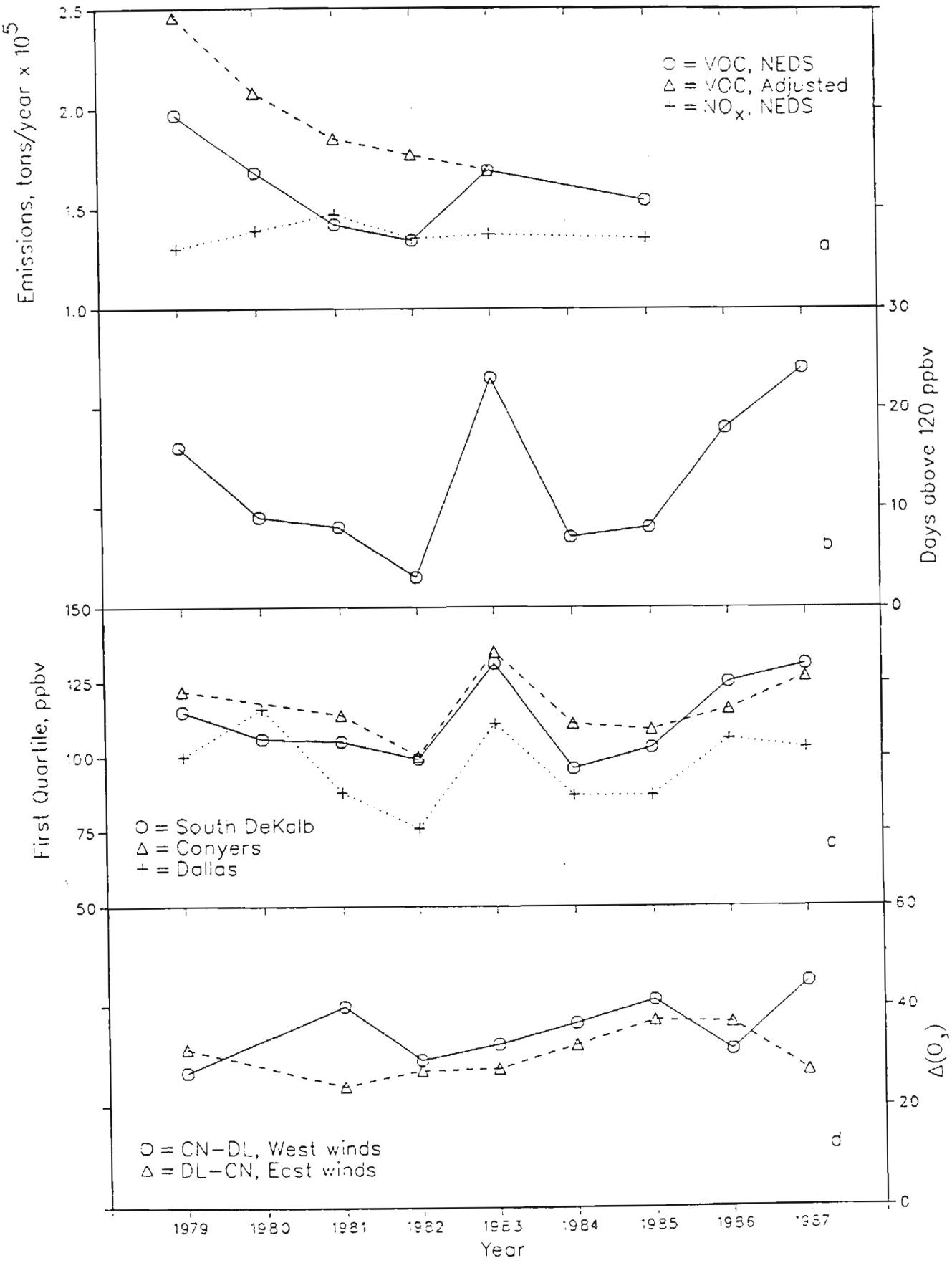
Emissions, tons/year x 10^5
2.5
2.0
1.5
1.0
○ = VOC, NEDS
△ = VOC, Adjusted
+ = NO_x, NEDS
a
30
b
20
10
0
Days above 120 ppbv
First Quartile, ppbv
150
125
100
75
50
○ = South DeKalb
△ = Conyers
+ = Dallas
c
60
40
20
0
$\Delta(O_3)$
○ = CN−DL, West winds
△ = DL−CN, East winds
d
1979
1980
1981
1982
1983
1984
1985
1986
1987
Year

Atlanta Metropolitan Area

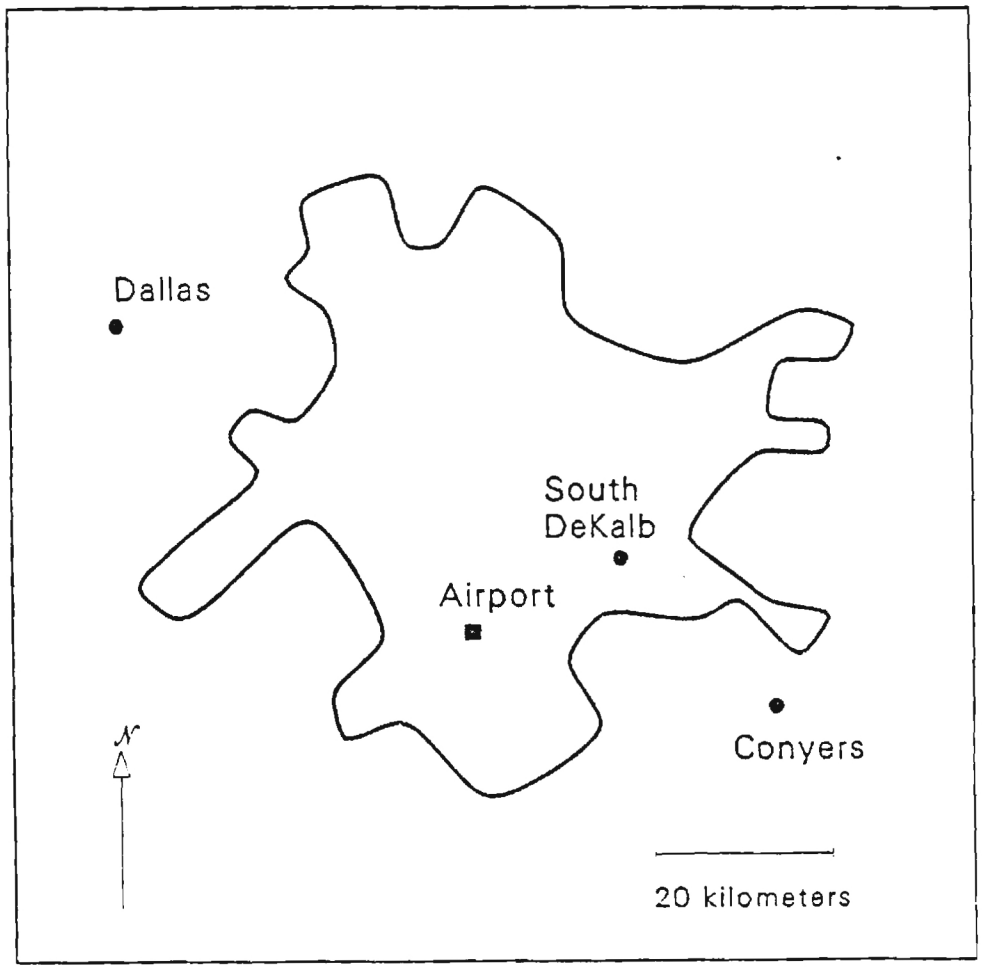

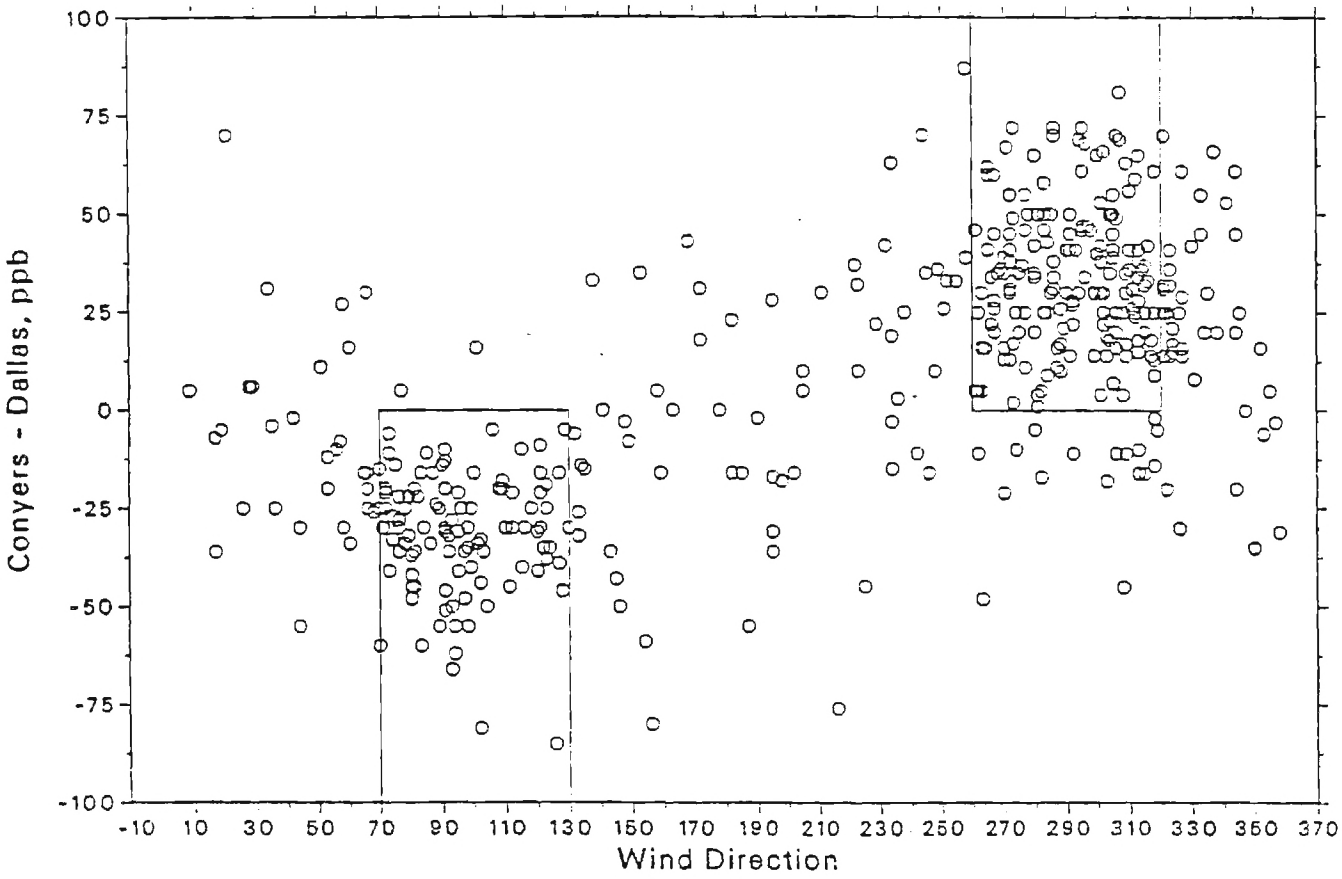
Conyers - Dallas, ppb
100
75
50
25
0
-25
-50
-75
-100
-10
10
30
50
70
90
110
130
150
170
190
210
230
250
270
290
310
330
350
370
Wind Direction

APPENDIX C

The Biochemistry of Ozone Deposition to Plant Leaves: The Role of Ascorbic Acid

William L. Chameides

School of Geophysical Sciences

Georgia Institute of Technology

Atlanta, GA 30332

June 3, 1988

Abstract

A mathematical formulation is derived which describes the transport and chemistry of atmospheric gases as they diffuse through the open stomata, inner air spaces, and cell walls of plant leaves before depositing on the mesophyllic plasmalemma. The formulation is applied to the problem of ozone deposition on plant leaves to determine if reactions in the mesophyllic cell-wall water can prevent ozone from reaching the plasmalemma and initiating harmful oxidation reactions. Calculations indicate that a major portion of the ozone diffusing through the leaf can react with ascorbic acid in the cell wall. Other mechanisms such as ozone reactions with biogenic olefins and ozone decomposition in the cell-wall water are found to be unimportant. These calculations suggest that plants may protect themselves from the harmful effects of ozone by concentrating ascorbic acid in their cell walls; by reacting with ozone in the cell wall, the ascorbic acid limits the amount of ozone that can penetrate through the cell wall and reach the more vulnerable material inside the wall.

Introduction

Approximately 1 billion metric tons of ozone (O_3) are removed from the atmosphere annually by dry deposition to vegetative surfaces. Much of this deposition occurs when O_3 diffuses into plant leaves through open stomata and reacts with the internal cell material of the leaf[1,2]. Because O_3 is phytotoxic[3,4,5] its deposition can have harmful biological effects; it has been suggested that in regions affected by air pollutants, enhanced O_3 levels may be a contributing factor in forest diebacks and crop loss[6,7]. Experimental studies have shown that the sensitivity of a plant to O_3 can vary widely from species to species and even from individual to individual within a given species[8]. While the factor or factors which determine a plant's sensitivity remain uncertain, ascorbic acid appears to often play a role. A number of investigators have found a strong inverse relationship between plant sensitivity and ascorbic acid levels within the plant leaf[9,10,11,12]. In this work a mechanism is proposed by which ascorbic acid protects a plant from O_3 damage.

To study the chemistry of ozone dry deposition, a mathematical formulation

is adopted which treats the process of gaseous diffusion through a leaf as a one-dimensional, molecular diffusion problem involving a series of diffusive layers. While this formulation represents a gross simplification of a very complex mass transfer problem, it has been found to adequately describe the transfer of carbon dioxide and water vapor between the leaf and atmosphere and should therefore also provide a reasonably quantitative framework from which to study the transfer of atmospheric O_3 to leaves.

Ozone Transfer Across The Mesophyllic Cell Wall

Similar to the uptake of atmospheric CO_2 by plants during photosynthesis, O_3 deposition onto the internal mesophyllic cells of a plant leaf must be preceded by O_3 transfer through a series of diffusive layers[13]. These layers are: 1. the thin laminar layer of air in contact with the leaf surface; 2. the stomatal openings on the leaf surface; 3. the inner air space inside of the leaf; and 4. the cell walls surrounding the mesophyllic plasmalemma. Once an O_3 molecule has penetrated through the cell wall to the plasmalemma, it can react rapidly with the polyunsaturated fatty acids (PUFA) in the lipid membrane and initiate destructive oxidation reactions[14,15]. In this section we focus on the processes which control the transfer of O_3 across the cell wall.

The cell wall in a leaf typically has two major components: a complex matrix of cellulose microfibrils, lignens, and other polymers, which give the cells their rigidity, and an aqueous solution surrounding the microfibrils which facilitates the transfer of CO_2 from the leaf's inner air spaces to the photosynthetically active cells[16]. To cross the cell wall and reach the plasmalemma, O_3, like CO_2, must diffuse through this aqueous solution. If O_3 was unreactive in this solution, then the one-dimensional diffusion equation

describing the time rate of change of ozone within the cell wall would be given by

$$\frac{\partial [O_3]}{\partial t} = D_w \frac{\partial^2 [O_3]}{\partial z^2} \qquad (1)$$

where $[O_3]$ is the aqueous-phase O_3 concentration within the cell-wall water in moles/liter (M), D_w is the aqueous phase molecular diffusion coefficient (2 x 10^{-5} cm^2/s), t is time, and z is distance within the cell wall. At steady state, the flux of O_3 in the cell wall is conserved and solution to Eqn. (1) yields

$$\Phi_{cw} = \Phi_p = \frac{H\ Av}{10^3\ r_{cw}} \left\{ X_{cw} - \frac{[O_3]_p}{H} \right\} \qquad (2)$$

where Φ_{cw} and Φ_p are the O_3 fluxes (in molecules/cm^2/s) crossing the inner-air-space/cell-wall boundary and cell-wall/plasmalemma boundary, respectively, Av is Avogrado's Number, X_{cw} is the O_3 partial pressure at the inner-air-space/cell-wall boundary, $[O_3]_p$ is the aqueous-phase O_3 concentration in moles/liter (M) at the cell-wall/plasmalemma boundary, H is the O_3 solubility constant (0.01 M/atm [17]), and r_{cw}, the transfer resistance of the cell wall, follows the standard form for an aqueous diffusive layer, e.g.,

$$r_{cw} = \frac{L}{D_w} \qquad (3)$$

In (3), L is the effective thickness of the cell wall.

If, on the other hand, O_3 reacts in the cell-wall water, the one-dimensional diffusion equation takes the form of

$$\frac{\partial[O_3]}{\partial t} = D_w \frac{\partial^2[O_3]}{\partial z^2} - k[O_3] \tag{4}$$

where k is the first-order loss coefficient (in s^{-1}) for O_3 in the cell-wall solution and is assumed for simplicity to be a constant. In this case the O_3 flux is not conserved and the steady state solution to (4) yields

$$\Phi_{cw} = \frac{H\ Av}{10^3\ r'_{cw}} \left\{ X_{cw} - \frac{[O_3]}{H \cosh(q)} \right\} \tag{5}$$

and

$$\Phi_p = \frac{H\ Av}{10^3\ r'_{cw}} \left\{ \frac{X_{cw}}{\cosh(q)} - \frac{[O_3]_p}{H} \right\} \tag{6}$$

where

$$q = \left(\frac{k}{D_w} \right)^{1/2} L \tag{7}$$

and r'_{cw}, the reactive transfer resistance of the cell wall, is given by

$$r'_{cw} = \tanh(q)/(kD_w)^{1/2} \tag{8}$$

The fraction, FR, of the total O_3 flux entering the cell wall that reacts before reaching the plasmalemma is, by mass conservation, given by

$$FR = (\Phi_{cw} - \Phi_p)/\Phi_{cw} \tag{9}$$

and from (5) and (6) we find that

$$FR = 1 - \coth(q) \qquad (10)$$

Values for FR as a function of k are plotted in Figure 1 for L = 1, 3, and 30 μm; this should represent a reasonable range for L given the thickness of cell walls (a few tenths to about 10 μm) and the fact that O_3 molecules diffusing through the wall must take a circuitous path around the microfibrils[16]. Figure 1 indicates that for intermediate values of k ranging from 0.1 to 10^4 s^{-1}, FR increases as both k and L are increased. Since an increase in k shortens the chemical lifetime of O_3 in the cell wall, FR is found to increase with increasing k. Since an increase in L lengthens the time an O_3 molecule requires to diffuse through the wall, an increase in L also causes an increase in FR. However for k-values outside this intermediate range, FR is essentially independent of both k and L. In the unreactive regime when $k \leq 0.1$ s^{-1}, FR is $\simeq 0$ and a negligibly small fraction of the O_3 reacts in the cell wall; in this case virtually all of the O_3 which enters the cell wall reaches the plasmalemma. In the reactive regime when $k \geq 10^4$ s^{-1}, FR $\simeq 1$ and virtually all of the O_3 reacts in the cell wall and never reaches the plasmalemma.

The results suggest that the impact of any given reaction on the flux of O_3 diffusing through the cell wall can be determined by evaluating that reaction's k-value. A reaction with a k in cell-wall water of 0.1 s^{-1} or less is in the unreactive regime and will not be important. A reaction with a k of 10^4 s^{-1} or more is in the reactive regime and can therefore represent a major sink for O_3 in the cell wall. Since the major organic components of cell walls (e.g., cellulose, lignens, and pectins, and other uronic acids) do not fall into the classes of compounds that are reactive with O_3 [8], it is likely that

reactions with these compounds would be in the unreactive regime. In the discussion below three other mechanisms are considered.

O_3 Decomposition and Peroxidation

It has been speculated that damage to plants by O_3 may be caused by peroxidation[18] where dissolved O_3 first decomposes into free radicals which then either react directly with the cell or form peroxides which react with the cell. Since O_3 must decompose for this process to be of importance, it is interesting to determine the extent to which O_3 can decompose to form free radicals as it diffuses through the cell-wall solution. In the bulk aqueous phase O_3 decomposition proceeds via reaction with hydroxyl ions with a bimolecular rate constant of about 50 M^{-1} s^{-1} [19,20]. Assuming that this rate constant can be applied to the aqueous-phase solution of the cell wall and using the fact that under physiological conditions $[OH^-]$ is at most 10^{-7} M [16], a first order loss coefficient, k_{decomp}, for O_3 decomposition in the cell wall of only 5×10^{-6} s^{-1} or less can be inferred. This value is well within the unreactive regime (see Figure 1) indicating that O_3 decomposition in the cell wall is far too slow to be of significance. A negligibly small fraction of the O_3 diffusing through the cell wall will decompose before reaching the plasmalemma.

O_3 Reaction with Biogenic Hydrocarbons

Plants emit a wide range of olefinic compounds[21,22]. In a deciduous forest the primary olefin emitted is typically isoprene while terpenes are generally the major species produced by a coniferous forest[23]. In addition plants generally emit small amounts of ethylene, often in response to environmental

stress[24]. During a typical summer day within a deciduous forest as much as 6000 μg-C cm^{-2} hr^{-1} can be emitted as olefins by the trees of a deciduous forest; ambient isoprene concentrations within the canopy of such a forest are typically a few ppbv (parts-per-billion by volume)[23].

Because O_3 is reactive with olefinic compounds[25], the possibility exists that O_3 reacts with these compounds as it diffuses through the inner air spaces and cell walls of leaves and that these reactions play an important role in the process of O_3 dry deposition to the leaves. In fact, in a recent series of experiments involving O_3 fumigation of pea seedlings, Mehlhorn and Wellburn[26] found a close correlation between O_3 damage and the amount of stress ethylene emitted by the plant. These investigators proposed that the release of stress ethylene determines the sensitivity of a plant to O_3 and that the reaction of O_3 with ethylene within the leaves may in fact initiate a series of reactions that ultimately leads to leaf necrosis.

In light of these observations it is interesting to determine if a significant fraction of the O_3 diffusing through the cell walls can react with olefinic compounds produced by the leaf before reaching the plasmalemma. Using a resistance model for mass transfer of olefinic compounds from the plasmalemma to the atmosphere (similar to the one described later in this work for O_3 transfer to the plasmalemma), the total concentration of olefinic compounds in the cell-wall water of leaves in a deciduous forest canopy can be estimated as a function of the abundance of olefins in the canopy and the rate at which olefins are produced by the leaves. Assuming a leaf area index of 5, a biogenic-olefin production rate of 1.6×10^{12} molecules cm^{-2} s^{-1} (equivalent to 6000 μg-C m^{-2} hr^{-1} for a five C-atom molecule such as isoprene), an olefin abundance in the canopy of 4 ppbv, and an olefin solubility of 0.01 M atm^{-1}, a cell-wall water concentration of about 10^{-7} M was obtained. Given that the bimolecular, rate

constants for aqueous-phase O_3-olefin reactions range from 10^5 to 10^6 M^{-1} s^{-1} [27,28], these calculations imply a first order loss coefficient, k_{cle}, for the reaction of O_3 with olefins in cell-wall water of only 0.01 to 0.1 s^{-1}. This loss coefficient falls within the unreactive regime indicating that, as in the case of O_3 decomposition, an insignificantly small fraction of the total O_3 flux diffusing through the cell wall reacts with olefins before reaching the plasmalemma. An equivalent analysis for the fraction of the O_3 flux which reacts with olefins in the laminar layer outside the leaf and in the inner air spaces of the leaf yields similar results.

Given the very small fraction of O_3 that can react with olefins before O_3 reaches the PUFA-rich plasmalemma and the fact that ethylene comprises a very small fraction of the total olefinic emission rate, it seems unlikely that a causal relationship exists between ethylene production and O_3 damage as proposed by Mehlhorn and Wellburn[26]. It seems far more likely on the basis of this analysis that enhanced ethylene release during O_3 fumigation is a result of O_3 damage rather than a cause of the damage. (In this regard it should be noted that Mehlhorn and Wellburn found that plants which would be otherwise damaged by O_3 fumigation showed no damage from O_3 if they were first sprayed with a 1 mM solution of aminoethoxyvinylglycine (AVG), an inhibitor of ethylene biosynthesis. While this finding was interpreted by the investigators to mean that O_3 damage was prevented by blocking ethylene production, it should be noted that AVG has a double C-bond and therefore should be reactive to O_3[25]. It is possible that the application of a 1 mM solution of AVG to the leaf surfaces rendered these surfaces highly reactive to O_3 and thereby prevented O_3 penetration to the plasmalemma.)

O_3 Reaction with Ascorbate

A number of investigators have found an anti-correlation between the ascorbic acid (AA) levels in a plant leaf and its sensitivity to O_3 [9,10,11,12]. However the mechanism by which AA protects leaves from O_3 damage remains unclear. A number of complex mechanisms have been proposed; these include AA scavenging of O_3-generated peroxides and AA repair of O_3-damaged PUFA in the lipid membrane. However little attention has been paid to the fact that AA, because it has a double C-bond, is reactive with O_3 and could therefore protect a plant from O_3 damage by simply scavenging the O_3 before it can react with the vulnerable components of the cell. We explore this possibility below.

AA levels in plant leaves generally range from about 0.1 to 1.0 μg/g leaf fresh weight (LFW)[29,30]. However to determine AA's effectiveness as an O_3 scavenger in the cell wall, the AA concentration in the cell-wall water is needed. Only a very little data exists on this parameter. Castillo et al.[31] measured about 2-3 μg/g LFW of AA in the intracellular fluid of Norway spruce needles; assuming that the cell wall comprises about 50% of the fresh weight of a cell and that the cell wall is about 60% water[32,16], this measurement implies an AA concentration in the cell-wall water of about 5×10^{-5} M. On the other hand, Castillo and Greppin[33] report an observation of AA in the cell-wall water of S. Album leaves exposed to O_3 of 10^{-3} M.

Under physiological conditions AA is essentially completely dissociated into ascorbate (the AA pKa is 4.19 M [34]); thus in order to determine AA's effectiveness as an O_3-scavenger in cell-wall water, the rate constant for the reaction between O_3 and ascorbate is needed. Giamalva et al.[15] measured a biomolecular rate constant for the aqueous-phase reaction between O_3 and ascorbate of 6×10^7 M^{-1} s^{-1}; J. Hoigne (private communication, 1987) reports a

lower limit of 10^7 M^{-1} s^{-1} for this reaction. Combining the kinetic data of Giamalva et al. with the AA concentration range noted above, a first order loss coefficient, k_{AA}, for the reaction of O_3 with ascorbate in the cell-wall water of 3,000 to 60,000 s^{-1} is inferred. These k-values are in the reactive regime (see Figure 1) and thus it appears that AA in the cell-wall solution can act as an effective chemical barrier to O_3. For the range of AA levels observed in the cell walls of two species, the calculations indicate that a very large fraction of the O_3 molecules diffusing through mesophyllic cell-walls will be scavenged by ascorbate before they reach the plasmalemma.

O_3 Deposition Model Calculations

The ability of cell-wall AA to limit the flux of O_3 reaching the plasmalemma can be further illustrated through simple model calculations simulating the transfer of O_3 from the atmosphere to the mesophyllic cells of a plant within a forest canopy. Using the standard resistance formulation for mass transfer, the flux, Φ_L of O_3 from the atmosphere to a single leaf can be represented by[16]

$$\Phi_L = \frac{x_a - X_{cw}}{r_a + r_s + r_i} \qquad (11)$$

where X_a is the ambient O_3 partial pressure, r_a is the transfer resistance across the laminar air layer in contact with the leaf surface, r_s is the stomatal resistance, and r_i is the resistance of the inner air spaces of the leaf. By conservation of mass it follows that

$$\Phi_L = A_{cw}\,\Phi_{cw} \tag{12}$$

where A_{cw} is the ratio of the surface area of the mesophyllic cell walls in contact with the inner air spaces of the leaf to the outside surface area of the leaf.

Equations (5), (6), (11), and (12) form a closed set in which Φ_L and Φ_p can be calculated in terms of X_a, $[O_3]_p$, r_a, r_a, r_i, A_{cw}, L, and k. For the illustrative calculations presented here, $[O_3]_p$, as before, is assumed to be small, $L = 3 \times 10^{-4}$ cm, $X_a = 20$ ppbv, $r_a = 1$ s/cm, $r_i = 0.4$ s/cm, $A_{cw} = 10$, and r_s is varied from 3 to 12 s/cm to allow for changes in the size of the stomatal openings. These values roughly correspond to those typical of a leaf in a deciduous forest during the summer.[16] The first order loss coefficient, k, is assumed to arise solely from the reaction of O_3 with ascorbate; thus

$$k = k_{AA} = (5 \times 10^7\ M^{-1}\ s^{-1})[AA]_{cw} \tag{13}$$

where $[AA]_{cw}$, the cell-wall asorbic acid concentration, is varied from 0 to 10^{-3}M.

The calculated fluxes, Φ_L and Φ_p, as a function of r_s and $[AA]_{cw}$ are illustrated in Figures 2 and 3. We find that while the gross rate of O_3 deposition to the leaves, Φ_L, is dependent upon r_s but only weakly influenced by $[AA]_{cw}$, the flux to the plasmalemma, Φ_p, is largely controlled by $[AA]_{cw}$ rather than by r_s. Note in the figures that, for $[AA]_{cw} > 5 \times 10^{-5}$ M, a factor of three increase in r_s causes a factor of 2 to 3 decrease in Φ_L but a factor of 10 increase in $[AA]_{cw}$ causes less than a 20% increase in Φ_L. On the other hand, a factor of 3 increase in r_s causes a relatively small decrease in Φ_p while a similar increase in $[AA]_{cw}$ causes a decrease in Φ_p of almost 3 orders of

magnitude. Figure 3 suggests how the AA level in the cell-wall water of a plant leaf can help to determine the plant's sensitivity to O_3. Two plants with the same external as well as stomatal properties, can experience orders of magnitude different O_3 fluxes to the mesophyllic plasmalemma of their leaves simply because of a difference of a factor of 2 or 3 in the amount of AA maintained in their cell walls.

It is useful to note that the results of the calculations have a number of characteristics that are consistent with observations. Φ_L is found to vary from about 2 to 10 x 10^{10} molecules cm^{-2} s^{-1} for X_a = 20 ppbv; for a forest canopy with a leaf area index of 5, this result implies an O_3 deposition velocity of 0.2 to 1.0 cm/s, which is within the range of O_3 deposition velocities that have been measured over forested areas[2]. The fact that Φ_L is found to be a strong function of the stomatal resistance, r_s, but only weakly dependent on the AA level is also consistent with field studies which have indicated that the gross rate of O_3 deposition to vegetation is generally dependent upon the stomatal characteristics of the leaves but largely independent of the internal properties of the leaves[2]. Finally the strong dependence of Φ_p upon AA and its independence upon r_s is consistent with observations which have indicated that a plant's sensitivity to O_3 is typically determined by the internal biochemical properties of the plant but independent of the plant's stomatal resistance[35,36,37].

Conclusion

Calculations indicate that the reaction of O_3 with AA in the cell-wall solution may often represent the major sink of atmospheric O_3 as it penetrates into the internal regions of a plant leaf. The calculations suggest that plants

may act to protect themselves from the harmful effects of O_3 dry deposition by placing AA in their mesophyllic cell walls, thereby limiting the amount of O_3 that can penetrate to their more vulnerable cell material.

In comparison to the O_3-ascorbate interaction, other reactions that have been proposed to take place in the cell wall, such as the reaction of O_3 with ethylene and O_3 decomposition followed by peroxide formation, appear to be unimportant. Furthermore it seems unlikely that these reactions would be important in the plasmalemma either; given the high levels of PUFA in the plasmalemma and the relatively high reactivity of O_3 with these compounds[15], direct ozonolysis of the PUFA seem a more likely reactive pathway for the O_3 molecules which reach the membrane.

In light of the conclusion that peroxidation reactions are unimportant it is interesting to take note of the observations of Castillo and Greppin[33]. These investigators found that S. Album leaves exposed to O_3 tended to release enhanced quantities of AA as well as an ascorbate-specific peroxidase into their intercellular fluid suggesting that the cells were attempting to defend themselves against attack from peroxidation rather than ozonolysis. However it should be noted that O_3 is not the only oxidant in the atmosphere and, in fact, regions of high O_3 levels often have high levels of peroxide, which is photochemically coupled to O_3. Thus it is conceivable that Castillo and Greppin, by exposing the S. Album leaves to O_3, were stimulating a generalized response of the plant to atmospheric oxidants rather than a specific response to O_3. Under this scenario a mesophyllic cell under stress from atmospheric oxidants would release AA as a protectant against ozonolysis and AA along with an ascorbate-peroxidase as a protectant against peroxidation.

While the O_3/AA mechanism proposed in this work appears to capture many of the key characteristics observed for O_3 dry deposition to plant leaves, many

more observations are needed. Measurements of the intercellular levels of AA in a diverse variety of plants having a wide range of O_3 sensitivities are needed to establish the general validity of the mechanism proposed here. In addition a more detailed understanding of the processes which control the production and release of AA to the cell wall are needed so that we may more accurately predict how plants might respond to the growing levels of atmospheric O_3 in large regions of the North American and European continents[38].

REFERENCES

(1) Galbally, I.E.; Roy, C.R.; *Quart. J. Roy. Met. Soc.* 1980, *106*, 599-620.

(2) Baldocchi, D.D.; Hicks, B.B.; Camara, P. *Atmos. Environ.* 1987, *21, No. 1*, 91-101.

(3) Lea, M.C. *Amer. J. Sci. Arts*, 1864, *37*, 373-376.

(4) Knight, R.C.; Priestley, *J. Ann. Bot.* 1914, *28*, 131-161.

(5) Homan, C. *Plant Physiol.* 1937, *12*, 957-978.

(6) Ashmore, M.; Bell, N.; Rutter, *J. Ambio*, 1985, 81-87.

(7) *Acid Rain and Transported Air Pollutants: Implications for Public Policy*, Washington, D.C., U.S. Congress, Office of Technology Assessment, 1984, OTA-O-204, 323 pp.

(8) *Ozone and Other Photochemical Oxidants, Committee on Medical and Biological Effects of Environmental Pollutants*, National Academy of Sciences, Washington, D.C. 1977.

(9) Fairbairn, H.T.; Taylor, O.C. *Proc. Am. Soc. Hortic. Sci.* 1960, *76*, 693 -699.

(10) Hansen, C.P.; Thorne, L.; Jativa, C.P. *Lasca Leaves*, 1970, *20*, 607.

(11) Lee, E.H.; Jersey, J.A.; Gifford, C.; Bennett, *J. Experimental Botany*, 1984, *24*, 331-341.

(12) Hanson, G.P.; Thorne, L.; Jativa, C.D. in *Proceedings of Second International Clean Air Congress*, (eds Englund, M.H.; Beery, W.T.), (Academic Press, New York, 1971), 261-266.

(13) Tingey, D.T.; Taylor, G.E. in *Effects of Air Pollution in Agriculture and Horticulture*, (eds Unsworth, M.H.; Ormond, D.P.), (Butterworth Scientific, London, 1982), 113-138.

(14) Pell, E.J.; Brennan, E. *Plant Physiol.* **1973**, *51*, 378-381.

(15) Giamalva, D.; Church, D.F.; Prior, W.A. *Biochemical and Biophysical Research Communications*, **1985**, 773-779.

(16) Nobel, P.S. *Introduction to Biophysical Plant Physiology*, W.H. Freeman & Co., **1970**, 488 pp.

(17) Chameides, W.L. *J. Geophys. Res.* **1984**, *89*, 4739-4755.

(18) Hoigne, J.; Bader, H. *Science*, **1975**, *190*, 782-784.

(19) Staehelin, J.; Hoigne, *J. Environ. Sci. & Technol.* **1982**, *16*, 676.

(20) Forni, L.; Bahnemman, D.; Hart, E.J. *J. Phys. Chem.* **1982**, *86*, 255-259.

(21) Went, F.W., *Nature*, **1960**, *187*, 641-643.

(22) Rasmussen, R.A. *Environ. Sci. Tech.* **1970**, *4*, 66-673.

(23) Zimmerman, P.R. EPA Rep. No. 904/9-77-028 (US EPA, 1979).

(24) Abeles, F.B. *Ethylene in Plant Biology*, (Academic Press, New York and London, **1973**). pp 302.

(25) Bailey, P.S. *Chem. Rev.* **1958**, *58*, 925-1010.

(26) Mehlhorn, H.; Wellburn, A.R. *Nature*, **1987**, *327*, 417-418.

(27) Williamson, D.G.; Cvetanovic, R.J. *J. Am. Chem. Soc.* **1968**, *90*, 4248-4252.

(28) Hoigne, J.; Bader, H. *Water Res.* **1983**, *17*, 173-183.

(29) Bessey, O.A.; King, *C.G. J. Biol. Chem.* **1933**, *103*, 687-698.

(30) Barnes, R.L. *Can. J. Bot.* **1972**, *50*, 215-219.

(31) Castillo, F.J.; Miller, P.R.; Greppin, H. *Experientia*, **1987**, *43*, 111-220.

(32) Carr, D.J.; Gaff, D.F. *UNESCO Arid Zone Res.*, **1962**, *16*, 117-125.

(33) Castillo, F.J.; Greppin, H. *Physiol. Plantarium*, **1986**, *68*, 201-208.

(34) Lewin, S. *Vitamin C: Its Molecular Biology and Medical Potential*, pp 231 (Academic Press, London, 1976).

(35) Dugger, W.M.; Taylor, O.C.; Cardiff, E.; Thompson, C.R. *Plant. Physiol.*, **1962**, *37*, 487-491.

(36) Evans, L.S.; Ting, I.P. *Amer. J. Bot.* **1974**, *61(6)*, 592-597.

(37) Gesalman, G.M.; Davis, D.D. *J. Amer. Soc. Hort. Sci.* **1978**, *103(4)*, 489 -491.

(38) Volz, A.; Kley, D. *Nature*, **1988**, *332*, 240-242.

FIGURE CAPTIONS

Figure 1. The calculated fraction, FR, of O_3 molecules diffusing through the cell wall that react before reaching the plasmalemma as a function of k, the first-order loss coefficient for O_3 in the cell-wall solution. The dotted line is for L = 1 μm, the solid line is for L = 3 μm, and the dashed line is for L = 30 μm.

Figure 2. The calculated O_3 flux, Φ_L, to a single leaf as a function of the ascorbic acid concentration, [AA], in the cell-wall water. The dotted line was obtained with a stomatal resistance, r_s, of 12 s/cm, the solid line with an r_s of 6 s/cm, and the dashed line with an r_s of 3 s/cm.

Figure 3. The calculated O_3 flux, Φ_p, to the plasmalemma of a single leaf as a function of the ascorbic acid concentration, [AA], in the cell-wall water. The dotted line was obtained with a stomatal resistance, r_s, of 12 s/cm, the solid line with an r_s of 6 s/cm, and the dashed line with an r_s of 3 s/cm.

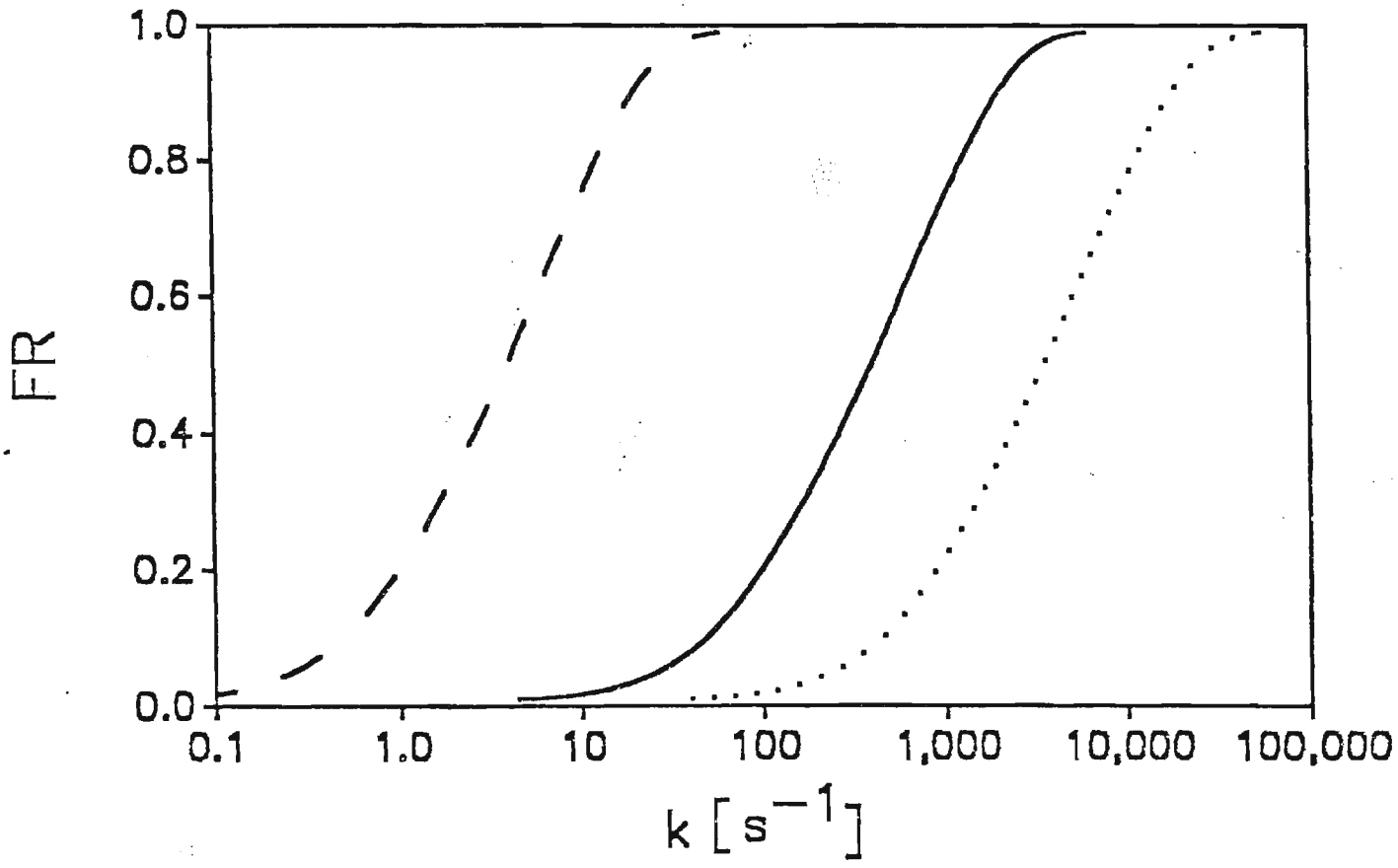

Figure 1. The calculated fraction, FR, of O_3 molecules diffusing through the cell wall that react before reaching the plasmalemma as a function of k, the first-order loss coefficient for O_3 in the cell-wall solution. The dotted line is for L = 1 μm, the solid line is for L = 3 μm, and the dashed line is for L = 30 μm.

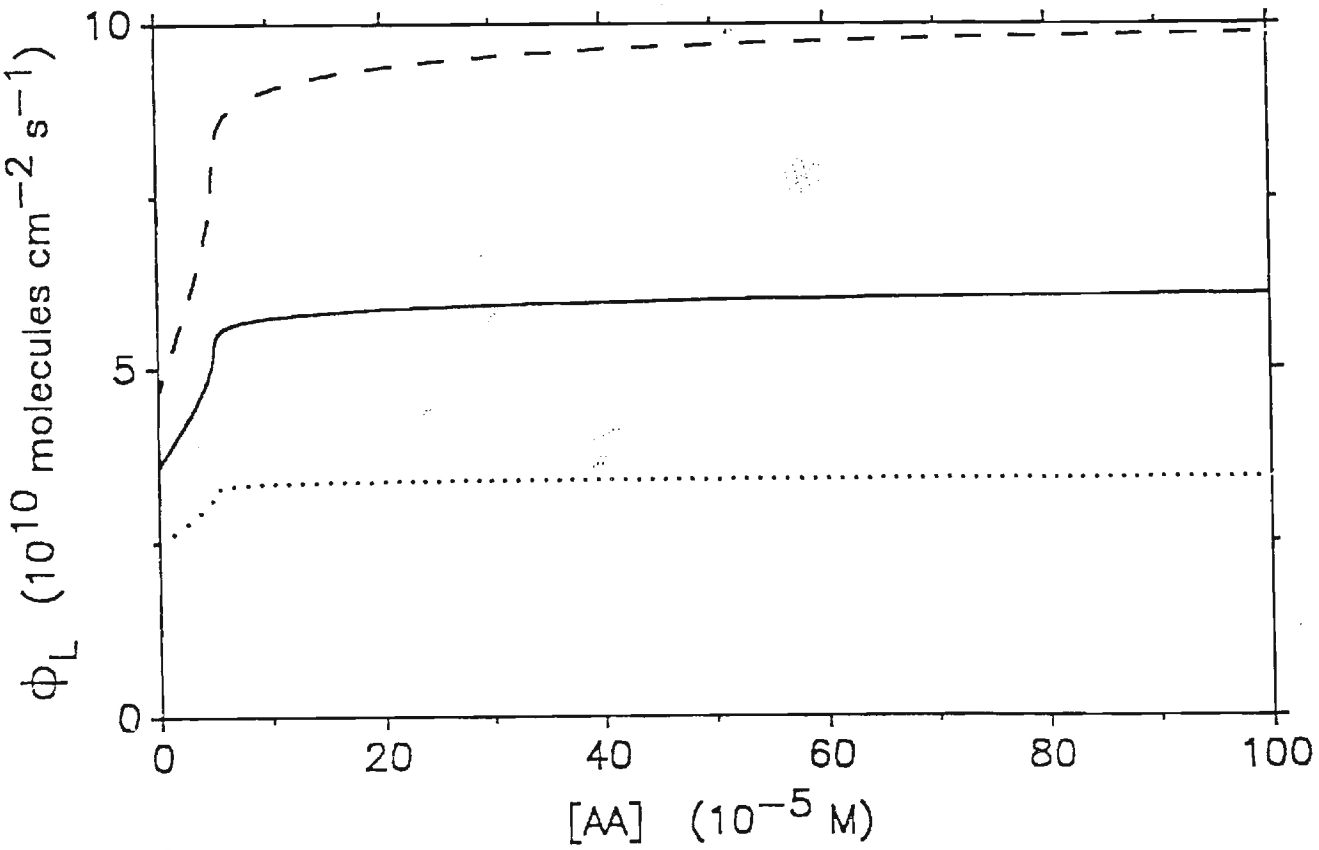

Figure 2. The calculated O_3 flux, Φ_L, to a single leaf as a function of the ascorbic acid concentration, [AA], in the cell-wall water. The dotted line was obtained with a stomatal resistance, r_s, of 12 s/cm, the solid line with an r_s of 6 s/cm, and the dashed line with an r_s of 3 s/cm.

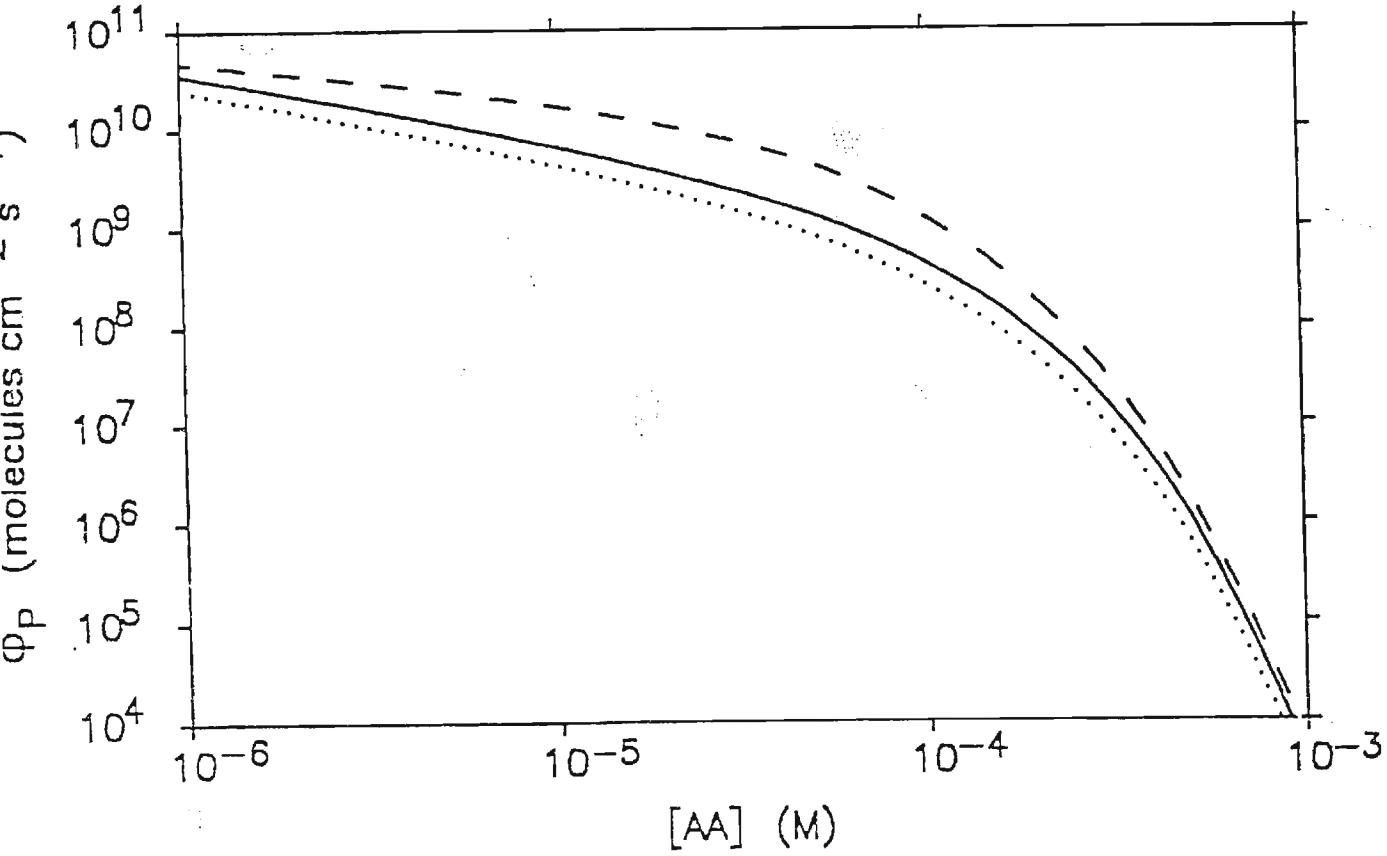

Figure 3. The calculated O_3 flux, Φ_p, to the plasmalemma of a single leaf as a function of the ascorbic acid concentration, [AA], in the cell-wall water. The dotted line was obtained with a stomatal resistance, r_s, of 12 s/cm, the solid line with an r_s of 6 s/cm, and the dashed line with an r_s of 3 s/cm.

APPENDIX D

THE ROLE OF BIOGENIC HYDROCARBONS IN URBAN PHOTOCHEMICAL SMOG: ATLANTA AS A CASE STUDY

W.L. Chameides, R.W. Lindsay, J. Richardson, C.S. Kiang

School of Geophysical Sciences

Georgia Institute of Technology

Atlanta, GA 30332

June 9, 1988

ABSTRACT: The effects of natural hydrocarbons need to be accounted for in order to develop a reliable plan for reducing ozone in the urban atmosphere. Trees can emit significant quantities of hydrocarbons to metropolitan areas such as Atlanta and model calculations indicate that these natural emissions can significantly affect urban ozone levels. By neglecting these compounds previous investigators may have over-estimated the effectiveness of an O_3-abatement strategy based on reducing anthropogenic hydrocarbons

INTRODUCTION

Haagen-Smit's pioneering work on photochemical smog first established that the photo-oxidation of hydrocarbons in the presence of nitrogen oxides produces ozone (O_3). [1] In urban areas with large emissions of anthropogenic hydrocarbons (AHC) and nitrogen oxides (NO_x), this mechanism often drives summer O_3 levels above the 0.12 ppmv National Ambient Air Quality Standard (NAAQS). In the U.S., a plan for O_3-abatement was implemented in the 1970's through the Clean Air Act. While the law called for emission reductions in either AHC or NO_x, its implementation by the U.S. Environmental Protection Agency (EPA) and the relevant state agencies has, for a variety of social, technological, and economic reasons, focused on AHC reductions. [2] However in spite of large reductions in AHC emissions over the past ten years and the expenditure of billions of dollars, O_3 in many locales has not decreased. [3,4] Sixty-eight cities remain in violation of the NAAQS; almost 40% of these are in the southeastern U.S. The apparent lack of success in the AHC-based O_3-abatement strategy suggests that there may be serious flaws in our understanding of the budget of urban hydrocarbons and/~~or of their~~ role in photochemical smog. In this work we examine one aspect of the urban hydrocarbon budget that has been neglected in the past: biogenic or natural hydrocarbons (NHC).

For an O_3-abatement strategy based on AHC reductions to be effective,

anthropogenic emissions must represent the dominant source of reactive, O_3-producing hydrocarbons. In this work we suggest that AHC emissions may not, in fact, be the only important source of reactive hydrocarbons to the urban atmosphere and that NHC emitted by trees and other vegetation can have a significant effect on urban O_3 levels.

The role of NHC is investigated by focusing on the chemistry of a specific city - Atlanta, Georgia. Atlanta is of interest for a number of reasons: it was the subject of an intense field study sponsored by the EPA in 1981 [5]; it is situated in the southeast where summertime NHC emissions are relatively high; [6] and while AHC emissions in the Atlanta area have been reduced by an estimated 50% since 1979, O_3 levels have not decreased.[4]

NATURAL HYDROCARBON EMISSIONS

In the U.S. trees are the principal emitters of biogenic non-methane hydrocarbons and isoprene and α-pinene are the primary species emitted. [6,7,8,9,10] It is estimated that nationwide this source amounts to about 30-60 Tg-C yr^{-1}; the nationwide source of AHC is only about 18 Tg-C yr^{-1}. [6,10] However while the importance of NHC in rural forested areas has been documented, [8,11] it is not widely known that NHC emissions can also be significant in urban areas. The Atlanta metropolitan area provides a useful example.

An analysis of digitized LANDSAT data (provided by Mr. N. Faust of the Georgia Tech Research Institute) and information from the Atlanta Regional Commission indicates that about 57% of the 900 km^2, eleven-county, EPA-designated Atlanta non-attainment area was wooded in 1985; these wooded areas are shrinking at a rate of only ~~about 2%~~ yr^{-1} due to urban growth. [12,13] Of this 57%, 23% was deciduous, 18% was mixed, and 16% was coniferous. Combining this data with Zimmerman's [9] 30°C biogenic emission factors for the three forest types, we estimate an Atlanta area-averaged, daytime emission rate of

2100 μg-C m^{-2} hr^{-1} for isoprene, which compares well with Westberg and Lamb's [5] isoprene estimate for Atlanta of 2500 μg-C m^{-2} hr^{-1}, and 1400 μg-C m^{-2} hr^{-1} for non-isoprene NHC. At night isoprene is not emitted and thus the total nighttime NHC emission rate is also about 1400 μg-C m^{-2} hr^{-1}.

For 15 hours of daylight in the summer, the above results imply integrated daytime sources of about 30 kg km^{-2} for isoprene and 50 kg km^{-2} for all NHC. Over a 24-hour period the integrated NHC source is about 65 kg km^{-2}. While these NHC emission rates are small compared to the maximum AHC emission rate of 600 kg km^{-2} day^{-1} found in a 10 km^2 area of downtown Atlanta, they are equivalent to the eleven-county area-averaged AHC emission rate of about 30 kg km^{-2} day^{-1} [4,5]. Furthermore, while biogenic emission rates in general have a large uncertainty (Lamb [6] estimates an uncertainty factor of 3), our estimates do not appear to be unrealistic; as we discuss later, model calculations using our estimates yield NHC concentrations that are reasonably close to observed levels. Finally, note that large NHC emissions are not unique to Atlanta. Independent estimates of the NHC emission rates in two other southeastern cities - Houston, Texas [14], Tampa Bay/St. Petersberg, Florida [8] - are roughly equivalent to our estimate for Atlanta. Thus large sources of NHC may be ubiquitous to cities in the southeast and possibly other regions of the country as well.

In spite of their large source, however, the role of NHC in urban photochemical smog has, for the most part, been discounted. This is especially surprising in light of smog chamber experiments which indicate that, for conditions common to the urban atmosphere, the O_3 forming potential of NHC is roughly equivalent to that of AHC (i.e., about 0.1 ppmv of O_3 for every 1 ppmv-C consumed). [15] Some investigators have concluded that NHC were negligible because their urban concentrations are much smaller than those of AHC. [5,10]

However because NHC are more reactive than AHC, they can have a significant impact in spite of their low concentrations. For instance, in the model calculations described below isoprene has a large effect even though it comprises only a few percent of the total hydrocarbon burden.

Lurmann, et al [16] claimed to show that NHC are unimportant through model simulations of the Tampa Bay/St. Petersberg area. Model simulations were reported with only AHC sources and with both AHC and NHC sources. Since the maximum O_3 level calculated with both sources was only about 10% larger than that calculated with only the AHC source, the authors concluded that NHC were not important. However, as Trainer et al [11] have pointed out, these results can be misleading; if the system is not limited by hydrocarbons then the O_3 production rate will respond non-linearly to the addition of AHC as well as NHC. In fact as the model calculations presented below demonstrate, NHC emissions can have a significant effect on urban O_3 levels.

MODEL SIMULATIONS

To illustrate the importance of NHC emissions to urban photochemical smog, model calculations simulating the formation of O_3 in Atlanta, Georgia were carried out using the city-specific Empirical Kinetics Modeling Approach (EKMA). [17,18,19] The EKMA model was developed by the EPA for state agencies trying to formulate O_3-abatement strategies. It simulates the photochemistry of a well-mixed column of air extending from the surface to the top of the mixed layer as the column advects from its initial, 0800 LST position at the city center to some evening position downwind of the city. During advection, surface emissions add hydrocarbons and NO_x to the column and variations in the mixing height cause air from above to be mixed into the column. The effects of changes in the local hydrocarbon source strength are explored with the model by simultaneously varying the initial, 0800 LST hydrocarbon concentration, and the daytime

surface emission rates. Changes in the local NO_x source strength are explored by varying the equivalent NO_x parameters.

The model utilizes a 34-species photochemical mechanism known as CB-4 to simulate the chemistry within the air column. CB-4 is a carbon-bond mechanism in which nine functional groups are used to represent the myriad of volatile organics emitted into the urban atmosphere. [20] One of the interesting aspects of CB-4 is that the chemistry of isoprene is explicitly included in the mechanism. However this portion of the mechanism is not typically used; EPA recommends to EKMA-users that isoprene be set equal to zero, thereby inactivating the NHC portion of the mechanism. [18]

For the calculations reported here, the model was tuned to simulate O_3 in an air column advecting from downtown Atlanta to Conyers, Georgia, located 40 km southwest of Atlanta, on June 4, 1984. This day was also simulated by the Georgia Department of Natural Resources (DNR) for their 1987 State Implementation Plan (Mr. R. Collom, private communication, 1988). June 4, 1984 was a typical ozone-episode day in Atlanta. Temperatures during the daylight hours averaged 28°C and peaked at 32°C. The winds were out of the northwest and by the end of the day O_3 at a DNR monitoring station in Conyers had peaked at 0.147 ppmv. Except for the inclusion of a NHC source, the input data for our simulations was the same as that used by DNR. To simulate present-day AHC and NO_x levels, the initial AHC and NO_x concentrations were set at 0.68 and 0.096 ppmv, respectively, in accordance with early morning observations from downtown Atlanta, and the total AHC and NO_x surface emissions from 0800 to 1900 LST were set at 34 and 28 kg/km^2, respectively. The emissions and their distribution as a function of time were chosen to correspond to the emissions an air column would encounter if it followed a trajectory from downtown to Conyers. The chemical speciation of the initial mix of AHC and NO_x and of the emissions was

based on the apportioning factors or 'reactivities' recommended by EPA. [18]

In addition to the AHC and NO_x emissions, a source of NHC was added to the EKMA model. Since vegetative emissions are light and temperature sensitive, the NHC emissions were distributed over the course of the day so that most of the NHC was emitted in the afternoon. The NHC emission rate was initially 0, increased linearly until 1200 LST, remained constant from 1200 to 1500 LST, and then decreased linearly to 0 at 1900 LST. (Slightly higher O_3 levels were obtained when the NHC emissions were held constant with time.) Calculations were carried out with total, integrated, daytime NHC emission rates ranging from 0 to 50 kg km^{-2}. In all cases the initial NHC concentration was set at 0.

For simplicity all NHC emissions were assumed to be isoprene. The chemistry of isoprene was simulated in two ways: 1. Using the isoprene chemistry specifically included in the CB-4 mechanism; and 2. Using the functional group chemistry of the CB-4 mechanism with each isoprene molecule represented as two olefins and one paraffin. [21] While the results described below and illustrated in Figures 1 and 2 were obtained using the first approach, both approaches generally yielded O_3 levels within a few percent of each other.

Figure 1 shows the maximum one-hour averaged O_3 level calculated as a function of AHC and NO_x with no NHC emissions. The dot indicates the result obtained for present-day AHC and NO_x levels. The calculated maximum O_3 at this point of 0.150 ppmv is in excellent agreement (although perhaps fortuitously) with the maximum O_3 measured at Conyers of 0.147 ppmv. On the basis of this figure one would project that a 30% reduction in AHC would be needed to reduce O_3 from 0.15 ppmv to the NAAQS of 0.12 ppmv. However as illustrated in Figure 2, this projection changes considerably if NHC are included.

In Figure 2 the maximum O_3 levels calculated as a function of AHC and NHC with NO_x held at present-day levels are illustrated. The vertical dotted-line

indicates the results when AHC are held constant at present-day levels; by following this line upward from the x-axis the effects of adding NHC emissions to the existing NO_x and AHC emissions can be explored. Similar to Lurmann et al, we find that adding NHC to the anthropogenic emissions has a very small effect on O_3; for instance the addition of 30 kg/km^2 of NHC causes only a 10% increase in O_3, from 0.15 ppmv to 0.165 ppmv. However it would not be correct to conclude that NHC can be neglected. For these high emission rates, there is an over-abundance of hydrocarbons and, as a result, O_3 responds non-linearly to any hydrocarbon addition. Thus note in Figure 2 that increasing AHC above present-day levels also has a very small impact on O_3. Furthermore NHC can generate significant O_3 levels by themselves. Note in Figure 2 that with AHC set to 0, maximum O_3 levels of 0.08, 0.11, and 0.12 ppmv were obtained for NHC emission rates of 30, 40, and 50 kg km^{-2}, respectively.

Because of O_3's non-linear response to hydrocarbons, the presence of NHC can have a profound impact on the effectiveness of an O_3-abatement strategy based on AHC reductions. With no NHC emissions, the results in Figure 2, similar to those in Figure 1, imply that a 30% reduction in AHC emissions would be adequate to reduce O_3 to 0.12 ppmv. However for an NHC emission rate of 30 kg/km^2 (our estimate of the Atlanta-area isoprene emission rate), a 70% AHC reduction would be needed. For NHC emissions of 50 kg/km^2 (our estimate of the total NHC emission rate), O_3 remains above the NAAQS even after AHC emissions are completely eliminated. In fact we find that for NHC emissions of 30 kg km^{-2} or greater, the percentage reduction in NO_x emissions needed to bring O_3 down to 0.12 ppmv is smaller than that required of AHC emissions.

While our results should be viewed cautiously because of the large uncertainties in the AHC and NHC emissions, a comparison of our results with the observations of Westberg and Lamb [5] suggests that the emission rates we have

used are not unreasonable. From early morning measurements at three Atlanta locations, Westberg and Lamb concluded that NHC constituted 2 to 7% of the city's total non-methane hydrocarbon burden. In the model, using present-day AHC levels and a NHC emission rate of 50 kg km^{-2}, the isoprene concentration never exceeded 2.5% of the total hydrocarbon burden.

CONCLUSION

While the effects of NHC are not currently factored into the nation's urban O_3-abatement strategy, calculations presented in this work suggest that it should. The emissions of NHC can be significant especially in cities in the southeastern U.S. such as Atlanta. Furthermore, EKMA model calculations tuned to simulate an O_3 episode in Atlanta indicate that NHC can have a major effect on O_3. In particular the calculations suggest that NHC can profoundly influence the predicted effectiveness of an O_3-abatement strategy based on AHC reductions. For a relatively modest NHC emission rate, the model indicates that NO_x reductions would more effectively reduce O_3 than would reductions in AHC. For a large but not unrealistic NHC emission rate, the model predicts that even if AHC emissions were completely eliminated, O_3 levels would still remain above the 0.12 ppmv NAAQS.

Because of the large uncertainties associated with our model calculations our results should be viewed with caution. In spite of these uncertainties however, the results demonstrate the potential importance of NHC to urban photochemical smog and the danger of pursuing an O_3-abatement strategy which ignores their effect. We believe that an intense investigation of NHC, focusing on their rates of production and atmospheric chemistry, is needed before a reliable strategy for O_3-abatement can be formulated.

REFERENCES

1. A.J. Haagen-Smit, *Ind. Eng. Chem.*, 44, 1362, (1952).

2. K.L. Schere, *Environ. Sci. Technol.*, 44, No. 5, (1988).

3. H.M. Walker, *J. Air Poll. Contrl. Ass.*, 35, 903, (1985).

4. R.W. Lindsay, W.L. Chameides, J.L. Richardson, submitted to *J. Air Poll. Contrl. Ass.*, (1988).

5. H. Westberg, B. Lamb, *Ozone Production and Transport in the Atlanta, Georgia Region*, EPA/600,S3-85/013, U.S. Environmental Protection Agency, (1985).

6. B. Lamb, A. Guenther, D. Gay, H. Westberg, *Atmos. Environ.*, 21, No. 8, (1987).

7. F.W. Went, *Proc. Natl. Acad. Sci.*, 46, (1960).

8. R.A. Rasmussen, *J. Air. Poll. Contrl. Ass.*, 22, No. 7, (1972).

9. P.R. Zimmerman, *Determination of Emission Rates of Hydrocarbons from Indigenous Species of Vegetation in the Tampa/St. Petersburg Florida Area, EPA 904/9-77-028*, U.S. Environmental Protection Agency, Atlanta, GA, (1979).

10. A.P. Altshuller, *Atmos. Environ.*, 17, No. 11, (1983).

11. M. Trainer, E.J. Williams, D.D. Parrish, M.P. Buhr, E.J. Allwine, H.H. Westberg, F.C. Fehsenfeld, S.C. Liu, *Nature*, 329, (1987).

12. Atlanta Regional Commission, *Atlanta Business Chronicle* Atlanta Regional Commission, p. 8B, (June 1, 1987).

13. J.L. Richardson, thesis, Georgia Institute of Technology, Atlanta, (1988).

14. P.R. Zimmerman, Natural Sources of Ozone in Houston: Natural Organics, *Proc. of Specialty Conference on Ozone/Oxidants - Interaction with Total Environment, Pittsburgh, PA*, Air Pollution Control Association, (1980).

15. R.R. Arnts, B.W. Gay, J.J. Bufalini, in *Atmospheric Biogenic Hydrocarbons*, 2, *Ambient Concentrations and Atmospheric Chemistry*, (Ann Arbor Science Publishers Inc., The Butterworth Group, 1981), pp. 117-138.

16. F.W. Lurman, B. Nitta, K. Ganesan, A.C. Lloyd, *Atmos. Environ.*, **18**, No. 6, (1984).

17. J. Seinfeld, *J. Air. Poll. Contrl. Ass.*, **38**, No. 5, (1988).

18. U.S. Environmental Protection Agency, *Guideline for Use of City-Specific EKMA in Preparing Post-1987 Ozone SIP's*, (1987).

19. Simulations were also carried out using a photochemical box model with a more complete photochemical mechanism based on the work of Lurman, F.W., A.C. Lloyd, and R. Atkinson, *J. Geophys. Res.*, **91**, (1986). The results of these calculations were similar to those presented here. [13]

20. G. Whitten, H. Hugo, J.P. Killus, *Environ. Sci. Technol.*, 14, (1980).

FIGURE CAPTIONS

Figure 1. Isopleths of the maximum, hourly O_3 levels (in ppmv) calculated as a function of NO_x and AHC with NHC emissions set to 0. The solid dot indicates the O_3 levels obtained for present-day conditions (i.e. an initial AHC concentration of 0.68 ppmv, and a total daytime AHC emission rate of 34 kg km^{-2}, an initial NO_x concentration of 0.096 ppmv, a total daytime NO_x emission rate of 10.8 kg km^{-2}). Variations in AHC or NO_x levels are explored in the model by varying the AHC or NO_x initial concentration and emission rate simultaneously. EPA recommends that diagrams like this one be used by state agencies making emission control projections. [18] Since a reduction in AHC emissions from 34 to 24 kg km^{-2} reduces O_3 from 0.15 to the NAAQS of 0.12 ppmv in this figure, we would project, following the EPA procedure, that a 30% reduction in AHC emissions would be needed to bring Atlanta into compliance with the Clean Air Act.

Figure 2. Isopleths of the maximum hourly O_3 levels (in ppmv) calculated as a function of AHC and NHC (as isoprene) with NO_x set at present-day levels. The dotted-line indicates the results obtained with AHC held at present-day levels. Note that even if AHC emissions are 20 or 30% higher than presently estimated, NHC emissions would still affect emission control projections.

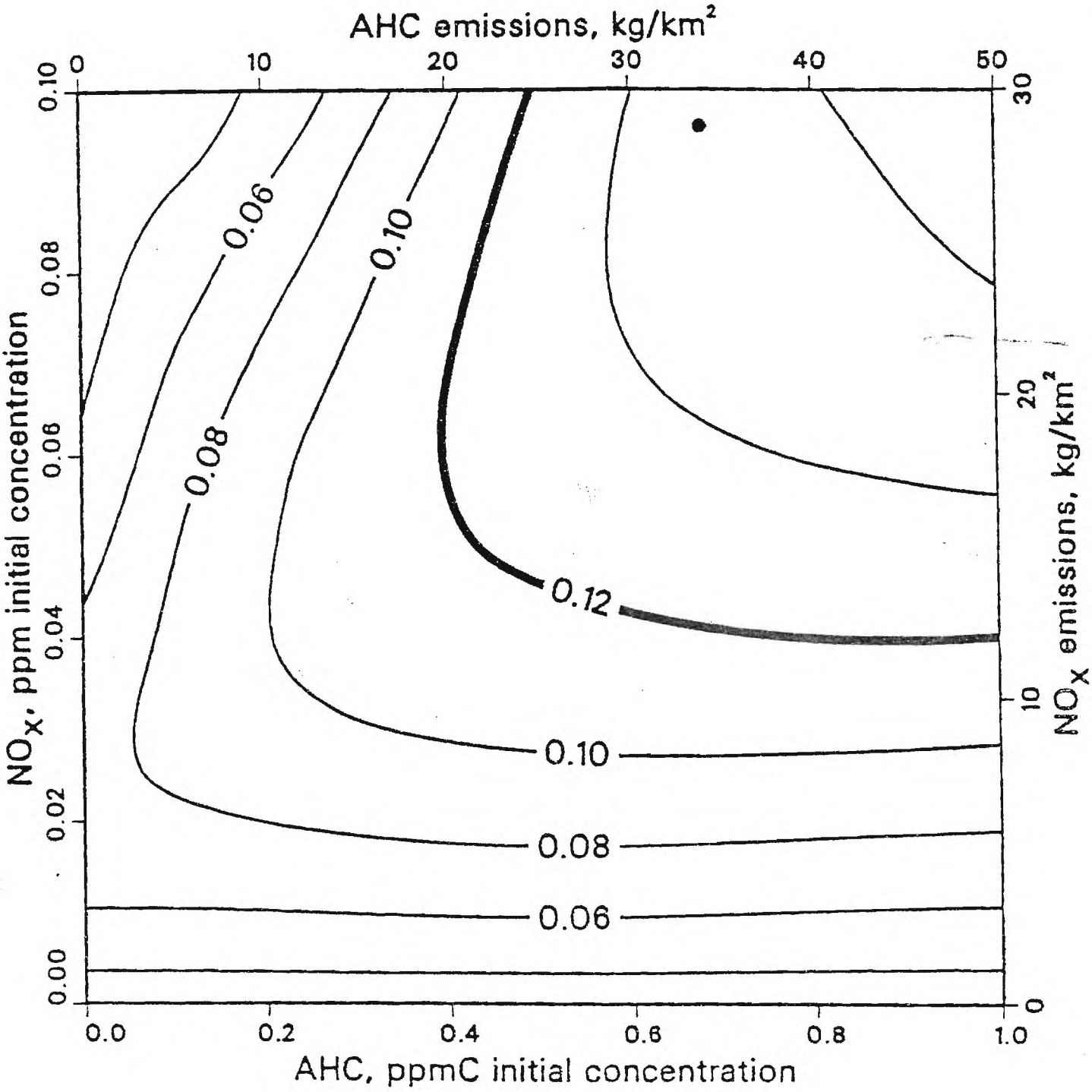

Figure 1. Isopleths of the maximum, hourly O_3 levels (in ppmv) calculated as a function of NO_x and AHC with NHC emissions set to 0. The solid dot indicates the O_3 levels obtained for present-day conditions (i.e. an initial AHC concentration of 0.68 ppmv, and a total daytime AHC emission rate of 34 kg km^{-2}, an initial NO_x concentration of 0.096 ppmv, a total daytime NO_x emission rate of 10.8 Kg km^{-2}). Variations in AHC or NO_x levels are explored in the model by varying the AHC or NO_x initial concentration and emission rate simultaneously. EPA recommends that diagrams like this one be used by state agencies making emission control projections. [18] Since a reduction in AHC emissions from 34 to 24 kg km^{-2} reduces O_3 from 0.15 to the NAAQS of 0.12 ppmv in this figure, we would project, following the EPA procedure, that a 30% reduction in AHC emissions would be needed to bring Atlanta into compliance with the Clean Air Act.

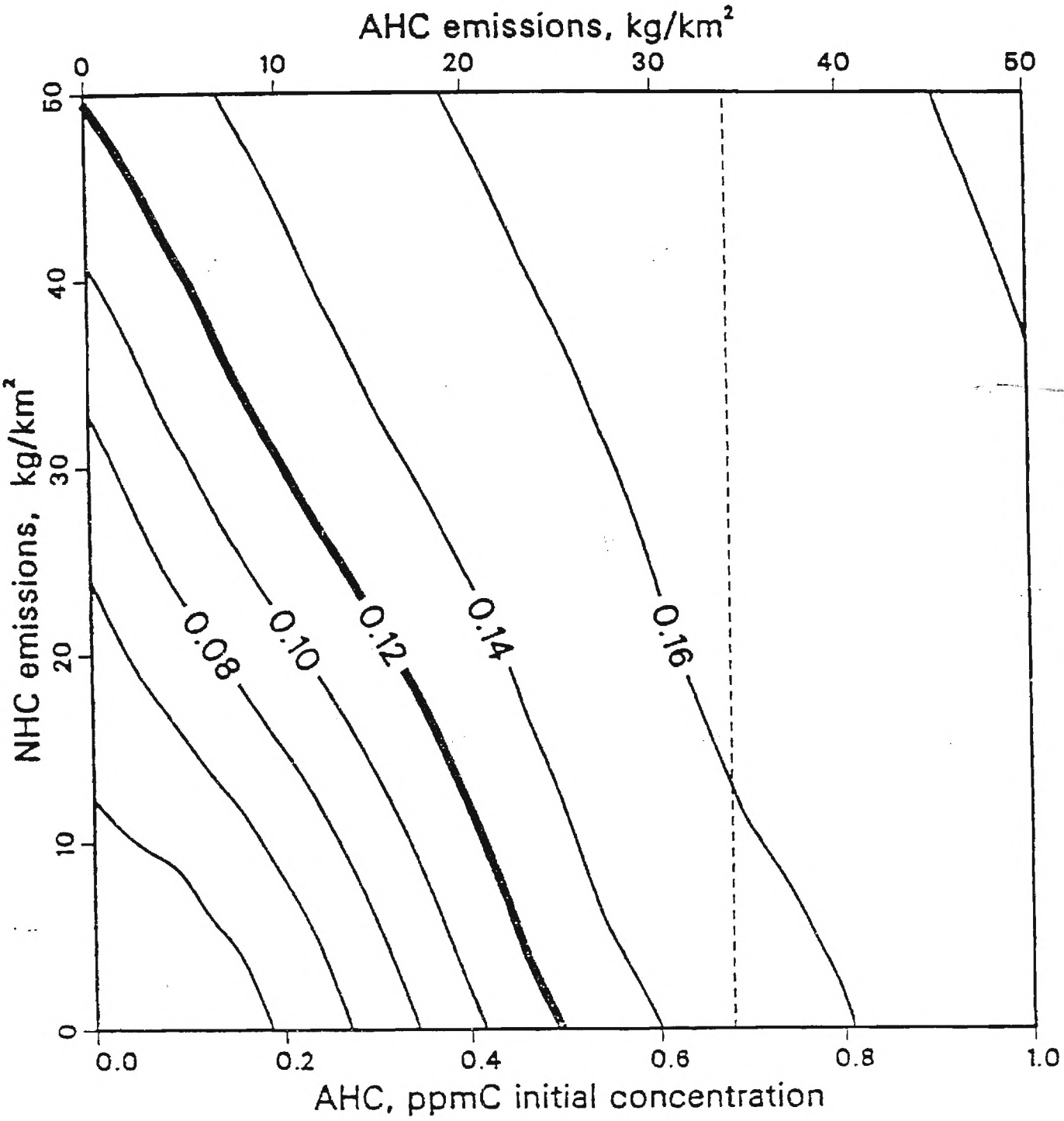

Figure 2. Isopleths of the maximum hourly O_3 levels (in ppmv) calculated as a function of AHC and NHC (as isoprene) with NO_x set at present-day levels. The dotted-line indicates the results obtained with AHC held at present-day levels. Note that even if AHC emissions are 20 or 30% higher than presently estimated, NHC emissions would still affect emission control projections.

G-35-646

Twenty-Four Month Interim Report on the Subject Grant

"Diagnostic Studies of the H_xO_y-N_xO_y-O_3 Photochemical System

Using Data from NASA GTE Field Expeditions"

NASA Grant NAG-1-786

PI: William L. Chameides

School of Geophysical Sciences

Georgia Institute of Technology

Atlanta, GA 30332

During the first two years of the three-year granting period the major focus of the research effort funded by NASA has been on the analysis of data gathered during the Spring, 1984 GTE CITE-1, the Summer, 1986 GTE CITE-2, and the Summer, 1988 GTE ABLE-3 field expeditions.

In the case of the Spring CITE-1 flights data from the field exercise was obtained from a GTE Data Archive Tape. Chemical and supporting meteorological data taken over the Pacific Ocean was statistically and diagnostically analyzed to identify the key processes affecting the concentrations of ozone and its chemical precursors in the region. The analysis has been completed and a paper has been submitted and accepted for publication in the Journal of Geophysical Research.

Our analysis of the GTE CITE-2 data was carried out in collaboration with Dr. D.D. Davis and other GTE scientists and focussed on a comparison of measured and calculated NO_2/NO ratios. Initial results of our analysis were presented at the Fall meeting of the American Geophysical Union in San Francisco and a draft paper describing our results has been completed and distributed to the CITE-2 Principal Investigators for input. The paper should be submitted to the Journal of Geophysical Research by the end of July.

We have initiated an analysis of chemical data gathered during the GTE CITE-3 mission to Alaska which is focussing on NO_x partitioning and ozone photochemistry. Preliminary results of

our analysis were presented at the Spring, 1989 AGU meeting.

In addition to the work described above, seven other papers have been completed with partial support from the subject grant. Titles of all papers completed with funds from NASA during the granting period are:

1. Acid dew and the role of chemistry in the dry deposition of reactive gases to wetted surfaces, W.L. Chameides, *J. Geophys. Res., 92*, 11,895-11,908, 1987.

2. Absorption cross sections and kinetic considerations of the IO species as determined by laser flash photolysis/laser-absorption spectroscopy, R.E. Stickel, A.J. Hynes, J.D. Bradshaw, W.L. Chameides and D.D. Davis, *J. Phys. Chem., 92,* 1862-1864, 1988.

3. High ozone events in Atlanta, Georgia, in 1983 and 1984, R.W. Lindsay and W.L. Chameides, *Environ. Sci. Technol., 22, No. 4,* 426-431, 1988.

4. Ozone precursors and ozone photochemistry over the eastern North Pacific Ocean during the spring of 1984 based on the NASA/CITE 1 airborne observations, W.L. Chameides, D.D. Davis, G.L. Gregory, G. Sachse and A.L. Torres, *J. Geophys. Res.,* in press, 1989.

5. Ozone trends in Atlanta, Georgia: Have emission controls been effective? R.W. Lindsay, J.L. Richardson, W.L. Chameides, *JAPCA*, **39**, 40-43, 1989.

6. The chemistry of ozone deposition to plant leaves: The role of ascorbic acid, W.L. Chameides, *Environmental Science and Technology,* **23**, 595-600, 1989.

7. The role of biogenic hydrocarbons in urban photochemical smog: Atlanta as a case study, W.L. Chameides, R.W. Lindsay, J.L. Richardson and C.S. Kiang, *Science, 241,* 1473-1475, 1988.

8. Model simulations of rainout and washout from a warm stratiform cloud, Lin Xing and W.L. Chameides, *J. Atmos. Chem.,* in revision, 1989.

Copies of papers 1-8 listed above have already been forwarded to NASA in previous Interim Reports.

Plans for research during the next 12 months of the granting period include:

1. An initial study of the data obtained during the GTE ABLE-2A and 2B experiments aimed at determining to what extent long-range transport of pollutants can affect oxidant levels in remote Brazilian locations.

2. A more in-depth analysis of NO measurements made during CITE-1 and 2 missions.

3. Collaborative analysis of ABLE-3 data gathered by J. Bradshaw and colleagues.

JOURNAL OF GEOPHYSICAL RESEARCH, VOL. 92, NO. D10, PAGES 11,895-11,908, OCTOBER 20, 1987

ACID DEW AND THE ROLE OF CHEMISTRY IN THE DRY DEPOSITION OF REACTIVE GASES TO WETTED SURFACES

William L. Chameides

School of Geophysical Sciences, Georgia Institute of Technology, Atlanta

Abstract. Using the resistance model for mass transfer, a formulation is derived for the dry deposition rate of a reactive, soluble gas depositing on a wetted, vegetative surface. The deposition velocity is expressed in terms of a dynamical resistance, which is a function of the physical state of the atmosphere, and a surface resistance, which is a function of the chemical and physical properties of the surface. This formulation is then used in a model to simulate the generation of acidic dew from the dry deposition of HNO_3 and SO_2, as well as the S_{IV} oxidants, H_2O_2 and O_3. Dewdrop pHs of about 4 are calculated by the end of the night, however these pHs can rapidly fall to potentially toxic levels soon after sunrise as the dewdrops evaporate. The deposition velocities to the dew for highly soluble species such as HNO_3 and H_2O_2 are found to be entirely determined by the dynamical resistance; for the conditions adopted here a value of 0.4 cm s^{-1} is calculated for these species. However, much smaller deposition velocities are predicted for SO_2 and O_3 because of their lower solubilities and hence larger surface resistances. In the case of SO_2, a nocturnally averaged deposition velocity of only about 0.03 cm s^{-1} is calculated for the standard model. Because the chemical lifetime of SO_2 in the dew is influenced by the atmospheric levels of H_2O_2, O_3, and SO_2, the SO_2 deposition velocity is found to be a strong function of these species' atmospheric abundances. These results imply that the deposition velocities of species such as SO_2 to wetted surfaces may be influenced by the chemical as well as the physical state of the atmosphere; the assumption typically adopted that dry deposition velocities are independent of the species' atmospheric abundance may not always be appropriate.

Introduction

The concern over the effects of atmospheric pollutants upon terrestrial ecosystems has led to a growing scientific interest in understanding the processes which control the deposition of trace species to the earth's surface. This deposition can occur via wet deposition, in which the species is deposited on the surface within precipitating hydrometeors, or via dry deposition, in which the species is deposited independently of precipitation. While the processes that control wet deposition are still not completely understood and uncertainties remain in wet deposition rates of many species, much larger uncertainties appear to be associated with dry deposition and its respective rates [cf. Calvert et al., 1983].

Paper number 7D0650.
0148-0227/87/007D-0650$05.00

These uncertainties arise from both the difficulties inherent in measuring in situ dry-deposition rates as well as the extremely complex nature of the phenomena that control this deposition, [cf. Hicks, 1986; Businger, 1986].

The rate of dry deposition of a given species, I, to a surface is typically represented in terms of a bulk dry deposition velocity, V_d, such that

$$\Phi_I = X_I(z_r)\, n_M\, V_d \qquad (1)$$

where Φ_I is the downward flux of species I to the surface (in molecules cm^{-2} s^{-1}), $X_I(z)$ is the volume mixing ratio of I at height z, n_M is the atmospheric number density at the surface, and z_r is some specified reference height. (In model calculations, z_r is often chosen to correspond to the lowest level of the model, while in a field experiment z_r is usually the minimum height at which X_I is measured.) The parameter V_d combines all the physical and chemical processes that ultimately control the rate of deposition into a single term. By analogy to the flow of electricity through a series of resistances, V_d can be expressed as the reciprocal of a sum of transfer resistances, each resistance representing the effects of a specific physical or chemical process and having units of seconds per centimeter. For instance, we can write

$$V_d = (r_d + r_s)^{-1} \qquad (2)$$

where r_d and r_s are defined here as the dynamic and surface resistances, respectively. The dynamic resistance term is used to denote the sum of all resistances related to the transport of the species from z_r to the surface. Note that the reciprocal of r_d is equivalent to a mass-transfer coefficient such that

$$\Phi_I = (1/r_d)\, n_M\, \{X_I(z_o) - X_I(0)\} \qquad (3)$$

where $X_I(0)$ is the effective concentration of I at the surface [cf. Welty et al., 1984].

The surface resistance term, on the other hand, combines those factors related to the surface which affect the deposition rate; in general, r_s is both a function of the surface type and the concentration of the species at the surface [cf. Garland, 1977]. Note that r_s is rarely if ever directly measured in field experiments; instead, it is usually inferred by measuring the flux of a species to a surface, the concentration of the species at z_r, and the meteorological parameters needed to calculate the dynamic resistance, r_d. The surface resistance is then assumed to be equal to the extra or residual resistance needed to bring the flux calculations from (1) and (2) into balance with the observed flux.

An assumption implicitly adopted in virtually all studies of dry deposition rates to date is that a species' deposition velocity is independent

of its atmospheric abundance. Hence it is typically assumed that once a species' deposition velocity has been determined through measurements and/or calculations for a given set of meteorological conditions and a given surface type, it can be directly applied via (1) to determine the species' dry-deposition flux without any consideration given to how changes in the composition of the atmosphere might affect this deposition velocity. In this work, calculations are presented which suggest that in the case of the dry deposition of soluble gases to a wetted surface, this assumption may not always be appropriate. The calculations involve the use of a simple mathematical model designed to simulate the dry deposition of soluble, reactive species to a surface covered by small drops of liquid water similar to those associated with dew. It should be noted at the outset that the calculations presented here highly simplify a very complex physical and chemical system and are not intended to be an exact simulation of the dry-deposition process to a particular wetted surface on a particular night; nevertheless, the calculations capture many of the key elements of this system and are therefore useful indicators of how various chemical and physical processes interact to control the deposition of a species to a wetted surface.

As a specific example, model calculations are presented simulating the nocturnal deposition of SO_2 to a dew-covered, vegetative surface in the presence of nitric acid and soluble, photochemical oxidants (i.e., H_2O_2 and O_3). These calculations are of interest for two reasons. In the first place, the deposition of acids such as HNO_3 and acid precursors such as SO_2 can represent a potentially toxic dosage of acidic solution to plants. Second, while the problem of SO_2 dry deposition to wetted surfaces has been considered previously by a number of other investigators, we still do not have a thorough and consistent understanding of the processes controlling the deposition of this important species. Field studies by Fowler and Unsworth [1974] and Fowler [1978] of the nocturnal deposition of SO_2 to agricultural crops wetted by dew indicated vanishingly small values for the surface resistance during the first half of the night. However, as the night progressed into the early morning hours, they observed a tendency for the surface resistance to increase and, as a result, for the deposition velocity to decrease. On the other hand, more recent studies by Pierson et al., [1986] and Mulawa et al., [1986] of the deposition of SO_2 and other gases to a surrogate surface covered with dewdrops indicated relatively large values for the SO_2 surface resistance throughout most of the night. In the case of the Pierson et al., [1986] investigation, the SO_2 deposition velocity to dew was found to be on average about an order of magnitude smaller than that of HNO_3 apparently because of sulfur dioxide's relatively large surface resistance. In contrast to these field studies most models of SO_2 dry deposition to wetted surfaces assume no surface resistance with V_d given simply by r_d^{-1} [cf. Sheih et al., 1979; Walcek et al., 1986].

It has been speculated by a number of investigators that large SO_2 surface resistances and correspondingly small SO_2 deposition velocities to dew or other wetted surfaces are caused by high acidity levels in the aqueous solutions which lower the SO_2 solubility and hence the ability of the solutions to absorb SO_2 from the atmosphere [cf. Fowler and Unsworth, 1974; Brimblecombe, 1978; Fowler, 1978; Pierson et al., 1986]. However little or no field data exist to support this conjecture. In the case of the SO_2 deposition studies of Fowler and Unsworth [1974] and Fowler [1978], pH measurements of the dew do not appear to have been made. In the case of the Pierson et al., [1986] study, there does not appear to be any evidence of a correlation between the observed SO_2 deposition velocities and the pH of the dew; for instance, this investigator calculated a Pearson-r correlation coefficient between the H^+ concentrations measured in the dew at the end of each night, and reported in Table 1 of Pierson et al., and the averaged SO_2 deposition velocities measured for those same nights, and reported in Table 6 of Pierson et al., of only 0.03. The lack of a correlation between these two parameters suggests that other surface-related phenomena besides pH may have played a role in controlling the SO_2 dry deposition rate during these experiments. In fact Mulawa et al., [1986] suggested on the basis of their observations that the limited availability of oxidants to convert dissolved SO_2 to sulfate may be an important factor. The model calculations presented in this work, by examining the effects of a variety of chemical and physical processes upon the dry-deposition rates of soluble, reactive gases such as SO_2 to dew-covered surfaces, may prove useful in helping to resolve these questions.

In the next section a brief review of the characteristics of dew is presented. This discussion is then followed by sections in which the formalism used to describe mathematically the dry deposition of gaseous species to a wetted surface is developed and in which this formalism is incorporated into a model designed to simulate the generation of acidic dew over a nocturnal period.

Dew Characteristics

While speculation on the origin and causes of dew can be documented back to antiquity (see, for instance, Aristotle's Meteorologica, Book I), the rigorous scientific study of dew apparently did not begin until the eighteenth and nineteenth centuries [Zikeev, 1952]. In 1725, Boyle was able to demonstrate experimentally that dew formed from the precipitation of water vapor onto cold surfaces, and in 1727, Perliczy developed the first balance capable of measuring dewfall amounts. In the nineteenth century the modern theory of dew formation (i.e., the radiational cooling of the surface during clear nights with high relative humidities resulting in the condensation of water vapor on the cooled surface) was first formulated by Wells [1814]. By the mid-twentieth century the experiments of Thornthwaite and Holzman [1942], Pasquill [1949], and Monteith [1957] had established the detailed mechanisms by which nocturnal, surface condensation is formed on vegetation.

In general, two processes can result in the formation of condensation on vegetative surfaces at night [c.f. Monteith, 1957]. One process

TABLE 1. Physical and Meteorological Conditions Assumed for Standard Model

Parameters	Symbol	Value Assumed
Surface pressure	P_o	1 atm
Surface temperature	T_o	290°K
Surface number density	n_M	2.5×10^{19} cm^{-3}
Reference height	z_r	10 m
Horizontal wind at z_r	u	2.5 m s^{-1}
Obukhov scale length	L	15 m
Surface roughness	z_o	0.05 m
Dewdrop concentration	N	50 cm^{-2}
Dewfall concentration	W	1.0×10^{-5} - 3×10^{-2} g cm^{-2}
Accumulation rate	dW/dt	0.0015 g cm^{-2} h^{-1}

involves the upward transport of water from the moist soil below the cool plant surface; this process is often referred to as distillation. The other involves the downward, turbulent transport of atmospheric water vapor to the plant and is referred to as dewfall or simply dew. It is this later process that will be the main focus of the present work. (In addition to these two processes involving condensation of water vapor onto the leaf surface, leaf wetness can also arise from the interception of precipitation and from guttation, that is, the exudation of water from inside the plant on humid nights).

As described by Monteith [1957], on extremely calm nights (with wind speeds of 0.5 m s^{-1} or less), turbulent transport is usually too slow to bring significant amounts of water vapor down from above, and the major source of surface condensation is due to distillation; however, on these occasions only trace amounts of surface condensation are typically found, even on nights with significant surface cooling. On the other hand, on nights with light winds (i.e., wind speeds of 0.5 - 3 m s^{-1}) as well as radiational cooling, much larger condensation rates are observed; measurements have shown that under these conditions by far the largest source of condensed water to the surface arises from dew rather than distillation. When the winds become significantly larger than about 3 m s^{-1}, little or no condensation is usually found because the enhanced turbulent exchange of heat between the atmosphere and the surface tends to keep the surface temperature above the dew point.

On nights with conditions favoring the formation of dew, accumulation rates can range from about (0.5-6) x 10^{-3}g cm^{-2} h^{-1}; as long as these conditions persist, dew formation will generally continue throughout the night. While dewfall accumulation of as much as 0.06 g cm^{-2} have been observed, total dewfall amounts of about 0.005 - 0.03 g cm^{-2} are typically found at the end of a night with favorable conditions [c.f. Monteith, 1957; Neumann, 1956; Lloyd, 1961; Wisniewski, 1982; Brimblecombe, 1978; Pierson et al., 1986]. Observations such as those of Lloyd [1961] and Drummond [1945] indicate that the evaporation of this surface condensation usually takes about 1 - 2 hours after sunrise, although the evaporation rate is likely to be highly variable, depending upon local meteorological and topographical features.

Since the outer surface of most leaves (i.e., the cuticle) is non wettable [c.f. Holman and Robbins, 1927], dew that forms on vegetation is generally found to be in the form of drops. Pierson et al., [1986] report drop densities of the order of 50 cm^{-2} of horizontal surface. Given total accumulation rates of (0.005-0.06) g cm^{-2} and assuming the drops to be perfect spheres, the above observation implies dewdrop radii of the order of 0.1 - 1 mm by the end of the night; a size which is consistent with the dewdrop sizes generally observed on vegetation [cf. Long, 1958].

In as much as the focus of the present work is to study the deposition of atmospheric gases to dew, rather than dew itself, no attempt is made here to simulate the actual dew-formation process. Instead, the physical and meteorological conditions, including the dewfall accumulation rates, typically observed on nights with significant surface condensation are specified, and then the resulting deposition rates of various species to this dew are calculated. The conditions adopted in the standard model calculations presented in this work are outlined in Table 1. In accord with the observations of Monteith [1957] and others that dew formation requires light but nonzero surface winds, we assume very stable conditions (i.e., Pasquill Category F) with a wind speed of 2.5 m s^{-1} at a height of 10 m and an Obukhov scale length of 15 m. (Note that these are identical to the conditions adopted by Sheih et al., [1979] to simulate the nocturnal deposition of SO_2 to dew-covered surfaces.) The surface itself will be assumed to

be a grassland with a surface roughness, z_o, of 0.05 m [cf. Panofsky and Dutton, 1984]; sensitivity calculations using other values of z_o will also be presented.

In order to simplify the numerics of the calculation a number of assumptions concerning the dewdrops are adopted. The first concerns the shape of the drops; for the calculations presented here it is assumed that the dewdrops form on the leaves as perfect spheres having contact angles of 180^o. In reality, dewdrops forming on the waxy surface of a plant leaf will most likely take the shape of spherical sections with contact angles of about 110^o [Archbold, 1943; Pruppacher and Klett, 1978]. However, it turns out that the results of the model calculations are not very sensitive to the specific geometry assumed for the dewdrops. Essentially equivalent results, with only minor quantitative differences, were obtained from model calculations assuming a planar geometry in which the dew was assumed to form a thin layer of water covering the leaf (i.e., a contact angle of 0^o).

The dewdrops are also assumed to be homogeneously distributed in both size and composition, an assumption which is perhaps not inappropriate given our present state of knowledge concerning the chemistry of dew. As indicated in Table 1, a dewdrop concentration, N, of 50 drops cm^{-2} of horizontal surface is adopted in accord with the observations discussed previously. The total amount a liquid water, W, is varied in the calculations from a nominally small value of 1×10^{-4} g cm^{-2} to a maximum of 3×10^{-2} g cm^{-2}. In the standard model the condensed water is assumed to accumulate at a rate, dW/dt, of 4×10^{-7} g cm^{-2} s^{-1} (i.e., 0.0015 g cm^{-2} h^{-1}); sensitivity calculations with dW/dt equal to 3×10^{-7} g cm^{-2} will also be presented. Finally, note that for a monodisperse distribution the radius $\underline{a}$ of the dewdrops is related to W and N by

$$\underline{a} = [3W/4N\pi\rho]^{1/3} \tag{3a}$$

where $\rho = 1$ g cm^{-3} is the density of water. Similarly, the rate of growth of the dewdrop radii is given by

$$d\underline{a}/dt = \frac{1}{3W}\ \underline{a}\ dW/dt \tag{3b}$$

Having characterized the nature of the dew-covered surface, we now turn to the problem of describing the rate at which a gas will be deposited to that surface.

Deposition Model

Following the formulation of (1), the rate of deposition of a species I to a surface can be expressed in terms of the dynamic and surface resistances, r_d and r_s, respectively. In this section, values for these two parameters are derived. It should be noted, however, that these parameters are dependent to some extent on the value chosen for the reference height, z_r. As indicated in Table 1, z_r is taken to be 10 m in the calculations presented here. While the choice of this particular value for z_r is somewhat arbitrary (in order to use micrometeorological similarity theory, z_r must be less than L) and a value of 5 or 15 m could just as easily have been chosen, it should be noted that the results presented here do not qualitatively change as z_r is varied over this range. Furthermore, in a later section the effects upon the deposition rate of a finite rate of transport of the species through the region lying above z_r will be considered.

Dynamical Resistance

The dynamical resistance, r_d, can be computed as a sum of three individual transfer resistances, such that

$$r_d = r_a + r_b + r_i \tag{4}$$

where r_a and r_b are the aerodynamic and sublayer resistances, respectively [cf. Weseley and Hicks, 1977], and r_i is an additional resistance term defined here as the impactive resistance. Each of these terms are discussed below.

The aerodynamic resistance, r_a, is related to the rate of turbulent mixing of the species from the reference height z_r to the surface and can be represented by

$$r_a = \{k\ u^*\}^{-1}\ [\ln(z_r/z_o) - C_1] \tag{5}$$

In (4), k is von Karmen's constant, equal to 0.4, u^* is the friction velocity, z_o is the surface roughness, and C_1 is a diabatic correction term [Weseley and Hicks, 1977]. The friction velocity can in turn be represented by

$$u^* = k\ u\ [\ln(z_r/z_o) - C_2] \tag{6}$$

where u is the wind velocity at z_r, assumed here to be 2.5 m s^{-1} (see Table 1), and C_2 is another diabatic correction term. Following Weseley and Hicks [1977], the diabatic correction terms can be approximated for the conditions adopted here by

$$C_1 = C_2 = -5\ z_r/L \tag{7}$$

where L is the Obukhov scale length assumed to be 15 m (see Table 1).

The sublayer resistance, r_b, is controlled by the rate of molecular and turbulent transport across the atmospheric sublayer in contact with the surface. Weseley and Hicks [1977] have shown that this parameter can be represented by

$$r_b = \{k\ u^*\}^{-1}/\{2[K_T/D]^{2/3}\} \tag{8}$$

where K_T is the thermal diffusivity and D is the molecular diffusivity. For a D equal to 0.13 cm^2 s^{-1}, the value appropriate for SO_2, (8) reduces to

$$r_b = 2.6\ /\ \{k\ u^*\} \tag{9}$$

which is the form of the sublayer resistance used in this study.

The impactive resistance, r_i, is related to the rate at which the species impacts and sticks to the dewdrop surface. Assuming spherical symmetry, appropriate if the drops are perfect spheres only touching the leaf surface at a single point, then the impactive resistance is given by [cf. Schwartz, 1986]

TABLE 2. Calculated Values for r_a, r_b, r_i, and r_d as a Function of u, z_s, and W

Input Parameters			Calculated Resistances, s cm^{-1}		
u,* m s^{-1}	z_o,* m	W, g cm^{-2}	r_a+r_b	r_i	r_d
2.5	0.05	$5x10^{-4}$	2.4	0.12	2.5
2.5	0.05	0.005	2.4	0.026	2.4
2.5	0.05	0.01	2.4	0.016	2.4
2.5	0.05	0.015	2.4	0.012	2.4
2.5	0.05	0.02	2.4	0.01	2.4
1.5	0.05	0.01	5.6	0.016	5.6
3	0.05	0.01	2.0	0.016	2.0
2.5	0.005	0.01	3.7	0.016	3.7
2.5	0.10	0.01	2.1	0.016	2.1

*Values for standard model are u = 2.5 m s^{-1} and z_o = 0.05 m.

$$r_i = [\pi \underline{a}^2 V N \alpha]^{-1} \quad (10)$$

where V is the thermal velocity and α is the species sticking or accommodation coefficient. In the calculations presented here a value of 0.01 is chosen for α. While significant uncertainties are associated with this parameter and it is likely that it varies from one species to another, measurements of the sticking coefficient of a variety of species impinging on a water surface suggest that for most species of interest α is probably of the order of 0.01 or larger [Chameides, 1984; Mozurkewich, 1987; Gardner et al., 1987]. In light of this fact it is interesting to note in Table 2, where the calculated resistances as a function of u, z_o, and W are listed, that for a wide range of conditions that might be encountered on a night with dewfall, the impactive resistance r_i is always much smaller than the sum of the aerodynamic and sublayer resistances. Thus it would appear that while uncertainties are associated with the parameter α used to determine r_i, this resistance is probably quite small and as a result has little or no effect upon the total dynamical resistance, r_d.

As indicated in Table 2, the dynamic resistance r_d for dry deposition to a dew-covered grassland is found to vary from about 2 to 6 s cm^{-1}; with the standard model values for u and z_o, a dynamic resistance of ~2.5 s cm^{-1} is obtained. Note from (2) that the inverse of the dynamic resistance represents the maximum value that the deposition velocity, V_d, can obtain for the meteorological conditions adopted. When the surface resistance r_s vanishes, or is relatively small, the deposition velocity is equal to $1/r_d$. On the other hand, as the surface resistance becomes large, V_d becomes increasingly less than the $1/r_d$. In the next section the surface resistance term is derived and combined with r_d to obtain an estimate for V_d.

Surface resistance

By equating (2) and (3), the surface resistance, r_s, can be shown to be given by

$$r_s = r_d \{X_I(0)/X_I(z_r)\}/\{1 - X_I(0)/X_I(z_r)\} \quad (11)$$

Thus the surface resistance is directly related to the concentration of the species at the effective surface of deposition [cf. Garland, 1977]. As $X_I(0)$ increases from 0 to $X_I(z_r)$, r_s increases from 0 to ∞. When $X_I(0)$ equals $X_I(z_r)$, r_s becomes infinitely large, causing V_d to go to zero, and the deposition to cease, as one would expect. In the present case, if we assume that deposition only occurs to the dewdrops and not to the dry leaf surface, then the effective surface of deposition is water and $X_I(0)$ is thermodynamically related to the concentration of I within the drops; i.e.,

$$X_I(0) = \frac{[I]_a}{H_I p_o} \quad (12)$$

In (12) H_I is the species' effective solubility or Henry's Law constant (in units of M atm^{-1} or moles per liter per atmosphere), p_o is the surface pressure (assumed to be 1 atm) and $[I]_a$ is the aqueous-phase concentration (in M) of species I at the dewdrop surface. (A species' effective solubility constant differs from the standard solubility constant in that it takes into account the effects of dissociation and complex formation upon the species' net solubility [cf. Chameides 1984]).

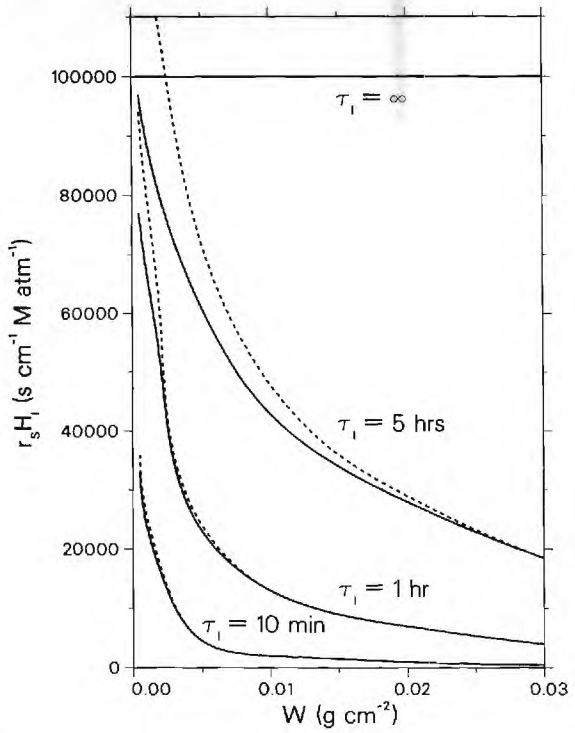

Fig. 1. Calculated values for the product of $r_s.H_I$ as a function of the liquid water accumulation, W, for various values of τ_I. Results are shown for $dW/dt = 4 \times 10^{-7}$ g cm^{-2} s^{-1} (solid line) and $dW/dt = 3 \times 10^{-7}$ g cm^{-2} s^{-1} (dashed line). Note that the value of r_s for a given H_I can be obtained by dividing the plotted product by H_I; thus for $\tau_I = \infty$ and $dW/dt = 4 \times 10^{-7}$, $r_s = 10^4$, 100, and 1 s cm^{-1} for H_I = 10, 10^3, and 10^5 M atm^{-1}, respectively.

Thus in order to evaluate the surface resistance, we must first obtain an expression for $[I]_a$. The concentration of I at the surface is a function of a variety of parameters, including the rate of deposition of I onto the dewdrop surface, the rate of diffusion of I away from the surface, and the reactivity of I within the drop. For illustrative purposes we first consider a simple chemical system in which a species is deposited on the drop surface and is consumed, but not produced, by chemical reactions within the drop. The species is assumed to have a constant chemical lifetime of τ_I. For these assumptions it can easily be shown that [Schwartz and Freiberg, 1981]

$$[I]_a = F\,[I] \tag{13}$$

where [I] is the mean concentration of I in the drop,

$$F = 1/3\,\{\coth(q)/q - 1/q^2\}^{-1} \tag{14}$$

and

$$q = \underline{a}/(\tau_I D_a)^{1/2} \tag{15}$$

and D_a is the aqueous-phase molecular diffusion coefficient, taken here to be equal to 2×10^{-5} cm^2 s^{-1}. For small values of $1/\tau_I$ and $\underline{a}$, F is essentially equal to 1 and $[I]_a \approx [I]$. On the other hand, as $1/\tau_I$ and/or $\underline{a}$ become large, molecular diffusion can no longer maintain a constant concentration in the drop and, as a result, F becomes greater than 1 and $[I]_a$ becomes greater than [I]. Calculations indicate that for dewdrops, whose radii are usually less than 1 mm, F is essentially equal to 1 and $[I]_a$ to [I] as long as τ_I is greater than about 1 min; in the calculations to be presented later, this turns out to be the case for SO_2, HNO_3, and H_2O_2, but not for O_3.

Having expressed $[I]_a$ in terms of [I], we now must solve for [I]. An estimate for this parameter can be obtained by noting that the time rate of change of [I] is given by

$$\frac{d[I]}{dt} = \frac{n_m}{A(W \times 10^{-3})}\,\frac{1}{r_d}\left(X_I(z_o) - \frac{F[I]}{H_I P_o}\right) - \frac{[I]}{W}\,\frac{dW}{dt} - \frac{[I]}{\tau_I} \tag{16}$$

where A is Avogadro's number and $(W \times 10^{-3})$ is equivalent to the number of liters of condensed water per square centimeter of horizontal surface. In (16) the first term on the right hand side of the equation represents the source of I to the dewdrop due to dry deposition from the atmosphere (see equation (3)), the second term arises from the dilution of I as the dewdrop grows, and the third term is the rate of loss of I due to chemical reactions. At equilibrium,

$$[I] = \left\{\frac{X_I(z_o)}{r_d}\,\frac{n_m}{A(W \times 10^{-3})}\right\} \div \left\{\frac{Fn_M}{A(W \times 10^{-3})r_d H_I} + \frac{1}{\tau_I} + \frac{1}{W}\,\frac{dW}{dt}\right\} \tag{17}$$

Substituting (13) and (17) into (11), a closed expression for the surface resistance is obtained, i.e.,

$$r_s = \frac{n_M F}{A\,H_I \times 10^{-3}}\,\{W/\tau_I + dW/dt\}^{-1} \tag{18}$$

Figure 1 quantitatively illustrates the resulting dependence of r_s upon H_I, W, dW/dt, and τ_I; r_s is found to decrease as H_I, W, and dW/dt increase and as τ_I decreases. The dependence upon H_I is easily understood; as H_I increases the capacity of the dewdrops to absorb the species increases and hence the resistance to deposition decreases. Since a decrease in τ_I and an increase in dW/dt tend to depress the concentration of I in the dewdrop, r_s decreases as these two parameters decrease and increase, respectively. However, while the dependence of r_s upon H_I is linear, the dependence of the surface resistance upon the other parameters is somewhat more complex. When the ratio W/τ_I is relatively small compared with dW/dt, r_s is found to be essentially independent of τ_I and W and inversely proportional to dW/dt. However, as W/τ_I increases, its effect upon r_s

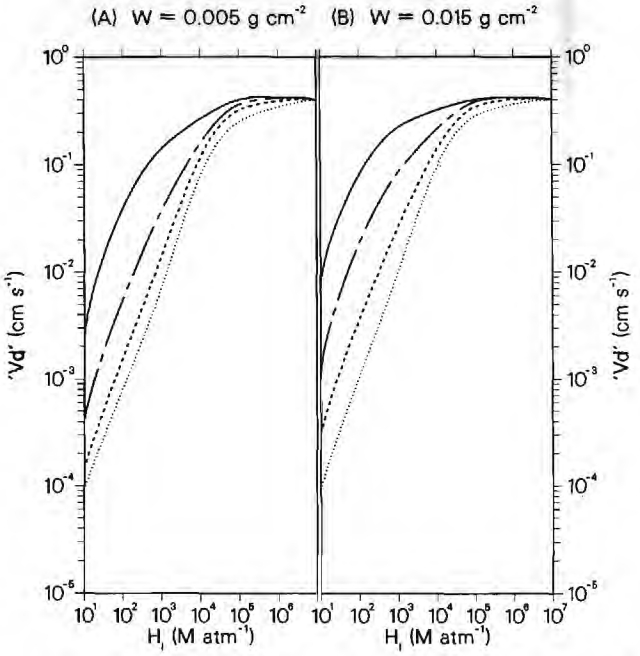

Fig. 2. Calculated values for V_d as a function of H_I for (a) W = 0.005 g cm^{-2} and (b) W = 0.015 g cm^{-2} and the conditions outlined in Table 1. Results are shown for τ_I = 10 min (solid line), 1 hour (dashed-dotted line), 5 hours (dashed line), and ∞ (dotted line).

becomes more pronounced; in fact, when this ratio becomes large compared with dW/dt, r_s becomes independent of dW/dt and inversely proportional to W and $1/\tau_I$ (see Figure 1).

Deposition Velocity

With r_d and r_s defined by (4), (5), (9), (10), and (18), the bulk deposition velocity, V_d, can be calculated by substitution into (2). The resulting values for V_d as a function of H_I, W, and τ_I are presented in Fig. 2. For species with relatively high solubilities (i.e., $H_I \geq 10^5$ M atm^{-1}), the surface resistance is too small to affect the deposition rate and V_d is essentially given by $1/r_d$; recall from Table 2 that for the conditions adopted here, $1/r_d$ = 0.4 cm s^{-1}. However, as H_I decreases, r_s increases until it eventually begins to slow the deposition rate and V_d falls below its maximum value of 0.4 cm s^{-1}. For extremely small H_I, $r_s \gg r_d$ and V_d is dominated by the surface resistance term; in this regime, V_d varies linearly with H_I and extremely small values for V_d are obtained. As indicated in Figure 2, the value of H_I where the transition occurs between a V_d dominated by r_d and a V_d dominated by r_s is dependent upon τ_I and W. Since r_s increases as τ_I increases (see Figure 1) and W decreases, the point where V_d begins to decrease as H_I decreases occurs at progressively larger values of H_I as τ_I increases and W decreases. A similar effect occurs for dW/dt as well, although this is not specifically illustrated in Figure 2.

The results illustrated in Figure 2 indicate that species with effective solubility constants of about 10^4 M atm^{-1} or less can have relatively large surface resistances and hence deposition velocities which are largely controlled by surface-related parameters, such as τ_I, W, and dW/dt. Since the effective solubility of SO_2 in solutions with pHs often encountered in dew (i.e., pH < 5) is considerably less than 10^4 M atm^{-1}, these results suggest that the deposition velocity of SO_2 to dew can be limited by its surface resistance. However, the extent to which the surface resistance reduces the SO_2 deposition velocity to a dew-covered surface is dependent on the reactivity of SO_2 in the dew solution. As indicated in Figure 2, if SO_2 is sufficiently reactive in a dewdrop, its deposition velocity to that drop would be relatively large in spite of its having a small solubility. On the other hand, as the reactivity of SO_2 in acidic dew decreases, its deposition velocity would become smaller.

From a qulitative point of view the results illustrated in Figure 2 suggest a potenital explanation for the wide range of SO_2 deposition velocities observed for dew-covered surfaces. The calculations suggest that the relatively large deposition velocities typically observed by Fowler and Unsworth [1974] and Fowler [1978] may have involved dewdrop solutions in which SO_2 was very reactive while the smaller deposition velocities inferred by Pierson et al., [1986] may have involved dewdrop solutions with lower SO_2 reactivities. To further test this hypothesis, the specific problem of SO_2 dry deposition to a dew-covered surface in the presence of other acidic and oxidative species is examined in a more comprehensive fashion in the next section.

Generation of Acid Dew From Dry Deposition of HNO_3 and SO_2

The results of the previous section illustrate in a general way how a species' solubility and reactivity can influence the rate at which that species is dry-deposited to a dew-covered surface. In this section the formalism developed in the previous section is incorporated into a model which simultaneously treats the atmospheric and aqueous-phase chemistry of a mixture of soluble trace gases as they are dry-deposited onto dewdrops over the course of a nocturnal period. Four species were chosen for this illustrative calculation; they are HNO_3, SO_2, O_3, and H_2O_2. (These four atmospheric species were chosen for a variety of reasons. Because they have a wide range of solubilities and a strong chemical interaction when present together within a solution, they provide a useful demonstration of the coupling between dewfall composition and dry-deposition rates. Furthermore, as will be discussed in more detail later, the deposition of these four species and their subsequent chemistry within the dewdrops represents a chemical mechanism which has many of the key elements believed to be responsible for the generation of acidic dew.) In Tables 3a - 3c the basic thermodynamic and kinetic data used in the model are listed.

Model Description

In the gas-phase portion of the model, the HNO_3, SO_2, O_3, and H_2O_2 mixing ratios (i.e., $X_I(z, t)$) are calculated as a function of time, t, and altitude, z, using a standard one-dimensional,

TABLE 3a. Chemical Mechanism Used in "Acidic Dew" Simulations: Species and Initial Concentrations

Gas-Phase		Aqueous-Phase	
Species	X_I^o, ppbv	Species	$[I]_o$, M
HNO_3	2	NO_3^-	0
SO_2	10	$S_{IV} = SO_2 + HSO_3^- + SO_3^=$	0
H_2O_2	1	H_2O_2	0
O_3	50	O_3	0
		$SO_4^=$	0
		H^+	2.5×10^{-6}

eddy-diffusion algorithm in which vertical transport is parameterized in terms of an eddy-diffusion coefficient, K(z). Because the nocturnal boundary layer is stable when dew forms, it is conceivable that for some species the rate of dry deposition to the dewdrops is actually limited by the rate of transport of the species down through the boundary layer to z_r rather than by the rate of transport from z_r to the surface [Weseley and Hicks, 1977]. In order to determine if and when this occurs, solutions for $X_I(z,t)$ are obtained for z ranging from z_r (the reference height of 10 m) to a maximum altitude z_T = 150 m. This later height is equivalent to 10 times the assumed Obukhov scale length, L, and is taken to be the nominal height of the nocturnal boundary layer.

Assuming the species to be unreactive in the nocturnal boundary layer, the continuity equations for the four gaseous species are given by

$$dX_I(z,t)/dt = -d\psi_I(z,t)/dz \qquad (19)$$

where I = HNO_3, SO_2, O_3, and H_2O_2, and $\psi_I(z,t)$ is the upward vertical flux of species I, and is in turn given by

$$\psi_I(z,t) = -K(z) \frac{dX_I(z,t)}{dz} \qquad (20)$$

Following Weseley and Hicks [1977], the profile for K(z) in the stable, nocturnal boundary layer is assumed to have the following form:

$$K(z) = ku^*L\,(0.05 + 0.12z/L)\ cm^2\ s^{-1} \qquad (21)$$

Solutions for $X_I(z,t)$ are obtained by integrating (19) using a standard Gear [1971] routine for each species subject to the boundary and initial conditions described below.

At $z = z_T$ a constant concentration condition is imposed so that

$$X_I(z_T,t) = X_I^o \qquad (22)$$

where X_I^o is a constant. At $z = z_r$ the flux to the surface is specified using the dry deposition formalism developed in the previous section. Thus from (3), (12), and (13)

$$\psi_I(z_r,t) = -\frac{\phi_I}{n_M} = \frac{1}{r_d}\left\{X_I(z_r) - \frac{F[I]}{H_I p_o}\right\} \qquad (23)$$

Note that in using (23) it is implicitly assumed for simplicity that the dry-deposition flux is limited to the wet parts of the surface and is excluded from the dry portions. Finally, as an initial condition on the gas-phase profiles, it is assumed that

$$X_I(z,0) = X_I^o \qquad (24)$$

TABLE 3b. Chemical Mechanism Used in "Acidic Dew" Simulations: Effective Solubility Constants

No.	Reaction	Effective Solubility Constant, M atm^{-1}
(RS1)	$HNO_3 \leftrightarrow H^+ + NO_3^-$	$5.8 \times 10^6/[H^+]$
(RS2)	$SO_2 \leftrightarrow S_{IV}$	$1.6\,(1 + 2.1 \times 10^{-2}/[H^+]$
(RS3)	$H_2O_2 \leftrightarrow (H_2O_2)_{aq}$	1.8×10^5
(RS4)	$O_3 \leftrightarrow (O_3)_{aq}$	1.5×10^{-2}

Data taken from Chameides [1984] with T = 290°K.

TABLE 3c. Chemical Mechanism Used in "Acidic Dew" Simulations: Aqueous-Phase Reactions

No.	Reaction	Rate Constant, M^{-1} s^{-1}
(R1)	$H_2O_2 + S_{IV} \rightarrow SO_4^= + 2H^+$	$5.7 \times 10^4/(0.1 + [H^+]/(1+2.1\times10^{-2}/[H^+])$
(R2)	$O_3 + S_{IV} \rightarrow SO_4^= + H^+$	$2.9 \times 10^5 + 9.3 \times 10^1/[H^+]$

*Data taken from Chameides [1984] with T = 290°K.

For the standard model calculations, X_I^o equals 2 parts per billion by volume (ppbv) for HNO_3, 10 ppbv for SO_2, 50 ppbv for O_3, and 1 ppbv for H_2O_2. These gas-phase concentrations were chosen to roughly correspond to the average lower-boundary levels observed by Pierson et al. [1986] during their study of dewfall composition in the Allegheny mountains.

In the aqueous-phase portion of the model, the dewdrop concentrations of NO_3^-, S_{IV} (= $SO_2 + HSO_3^- + SO_3^=$), O_3, H_2O_2, $SO_4^=$, and H^+ are determined as a function of time. As outlined in Table 3, the presence of NO_3^-, S_{IV}, O_3, and H_2O_2 in the dew arises in the model from the deposition and dissolution of atmospheric HNO_3, SO_2, O_3, and H_2O_2, respectively. The $SO_4^=$ ion on the other hand is generated in the dewdrops from the oxidation of S_{IV} by dissolved H_2O_2 and O_3. (Note that for the conditions adopted here, oxidation by H_2O_2 is responsible for roughly 70% of the total sulfate generated in the dewdrops.) Finally, the presence of H^+ in the dew is the result of the dissociation of nitric, sulfuric, and, to a very small extent, sulfurous acid.

The values of $[NO_3^-]$, $[S_{IV}]$, $[O_3]$, and $[H_2O_2]$ as a function of time are obtained by integrating a coupled set of equations of the form of (16), with the values of X_I at z_r being supplied from the solutions of the gas-phase equations described earlier. In these equations, expressions for τ_I are appropriately formed from the chemical mechanism outlined in Table 3. Thus in the case of S_{IV},

$$1/\tau_{SIV} = [H_2O_2]\ (R1) + [O_3]\ (R2) \qquad (25)$$

while for NO_3^-, which is unreactive, $1/\tau$ is zero. For the special case of $SO_4^=$, which is chemically generated in the dewdrops but not consumed, the chemical loss term in (16) is replaced by an appropriate source term and the term relating to the source of the species from dry deposition is set equal to zero. For simplicity, the initial concentrations of each of these species is assumed to be zero. The H^+ concentration as a function of time is solved for by demanding charge balance subject to the initial condition that at t = 0 the pH is 5.6.

The nocturnal period during which dew is allowed to accumulate in the model is assumed to be 10 hours. During this period, W, the concentration of liquid water on the leaf surfaces, is assumed to accumulate in the standard model at a constant rate of 4×10^{-7} g cm^{-2} s^{-1}. This results in a total accumulation by the end of the night of 0.015 g cm^{-2}, a value consistent with the observations discussed earlier. (In order to avoid numerical problems related to dividing by zero, a small amount of liquid water is assumed to be present at t = 0; in the calculations presented here this amount is 1×10^{-5} g cm^{-2} s^{-1}; however, the results are not sensitive to the exact amount chosen.) In addition to the standard model, calculations are presented for a constant liquid water model in which W is held fixed at 0.015 g cm^{-2}. The resulting variations in W as a function of time for the two models are illustrated in Figure 3.

An additional simplification in the chemical mechanism adopted here which should be noted relates to interactions between the dewdrops and the leaf surfaces. It is quite possible that the presence of soluble impurities on the leaves and the exchange of ions between the plant cells and the dewdrops through the leaf cuticle may play a significant role in influencing the acidity of dew [Brimblecombe and Todd, 1977]. However, in the calculations presented here the vegetative surface is assumed to be inert and impermeable, and thus these effects are neglected.

While this mechanism undoubtedly represents a gross simplification of the actual chemistry of dewdrops, it is nevertheless interesting to note that the mechanism does appear to capture the main elements currently believed to lead to the generation of acidity in dew. For instance, limited observations suggest that nitric and sulfuric acid, the two acids included in the model, might often be the principal acids in dew in the continental United States, [Pierson et al., 1986; Mulawa et al., 1986]. Furthermore, the measurements by Pierson et al., [1986] of dew in a remote location indicate that similar to the mechanism adopted here, the primary source of nitric acid in the dew was from the dry deposition

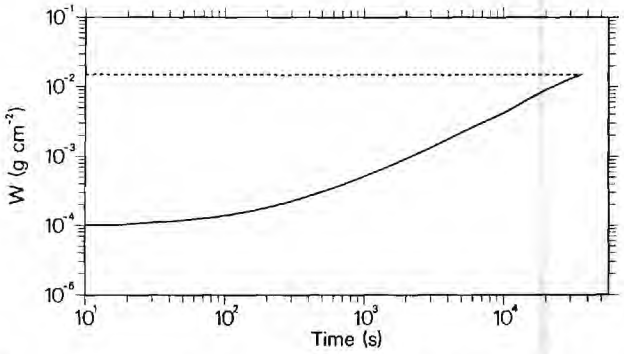

Fig. 3. Assumed variation in the total accumulation of liquid water, W, as a function of time, t. W is shown for the standard model (solid line) and for a constant liquid water model (dashed line).

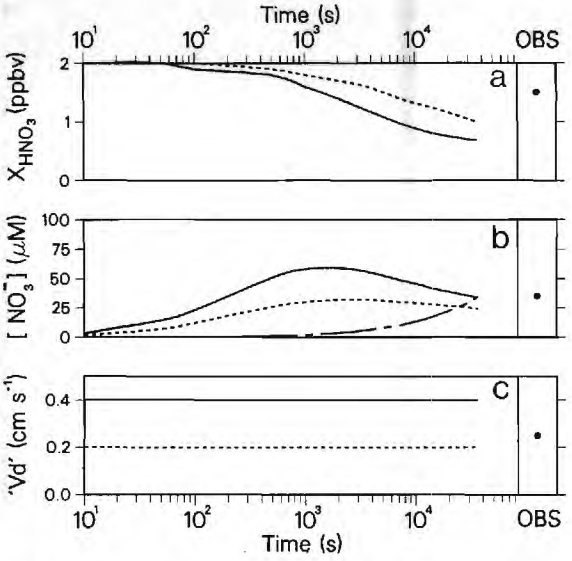

Fig. 4. Calculated variations in X_{HNO3} at $z=z_r$, $[NO_3^-]$, and "$V_d(HNO_3)$" as a function of time. Results are shown for the standard model (solid line), r_d = 5 s cm^{-1} (dashed line), and for a constant W of 0.015 g cm^{-2} (dashed-dotted line). Note "$V_d(HNO_3)$" and X_{HNO3} for the constant W case were identical to those obtained for the standard model. On the far right-hand side of Figure 4 are the averaged observations of Pierson et al., [1986].

and dissolution of gaseous HNO_3, while for sulfuric acid it was from the deposition of SO_2 and its subsequent aqueous-phase oxidation. Finally, while a wide range of species are capable of oxidizing S_{IV} to sulfate, O_3 and H_2O_2 are two ubiquitous oxidants currently believed to often play a major role in the conversion of S_{IV} to sulfate in cloud water and fogs [Penkett et al., 1979; Moller, 1980; Jacob and Hoffman, 1983; Calvert et al., 1983; Martin, 1983; Chameides, 1984]. Thus in addition to simply illustrating the interaction between dry-deposition rates to dew-covered surfaces and dewdrop chemistry for a variety of species of interest, these model calculations may ultimately prove useful in further elucidating the actual processes which govern the generation of acidity in dew. The results of these calculations are presented in the next section.

Model Results

Results from the model calculations are illustrated in Figures 4, 5, and 6; these include those obtained from the standard model as well as those obtained from calculations with varying values for r_d, dW/dt, X_{H2O2}^o, and X_{SO2}^o. In Figures 4 and 5, results related to the nitrogen and sulfur oxides, respectively, are presented; in Figures 4 and 5 the calculated gas-phase concentrations at the reference height, z_r, and the mean aqueous-phase concentrations in the dewdrops as well as the effective deposition velocity, "V_d," for the relevant species are plotted as a function of time. A species' effective deposition velocity is defined as the ratio of the average flux of the species to the dewdrops divided by its average concentration at z_r. Thus for SO_2 at time t,

$$"V_d(SO_2)" = \frac{([S_{IV}]_t) + [SO_4^=]_t)\ A\ (W \times 10^{-3})}{t\ X_{SO2}(z_r)_t} \quad (26)$$

where $[S_{IV}]_t$ and $[SO_4^=]_t$ are the average concentrations of S_{IV} and $SO_4^=$ in the dewdrop solutions and $X_{SO2}(z_r)_t$ is the average level of SO_2 at z_r; the average for these three parameters being carried out from time 0 to time t. (Note that because of the limited solubility of sulfurous acid, the calculated S_{IV} levels were, except for the first minute or two of the integration, much lower than those calculated for $SO_4^=$.) Similarly, for HNO_3

$$"V_d(HNO_3)" = \frac{[NO_3^-]_t\ A\ (W \times 10^{-3})}{t\ X_{HNO3}(x_r)_t} \quad (27)$$

where $[NO_3^-]_t$ and $X_{HNO3}(z_r)_t$ represent the appropriate averages of the NO_3^- and HNO_3 concentrations.

The variations of nitric acid and its aqueous-phase counterpart, NO_3^-, illustrated in Figure 4 are characteristic of a highly soluble species whose deposition rate is controlled by dynamical processes. Because of nitric acid's high solubility, its surface resistance is always vanishingly small, and as a result, "$V_d(HNO_3)$" $\approx r_d^{-1}$ (see equation (3)). Hence in the standard model case, "$V_d(HNO_3)$" was calculated to be 0.4 cm

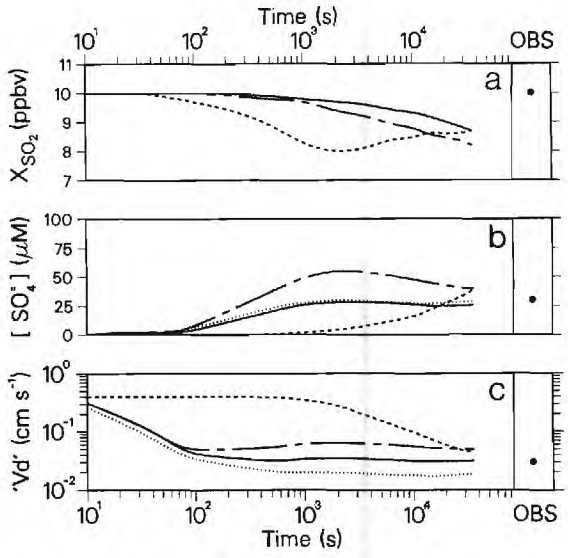

Fig. 5. Calculated variations in X_{SO2} at $z = z_r$, $[SO_4^=]$, and "$V_d(SO_2)$" as a function of time. Results are shown for the standard model (solid line), for a constant W of 0.015 g cm^{-2} (dashed line), for X_{H2O2}^o = 2 ppbv (dashed-dotted line), and for X_{SO2}^o = 20 ppbv (dotted line). Note results with r_d = 5 s cm^{-1} were indistinguishable from those illustrated for the standard model. On the far right-hand side of Figure 5 are the averaged observations of Pierson et al., [1986].

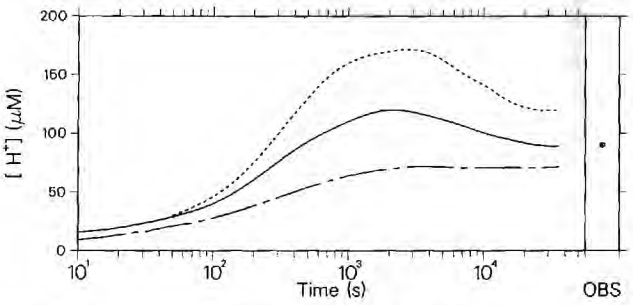

Fig. 6. Calculated variations in $[H^+]$ as a function of time. Results are shown for the standard model (solid line), for r_d = 5 s cm^{-1} (dashed-dotted line), and for X_{H2O2}^o = 2 ppbv (dashed line). On the far right-hand side of Figure 6 are the averaged observations of Pierson et al., [1985].

s^{-1} throughout the integration, while a value of 0.2 cm s^{-1} was obtained in the case when r_d was set equal to 5 s cm^{-1} (see Figure 4c).

As illustrated in Figure 4b, the aqueous-phase concentration of NO_3^- was found to rise rapidly to the 10-μM level after only a few minutes and reach a maximum concentration of almost 70 μM after a half an hour in the standard model. The nitrate concentration then decreased slightly and eventually reached a fairly constant level of about (30-40) μM in the standard model. The relatively constant value for $[NO_3^-]$ over the later portion of the integration was the result of an approximate equilibrium established between the source of nitrate to the dew from HNO_3 deposition and dilution of nitrate caused by the continued growth of the dewdrops (see Figure 3). (The effect of the dilution term upon $[NO_3^-]$ levels is apparent in Figure 4b by comparing the standard model result with that obtained when W was held constant at 0.015 g cm^{-2}; for the constant W case there is no dilution, and as a result, $[NO_3^-]$ was found to increase continuously throughout the integration.)

It is interesting to note in Figure 4b that when "$V_d(HNO_3)$" was decreased by a factor of 2 by changing r_d from 2.5 to 5 s cm^{-1}, the resulting $[NO_3^-]$ level only decreased by a factor of about 1.5. For instance, in the standard model case, $[NO_3^-]$ was calculated to be about 35 uM by the end of the night, while a level of 25 uM was obtained when r_d was set equal to 5 s cm^{-1}. This result is indicative of the fact that an additional process, other than the transport of HNO_3 from z_r to the surface, is acting to limit the rate of HNO_3 deposition. This other process is the downward transport of HNO_3 through the stable, nocturnal boundary layer. Note in Figure 4a that because this later process is not fast enough to balance the rapid loss of HNO_3 due to deposition, the lower-boundary layer tends to become depleted in this species as the night progresses. Furthermore, the size of the HNO_3 depletion is a function of r_d. When r_d was changed from its standard model value to 5 s cm^{-1}, thereby halving "V_d," the HNO_3 depletion over the course of the night became less pronounced; in the standard model case, $X_{HNO3}(z_r)$ decreased from 2 to 0.7 ppbv, while it only decreased to about 1 ppbv when r_d equaled 5 s cm^{-1}. Because the amount of HNO_3 depletion decreases as the deposition velocity decreases, the resulting level of $[NO_3^-]$ in the dewdrops does not vary linearly with V_d. This result serves to reinforce the point made by Weseley and Hicks [1977] relating to the importance of including the effects of slow transport through the boundary layer when simulating the dry deposition of species with little or no surface resistance under stable conditions.

In contrast to nitric acid, the model calculations indicate that the deposition of SO_2 can be controlled by the surface rather than dynamic resistance. For instance, while the HNO_3 mixing ratio at z_r was found to drop well below its initial value after an hour or so, only a very small decrease in $X_{SO2}(z_r)$ was calculated (see Figure 5a). The SO_2 effective deposition velocity, illustrated in Figure 5c, was also found to vary very differently from that of HNO_3. While "$V_d(SO_2)$" was found to be close to r_d^{-1} at the very early stages of the integration, "$V_d(SO_2)$" quickly decreased to much smaller values as time progressed and the S_{IV} levels in the dewdrops built up. In the standard model case an effective deposition velocity of about 0.03 cm s^{-1} was calculated for times greater than about 2 min (see Figure 5c). Furthermore, while "$V_d(SO_2)$" was found to be essentially independent of the value chosen for r_d, it was calculated to be a strong function of surface-related parameters such as W and dW/dt as well as to X_{H2O2}^o and X_{SO2}^o, which affect the chemical lifetime of S_{IV} in the dewdrops.

Of particular interest is the calculated sensitivity of "$V_d(SO_2)$" to the values assumed for X_{H2O2}^o and X_{SO2}^o. Note, for instance in Figure 5 that doubling X_{H2O2}^o from its standard model value of 1 ppbv to 2 ppbv caused "$V_d(SO_2)$" to increase from about 0.03 to 0.05 cm s^{-1} and the $[SO_4^=]$ level calculated for the end of the night to increase from about 25 uM to about 40 uM. Calculations with X_{H2O2}^o equal to 10 ppbv yielded a "$V_d(SO_2)$" of 0.32 cm s^{-1}, a value almost identical to that obtained for HNO_3; note that the results of this calculation are not illustrated in Figure 5. This increased SO_2 deposition rate and corresponding increase in $[SO_4^=]$ levels is caused by the fact that increasing atmospheric H_2O_2 raises the concentration of H_2O_2 in solution, which in turn lowers the aqueous-phase SO_2 lifetime, τ_{SIV}. As discussed in the previous section, a decrease in the τ of a species whose deposition rate is controlled by the surface resistance has the net effect of increasing V_d. However, note in Figure 5 that not only is "$V_d(SO_2)$" affected by changes in X_{H2O2}^o, but it is also affected by variations in X_{SO2}^o. Because for the conditions adopted here (i.e., $X_{SO2} > X_{H2O2}$) a doubling in atmospheric SO_2 causes a depletion of H_2O_2 in the dewdrops, it results in an increase in τ_{SO2}; the increase in τ_{SO2} in turn causes a decrease in "$V_d(SO_2)$."

It is also interesting to note that while several investigators have speculated that the pH of dewdrops may play a major role in determining the rate at which SO_2 is dry-deposited to dew, the present results indicate that this does not necessarily have to be the case. While large variations in pH can affect the SO_2 deposition (calculations indicate that the presence of a few

ppbv of NH_3 in the boundary layer can neutralize the dewdrops and increase "$V_d(SO_2)$"), other chemical processes can also be important. For instance, note in Figure 6, where the calculated values of $[H^+]$ are plotted as a function of time, that the pH hardly changed at all when X_{SO2}^o was varied from 10 to 20 ppbv, but "$V_d(SO_2)$" changed from about 0.03 to 0.02 cm s^{-1}. These results serve to illustrate the potential importance of the chemical state of the atmosphere in determining the deposition velocity of SO_2 and similar species to wetted surfaces; while much attention has been paid to the role of meteorological phenomena in the dry-deposition process, the chemical composition of the atmosphere can also play a role. Furthermore,while it is typically assumed that a species' deposition velocity is independent of its concentration, the calculations presented here indicate that under some conditions and for some species this assumption could be erroneous.

Although not specifically illustrated here, the variations in H_2O_2 and O_3 are similar to those of HNO_3 and SO_2, respectively. H_2O_2, which has a solubility constant of about 10^5 M atm^{-1}, is sufficiently soluble to have its deposition controlled by dynamical processes, and as a result, "$V_d(H_2O_2)$" was always calculated to be about $1/r_d$. O_3, on the other hand, has a solubility constant of only about 10^{-2} M atm^{-1}, and its deposition velocity was found to be controlled by the surface resistance term. For the standard model case, a "$V_d(O_3)$" of about 2 x 10^{-3} cm s^{-1} was calculated.

The variations in $[H^+]$ illustrated in Figure 6 generally reflect the variations calculated for $[NO_3^-]$ and $[SO_4^=]$ illustrated in Figures 4b and 5b. For the standard model, about two thirds of the calculated free acidity arose from sulfuric acid and the remaining one third from nitric acid; the contribution to the acidity from sulfurous acid was for the most part negligible. The calculations yield a dewdrop pH of about 4 by the end of the night, a result which is roughly consistent with previously measured acidity levels measured in dew over the continental United States [Pierson et al., 1986; Mulawa et al., 1986]. However, while these calculated and observed dewdrop pHs are fairly modest and imply a relatively small total flux of acid to the Earth's surface when compared to that in rain [cf. Brimblecombe, 1978; Mulawa et al., 1986], acidified dewdrops may still have a significant and deleterious impact upon terrestrial ecosystems. Recall that once the sun rises, dewdrops rapidly evaporate. As the drops evaporate the pH within these drops can drop to extremely low values, possibly low enough to damage the leaf surfaces upon which the dewdrops originally formed (cf. Sigal and Johnston, 1986; Wood and Bormann, 1975; Lee et al., 1981; Haines et al., 1980) .

On the far right-hand side of Figures 4, 5, and 6, the averaged concentrations and deposition velocities of Pierson et al., [1986] are indicated. Recall that the conditions for the model calculations were chosen to resemble those encountered by Pierson et al., [1986]. While the good agreement between these observations and the model calculations do not in any sense validate the model presented here, it does indicate the reasonableness of the model results. Of particular significance is the agreement between the calculated and observed deposition velocities for HNO_3 and SO_2; this agreement strongly supports the conclusion that SO_2 deposition to wetted surfaces can be limited by chemical rather than physical phenomena. On the other hand, the results illustrated here should not be interpreted to mean that the SO_2 deposition velocity to a wetted surface must always be relatively small. In fact, the calculations indicate that if there are sufficient levels of S_{IV} oxidants such as H_2O_2 available the SO_2 deposition velocity can be almost as large as that of HNO_3. For this reason, it is extremely important to characterize the chemical as well as the physical state of the surface and atmosphere when measuring dry-deposition rates of reactive gases such as SO_2.

Conclusion

A formalism has been developed to describe the dry deposition of soluble, reactive gases to wetted surfaces in terms of the relevant meteorological conditions, the surface roughness, the total amount of liquid water present on the surface, the rate of accumulation of this liquid water, and the species' solubility and reactivity in the surface water. For the case of nocturnal, dry deposition to a dew-covered surface, the deposition velocity of species with solubility constants larger than about 10^4 M atm^{-1} were found to be controlled by dynamical processes. The deposition velocities of species with lower solubilities were found to be determined by the surface resistance, which is in turn a function of chemical as well as physical parameters.

A model using this formalism was found to be able to explain observed nitrate, sulfate, and hydrogen ion levels in dew in terms of the dynamically controlled dry deposition of gaseous HNO_3 and the chemically controlled dry deposition of SO_2 and its subsequent oxidation. The oxidation of the dissolved SO_2 was accomplished in the model by reactions with hydrogen peroxide and ozone which also had been deposited and dissolved in the dew from the atmosphere. However, other oxidants and/or catalysts may also play a significant role in generating sulfate in dew in some locations and under some conditions; this possibility requires further study as does the determination of how the action of these other oxidants and catalysts might affect the SO_2 deposition velocity. Consideration also needs to be given to the effect of the deposition of alkaline material, such as NH_3 and dust particles, upon the SO_2 deposition rate. Finally, further work is needed to define the role of species derived from the plant itself in the chemistry of dew and its associated deposition velocities.

Similar to observations of dew in the continental United States, the model generates a dewdrop pH of about 4 by the end of the night. However, the rapid evaporation of these drops soon after sunrise can lead to much lower pHs. The possibility that these highly concentrated, evaporating droplets have a deleterious effect upon plant leaves deserves further investigation.

It should be noted that the calculations presented here are not intended to be an exact simulation of the deposition process at some specified time and location; indeed, the many

simplifications adopted in the model and the natural variability of many of the parameters used in the model would preclude such a claim. Instead, the calculations should be viewed in a more qualitative fashion as an exploratory assessment of the role of chemical processes in the dry deposition of soluble, reactive gases to wet surfaces. In this light the finding that the chemical rather than the physical state of the atmosphere can control the deposition rate of sparingly soluble species such as SO_2 to wetted surfaces is of particular interest. While this result was obtained for a model simulating dry deposition to dew, the qualitative features of this result may have much wider applicability. In this regard it should be noted that dry deposition in many cases ultimately involves deposition to some sort of wetted surface; this surface can be on the outside of leaves, as in the case of dew, or, in the case of deposition to the interior of plant leaves, the aqueous layer bathing the internal cell walls. Thus the finding that variations in atmospheric SO_2 levels can affect the SO_2 deposition velocity to dew implies the possibility that a similar effect may occur for the SO_2 dry-deposition velocity to a much wider range of surfaces. Further work, including more sophisticated model calculations as well as field measurements, are needed to more accurately establish the coupling between atmospheric composition and dry-deposition velocities in the case of SO_2 and other species with limited solubility.

Acknowledgements. This work was supported in part by funds from the National Aeronautics and Space Administrations under grant NAG-1-385 and from the National Science Foundation under grants ATM-8208828 and ATM-8600888. The author would like to thank Barry Huebert for serving as Editor for this paper.

References

Archbold, J. W., Preliminary note on condensation in the form of clouds and dew, Philos. Mag., 34, 632-642, 1943.

Brimblecombe, P., "Dew" as a sink for sulfur dioxide, Tellus, 30, 151-157, 1978.

Brimblecombe, P., and I. J. Todd, Short communications - Sodium and potassium in dew, Atmos. Environ., 11, 649-650, 1977.

Businger, J. A., Evaluation of the accuracy with which dry deposition can be measured with current micrometeorological techniques, J. Clim. and Appl. Meteorol., 25, 1100-1124, 1986.

Calvert, J., J. N. Galloway, J. M. Hales, G. M. Hidy, J. Jacobson, A. Lazrus, J. Miller, and V. Mohnen, Acid Deposition - Atmospheric Processes in Eastern North America, National Academy Press, Washington, D.C. 1983.

Chameides, W. L., The photochemistry of a remote marine stratiform cloud, J. Geophys. Res., 89, 4739-4755, 1984.

Drummond, A. J., The persistence of dew, J. Roy. Meteorol. Soc., 71, 415-417, 1945.

Fowler, D., Dry deposition of SO_2 on agricultural crops, Atmos. Environ., 12, 369-373, 1978.

Fowler, D. and M. H. Unsworth, Dry deposition of sulphur dioxide on wheat, Nature, 249, 389-390, 1974.

Gardner, J. A., L. R. Sharfman, Y. G. Adequyi, P. Davidovits, M. S. Zahniser, D. R. Worsnop, and C. E. Kolb, Measurement of the sticking coefficient of $SO_2(g)$ on water droplets, J. Geophys. Res., in press, 1987.

Garland, J. A., The dry deposition of sulphur dioxide to land and water surfaces, Proc. R. Soc. London, Ser. A, 245-268, 1977.

Gear, C. W., Numerical Initial Value Problems in Ordinary Differential Equations, Prentice Hall, Englewood Cliffs, N.J., 1971.

Haines, B., M. Stefani, and F. Hendrix, Acid rain: Threshold of leaf damage in 8 plant species from a southern Appalachian forest succession, Water Air Soil Pollut., 14, 403-404, 1980.

Hicks, B. B., Measuring dry deposition: A re-assessment of the state of the art, Water Air Soil Pollut., 30, 75-90, 1986.

Holman, R. M., and W. W. Robbins, Textbook of General Botany, 2nd ed, John Wiley & Sons, New York, 1927.

Jacob, D. J., and M. R. Hoffman, A dynamic model for the production of H^+, NO_3^-, and $SO_4^=$ in urban fog, J. Geophys. Res., 88, 6611-6621, 1983.

Lee, J. J., G. E. Neely, S.C. Perrigan, and L. C. Grothaus, Effect of simulated sulfuric acid rain on yield, growth and foliar injury of several crops, Environ. Exp. Bot., 21, 171-185, 1981.

Lloyd, M. G., The contribution to dew to the summer weather budget of northern Idaho, Bull. Am. Meteorol. Soc., 42 (8), 572-580, 1961.

Long, I. F., Some observations on dew, Meteorol. Mag., 87, (1,032), 161-168, 1958.

Martin, L. R., Kinetic studies of sulfite oxidation in aqueous solution, in Acid Precipitation, edited by J. G. Calvert, Butterworth, Stoneham, Mass, 1983.

Moller, D., Kinetic model of atmospheric SO_2 oxidation based on published data, Atmos. Environ., 14, 1067-1076, 1980.

Monteith, J. L., Dew, J. Roy. Meteorol. Soc., 83, 322-341, 1957.

Mozurkewich, M., P. H. Murphy, A. Gupta, and J. G. Calvert, Mass accommodation coefficient for HO_2 radicals on aqueous particles, J. Geophys. Res., in press, 1987.

Mulawa, P. A., S. H. Cadle, F. Lipari, C. C. Ang and R.T. Vandervennet, Urban dew: Its composition and influence on dry deposition rates, Atmos. Environ., 20, 7, 1389-1396, 1986.

Neumann, J., Estimating the amount of dewfall, Archiv. Meteorol. Geophys. Bioklimatol., Ser. A, 9, 197-203, 1956.

Panofsky, H. A., and J. H. Dutton, Atmospheric Turbulence - Models and Methods for Engineering Applications, John Wiley, New York, 1984.

Pasquill, F., Some estimates of the amount and diurnal variation of evaporation from a clayland pasture in fair spring weather, J. Meteorol. Soc., 75, 249-255, 1949.

Penkett, S. A., B. M. R. Jones, K. A. Brice, and A. E. J. Eggleton, The importance of atmospheric ozone and hydrogen peroxide in oxidizing sulphur dioxide in cloud and rainwater, Atmos. Environ., 13, 123-137, 1979.

Pierson, W. R., W. W. Brachaczek, R. A. Gorse, Jr., S.M. Japar, and J.M. Norbeck, On the acidity of dew, J. Geophys. Res., 91, 4083-4096, 1986.

Pruppacher, H. R., and J. D. Klett, Microphysics of Clouds and Precipitation, 714 pp., D. Reidel Co., Hingham, Mass, 1978.

Schwartz, S. E., Mass-transport considerations pertinent to aqueous phase reactions of gases in liquid-water clouds, Chemistry of Multiphase Atmospheric Systems, NATO ASI Series, vol. 6, edited by W. Jaeschke, Springer Verlag, New York, 1986.

Schwartz, S. W., and J. E. Freiberg, Mass-transport limitation to the rate of reaction of gases in liquid droplets: Application to oxidation of SO_2 in aqueous solutions, Atmos. Environ., 15, 1129-1144, 1981.

Sheih, C. M., M. L. Weseley, and B. B. Hicks, Estimated dry deposition velocities of sulfur over the eastern United States and surrounding regions, Atmos. Environ., 13, 1361-1368, 1979.

Sigal, T., and J. W. Johnston, Jr., Effects of simulated acidic rain on one species each of pseudoparmelia, ushea, and umbilicaria, Water Air Soil Pollut., 27, 315-322, 1986.

Thornthwaite, C. W. and R. M. Holzman, Measurements of evaporation from land water surfaces, U.S. Dep. Agric. Tech. Bull., 817, 1942.

Walcek, C. J., R. A. Brost, J. S. Chang, and M. L. Weseley, SO_2 sulfate and HNO_3 deposition velocities computed using regional land use and meteorological data, Atmos. Environ., 20, 949-964, 1986.

Wells, W. C., Essay on Dew, T. Davidson, London 1814.

Welty, J. R., C. E. Wicks, and R. E. Wilson, Fundamental of Momentum, Heat, and Mass Transfer, 3rd ed. John Wiley, New York, 1984.

Weseley, M. L., and B. B. Hicks, Some factors that affect the deposition rates of sulfur dioxide and similar gases on vegetation, J. Air Pollut. Control Assoc., 27, 1110-1116, 1977.

Wisniewski, J., The potential acidity associated with dews, frosts, and fogs, Water Air Soil Pollut., 17, 361-377, 1982.

Wood, T., and F. H. Bormann, Increases of foliar leaching caused by acidification of an artificial mist, Ambio, 4, 169-171, 1975.

Zikeev, N. T., Annotated bibliography on dew, II, Meteorol. Geostrophys. Abstr. Bibliog., 3, 360-391, 1952.

W. L. Chameides, School of Geophysical Sciences, Georgia Institute of Technology, Atlanta, GA 30332

(Received April 15, 1987;
revised July 31, 1987;
accepted August 4, 1987.)

Ref. # JP8611432

Absorption Cross Sections and Kinetic Considerations of the IO species as Determined by Laser Flash Photolysis/Laser-Absorption Spectroscopy

R.E. Stickel, A.J. Hynes, J.D. Bradshaw,

W.L. Chameides and D.D. Davis*

School of Geophysical Sciences

Georgia Institute of Technology

Atlanta, GA 30332

In Press
J. Phys. Chem.

Abstract

Reported are independent measurements of the absorption cross section of the IO radical for the $A^2\Pi - X^2\Pi$ band system. A value of $(3.1 \pm 0.6) \times 10^{-17}$ cm^2 was observed for the (4,0) bandhead in good agreement with an earlier investigation. Results are also reported for the (5,0),(3,0), (2,0), and (1,0) bands over the wavelength range of 410 to 470 nm. However, no measurable ($<2 \times 10^{-18}$ cm^2) absorption was found for the (0,0) band. The atmospheric photodissociation rate constant, J_{IO}, for solar zenith angles of 0^o to 40^o was calculated to have a value of (0.06 ± 0.01) sec^{-1}. This value is a factor of five lower than previous estimates. Finally, the rate coefficient for the reaction IO + IO → products (3) has been measured at 760 torr N_2 and 300^oK. The measured effective bimolecular rate constant was found to be $(6 \pm 2) \times 10^{-11}$ $cm^3 \cdot molec^{-1} \cdot sec^{-1}$, in good agreement with recent results by Sander (1986).

Introduction

The role of iodine in tropospheric photochemistry has been the subject of speculation for several years.[1,2,3] It has been proposed, for example, that methyliodide as well as iodine in other chemical forms from marine sources or nuclear reactors can be photolyzed in the atmosphere to produce atomic iodine. It is further postulated that in the natural troposphere atomic iodine may participate in free radical driven chemical cycles that alter tropospheric levels of ozone, H_xO_y, and NO_x species[3]. Concerning the possible accidental release from nuclear reactors, the question posed is that concerning the atmospheric lifetime of radioactive iodine, and hence, its dispersal over large geographical areas via atmospheric transport processes.

The IO molecule has been identified as one of the key intermediates in the atmospheric iodine cycle [3,7,8]; thus, both its photolytic and gas kinetic lifetime are in need of careful evaluation. The solar photolysis of IO occurs primarily via the $A^2\Pi \leftarrow X^2\Pi$ band system in the 417 -470 nm spectral range. This system was discovered[4] and, analyzed[5,6] previous to 1961. However, no absolute photoabsorption cross section data were available until a low resolution spectrum was published in 1983[7]. Subsequently, the latter result has been substantially revised [8]. The present work includes an independent measurement, at higher resolution, that confirms the original study by Cox and Coker[7] while differing somewhat in the relative band intensities, particularly in regards to the (0,0) transition. The rotationally resolved (2,0) band spectrum presented here also supports the J-dependent predissociation suggested by a recent laser-induced fluorescence measurement[9].

Experimental

Iodine monoxide was photochemically generated in this study by the laser flash photolysis of ozone in the presence of iodine. The source mixture was prepared by mixing two flows of nitrogen carrier gas; one that had been passed through a trap containing reagent grade iodine crystals and the other that had

been doped with zero grade air and passed through a discharge-type ozone generator. The ozone and iodine concentrations were monitored via optical absorption at 254 nm ($\sigma = 1.13 \times 10^{-17}$ cm^2, ref. 10) and 500 nm ($\sigma = 2.19 \times 10^{-18}$ cm^2, ref. 11), respectively. As shown in Fig. 1, optical absorption measurements of IO were recorded using the output of a XeCl excimer pumped dye laser. The dye laser output bandwidth was approximately 0.01 nm (FWHM). The analysis beam was typically passed through the sample chamber 60 times using a White cell[15] configuration; however, the actual number of passes was limited by films forming on the AR coated chamber windows, presumably due to thermal reactions of the type:

$$I_2 + O_3 \rightarrow \text{Products}$$

The photolysis laser consisted of a KrF excimer laser which produced 30 mJ per pulse at 248 nm in a 12 mm x 12 mm beam. For absolute cross section measurements, the beam was apertured to 10mm x 10mm. The spatial homogeneity of the beam was verified by scanning a pinhole aperture across the beam profile and by inspecting burn patterns on photosensitive paper. Spatial variations were 10% or less. The photolysis energy was measured by a calibrated thermopile (Scientech) that was positioned immediately behind the sample cell. These raw measurements were then corrected for Fresnel losses using the measured transmissivity of the cell. Absorption of the photolysis beam by the sample gas was found to be negligible.

The total path length of the analysis beam through the photo active region of the sample chamber was defined by the product of the 10mm width photolysis beam and the number of passes through the chamber as determined both by direct count and by measurement of the time delay between input and output pulses. The validity of the latter approach was further confirmed by absorption measurements of NO_2 produced from the photolysis of HNO_3.

For relative cross section measurements the 10mm x 10mm aperture was removed and the thermopile was replaced by a mirror which reversed the

photolysis beam for a second pass through the sample, roughly doubling the IO concentrations. Stability of the [IO] was verified by frequent checks of the reference wavelength at 427 nm.

The pre-photolysis concentrations of I_2 and O_3 were varied over the range of 2.8 to 11×10^{14} molec.cm^{-3} and 1.7 to 4.3×10^{14} molec.cm^{-3}, respectively. In all cases the ozone level was near 1% of the oxygen level and the total pressure was ~ 760 Torr. The initial O atom concentration was computed as the product of the photolysis photon flux and an ozone absorption cross section [10] of $1.0 \times 10^{-18} cm^2.molec^{-1}$. The range of initial [O] observed was 2.7 to 4.5×10^{13} cm^{-3} with a single photolysis pass and roughly double that with two photolysis passes. Note that under our experimental conditions the primary process $O_3 + h\nu \xrightarrow{\lambda=248\ nm} O(^1D) + O_2$ results in the production of $O(^3P)$ within nanoseconds of the photoflash due to the rapid quenching by nitrogen. Thus, the formation of IO involved the reactions:

(1) $O(^3P) + I_2 \rightarrow IO + I$

and (2) $I + O_3 \rightarrow IO + O_2$

Other potentially important reactions in this system include:

(3) $IO + IO \rightarrow$ products (e.g. I_2O_2, $I_2 + O_2$, and/or $2I + O_2$)

(4) $O(^3P) + O_3 \rightarrow 2O_2$

(5) $O(^3P) + O_2 \xrightarrow{M} O_3$

and (6) $I + I \xrightarrow{M} I_2$

Results and Discussion

The rate equations resulting from reactions (1) through (6) were integrated numerically using a piecewise linear approximation[12] to determine the concentration of IO in time. The rate coefficients used in this analysis were $k_1 = 1.38 \times 10^{-10}$[13], $k_2 = 9.6 \times 10^{-13}$[8], $K_3 = 6 \times 10^{-11}$, $k_4 = 8.9 \times 10^{-15}$[14], $K_5 = 1.5 \times 10^{-14}$[14] and $K_6 = 9.3 \times 10^{-13}$[3]. All k values are expressed here in $cm^3 \cdot molec^{-1} \cdot s^{-1}$. The uppercase K's represent bimolecular equivalent k's using a third body N_2 concentration of 2.5×10^{19} $molec \cdot cm^{-3}$; however, K_3 represents the effective bimolecular K value, at one atmosphere pressure of N_2, that encompasses the three different product channels as shown in equation (1). The value used here for K_3 is based on curve fitting the observed temporal variation in the IO absorption with model curves using several different values of K_3. An example of such a comparison is illustrated in Fig. 2. For this experiment the initial I_2 and O concentrations were 6.2×10^{14} and 3.4×10^{13} $molec.cm^{-3}$ respectively. Each experimental point is an average of 15 individual absorbance measurements, each involving one photolysis pulse and two analysis/probe pulses. Although some of the values are negative none of them is more than one standard deviation below zero. The four smooth curves represent model results with K_3 values of 2, 4, 8 and 16($\times 10^{-11} cm^3 \cdot molec^{-1} \cdot s^{-1}$), respectively, from top to bottom.

From Fig. 2, two important findings are apparent. Firstly, with a factor of 8 change in K_3, the peak [IO] concentration varies from 79% to 95% of the initial [O]. The cross section values computed from these data are thus largely insensitive to errors in K_3. Secondly, at a total pressure of one atmosphere the value of K_3 of $\sim 2 \times 10^{-10} cm^3 \cdot molec^{-1} \cdot sec^{-1}$, published in earlier works[7,8], is clearly inconsistent with the observations of this work. The best fit to the current data from 7 experiments involving a range of [O] and [I_2] levels indicates a K_3 value of $(6 \pm 2) \times 10^{-11}$ $cm^3 \cdot molec^{-1} \cdot sec^{-1}$, in good agreement with the recent measurement by Sander[20].

Iodine monoxide cross sections as a function of wavelength were assembled by first measuring the (4,0) bandhead cross section and then scanning the remainder of the spectrum with frequent references to the (4,0) head. Fig. 3 shows a composite of this spectrum numerically smoothed to an effective resolution of 0.3 nm for comparison with a previously published spectrum[7]. The (4,0) band is virtually identical in both works, and the current value of $3.1 \pm 0.6 \times 10^{-17}$ cm^2 for the (4,0) band head also agrees very well with more recent results[20]. The relative intensities of the other bands are somewhat different from those of ref.(7), but the most striking discrepancy is the absence of the (0,0) band in the present work. Taking the noise level in the present data as an upper bound yields a (0,0) bandhead cross section of $< 2 \times 10^{-18}$ cm^2 or roughly 20 times below the value observed here for the (2,0) head. A theoretical estimate of the Franck-Condon factors(16) results in a predicted 9:1 ratio and a laser-induced fluorescence observation revealed the (0,0) band to be less than one tenth the (2,0) intensity(9). However, interpretation of the latter result[9] is complicated by the predissociation of the $A^2\Pi$ state. In fact, the apparent rotational temperature of 70°K exhibited by the fluorescence spectrum was ascribed to a rotational dependence in the predissociation. This hypothesis would seem to be confirmed by the high resolution (2,0) band spectrum shown here in Fig. 4 which compares favorably to the 300°K prediction of ref. 9. The fluorescence spectrum of the (0,0) band was observed to have a more normal 300°K distribution suggesting that the (2,0) band may lose more in intensity to predissociation than the (0,0) transition, making the (0,0) band relatively more prominant in fluorescence than in absorption. The latter argument would seem to be in agreement with the current result.

The (3,1) band has been included in Fig. 3 but the relative intensity can not be interpreted in a straightforward manner because of the transient character of the vibrationally excited ground state. This band was not included in our estimate of the solar photolysis rate. An absorption feature near 410

nm, consistent with the (6,0) band of IO, was observed but a positive identification was not possible. This new band was well below the (5,0) band in intensity and did not contribute substantially to the evaluation of the atmospheric photolysis rate.

The rate of IO photolysis in the troposphere has been estimated from the data of Fig. 3 and the calculated solar fluxes from Peterson[19]. The resulting J value is 0.06 $\pm$0.01 s^{-1} for solar zenith angles from 0^0 to 40^0 and declines to 0.04 $\pm$ 0.01 s^{-1} at 80^0. This value differs sharply from the value of 0.3 reported by Cox and Coker[7]. Apparently there are two sources for this discrepancy. Firstly, the average cross section values of Table II in Cox and Coker's work seem to be inconsistent with the data they present in their Fig. 1 which displays the IO cross section vs. wavelength. Secondly, they observed a greater degree of absorption between the individual IO bands than was seen in the present work.

The impact of our reported values of K_3 and J_{IO} on the tropospheric photochemistry of iodine will be addressed in a subsequent publication. The authors note, however, that meaningful modelling evaluations of this system must deal with not only new values for $J_{(IO)}$ and K_3 but must also assess the atmospheric photochemical fate of other key iodine species such as I_2O_2 and HOI, as well as various possible gas kinetic processes involving these same species. At this time, information on both I_2O_2 and HOI appears to be very limited and new studies, relevant to natural atmospheric conditions, would seem to be needed.

Acknowledgements

The authors would like to thank S. Fischer for providing the computer program used to integrate the kinetic rate equations. We also acknowledge the support of this research by NSF Grant #ATM 8113237.

References

1) Moyers, J.L.; and R. A. Duce, J. Geophys. Res. 1972 ,77, 5229.

2) Zafiriou, O.C., J. Geophys. Res., 1974, 79, 2730 .

3) Chameides, W.L.; and D. D. Davis, J. Geophys. Res., 1980, 85, 7383 .

4) Vaidya, W.M., Proc. Ind. Acad. Sci. 1937, 6A, 122.

5) Coleman, E.H.; A.G. Gaydon and W.M. Vaidya, Nature, 1948, 162, 108 .

6) Durie, R.A.; F. Legay and D.A. Ramsay, Can. J. Phys., 1960, 38, 444 .

7) Cox, R A.; and G.B. Coker, J. Phys. Chem., 1983, 87, 4478 .

8) Jenkin, M.E.; and R.A. Cox, J. Phys. Chem., 1985, 89, 192 .

9) Inoue, G.M.; Suzuki and N. Washida, J. Chem. Phys., 1983, 79, 4730 .

10) Griggs, M.J.; J. Chem. Phys., 1968, 49, 857 .

11) Tellinghuisen, J.; J. Chem. Phys., 1973, 58, 2821 .

12) Hesstvedt, E.O.; Hov and I.S.A. Isaksen, Int. J. Chem. Kinet., 1978, 10, 971

13) Ray, G.W.; and R.T. Watson, J. Phys. Chem., 1981, 85, 2955 .

14) JPL, Publication 81-3, "Chemical Kinetic and Photochemical Data for use in Stratospheric Modeling - Evaluation Number 4: NASA Panel for Data Evaluation", Jet Propulsion Laboratory, California Institute of Technology, Pasadena, CA, 1981.

15) White, J.U.; J. Opt. Soc. Am., 1942, 32, 285 .

16) Rao, M.L.P.; D.V.K. Rao and P.T. Rao, Phys. Lett., 1974, A50, 341 .

17) Moyers, J.L.; and R. A. Duce, J. Geophys. Res., 1972, 77, 5229 .

18) Zafiriou, O.C.J.; J. Geophys. Res., 1974, 79, 2730 .

19) Peterson, J.P.; EPA Report 600/4-76-025, U.S. EPA, Research Triangle Park, NC, 1976, "Calculated Actinic Fluxes (290-700 nm) for Air Pollution Photochemical Applications".

20) Sander, S.P.; J. Phys. Chem., 1986, 90, p. 2194 .

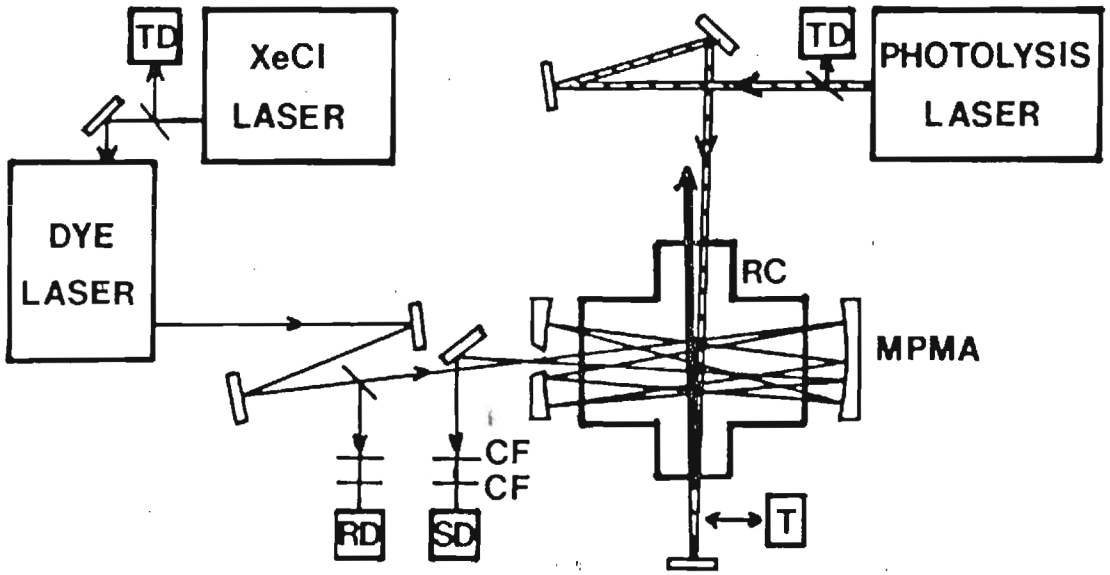
TD
XeCl
LASER
TD
PHOTOLYSIS
LASER
DYE
LASER
RC
MPMA
CF
CF
RD
SD
T

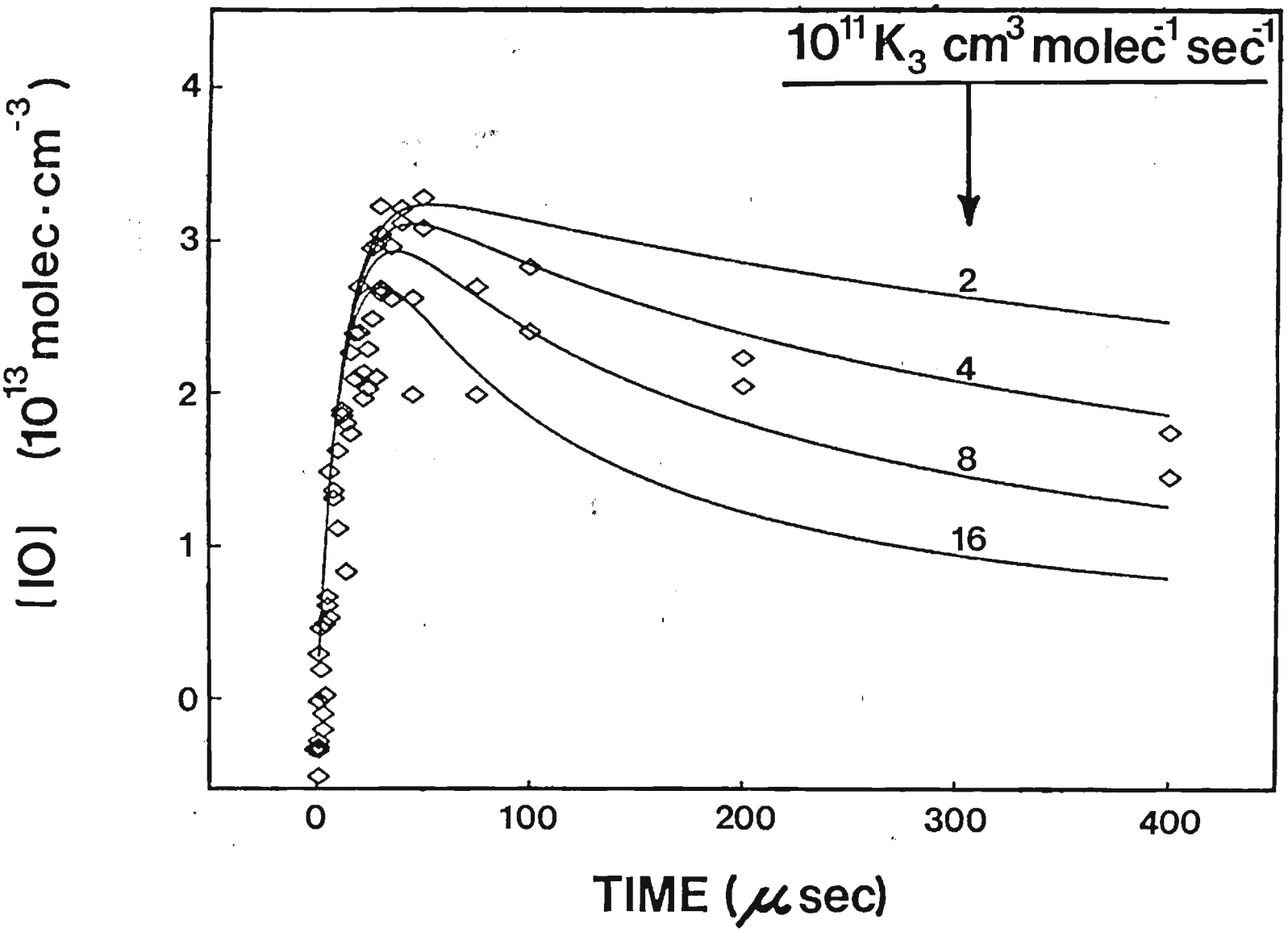
$10^{11} K_3$ cm^3 molec^{-1} sec^{-1}
2
4
8
16
[IO] (10^{13} molec·cm^{-3})
0
1
2
3
4
0
100
200
300
400
TIME (μsec)

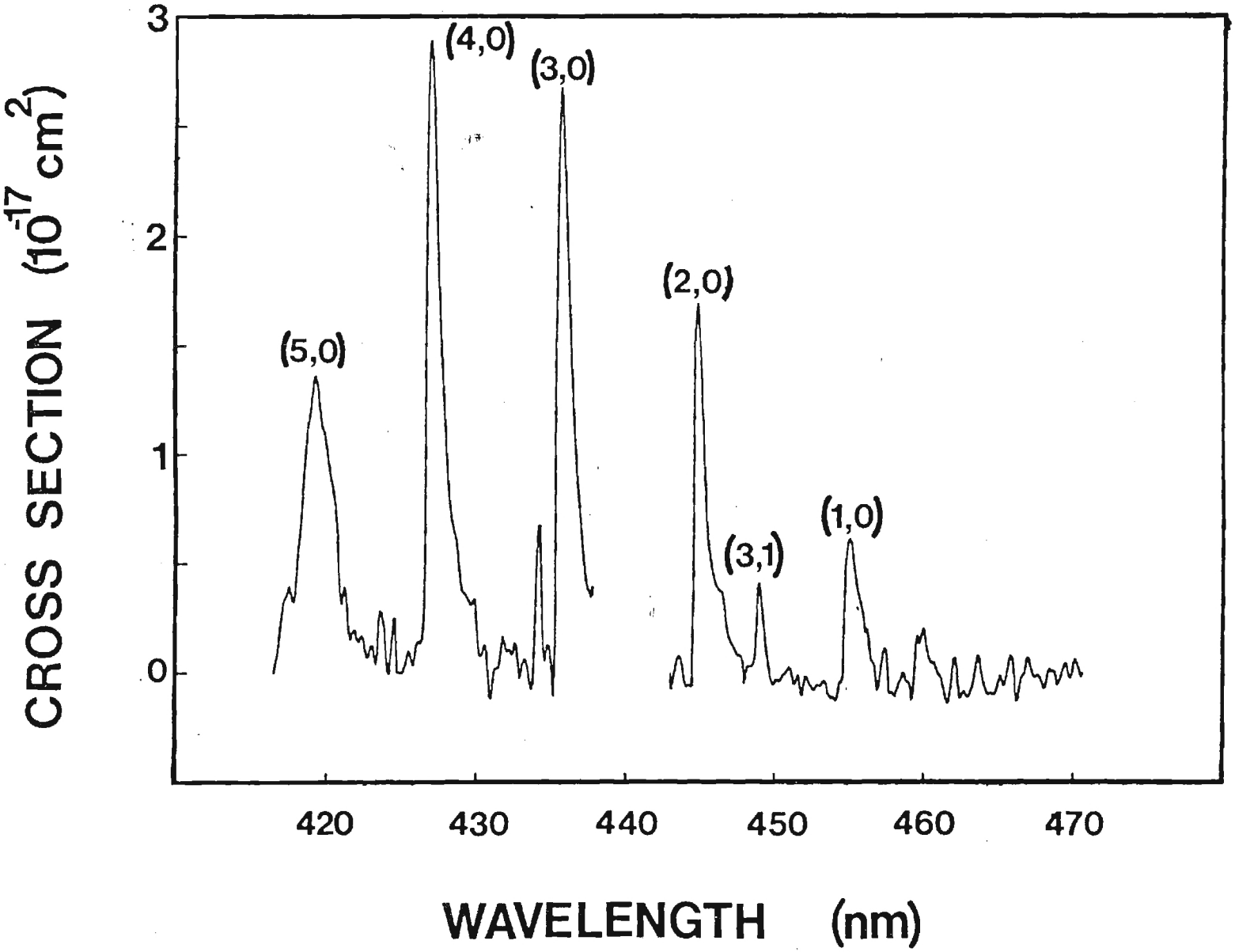
CROSS SECTION (10^{-17} cm^2)
3
2
1
0
(4,0)
(3,0)
(5,0)
(2,0)
(3,1)
(1,0)
420
430
440
450
460
470
WAVELENGTH (nm)

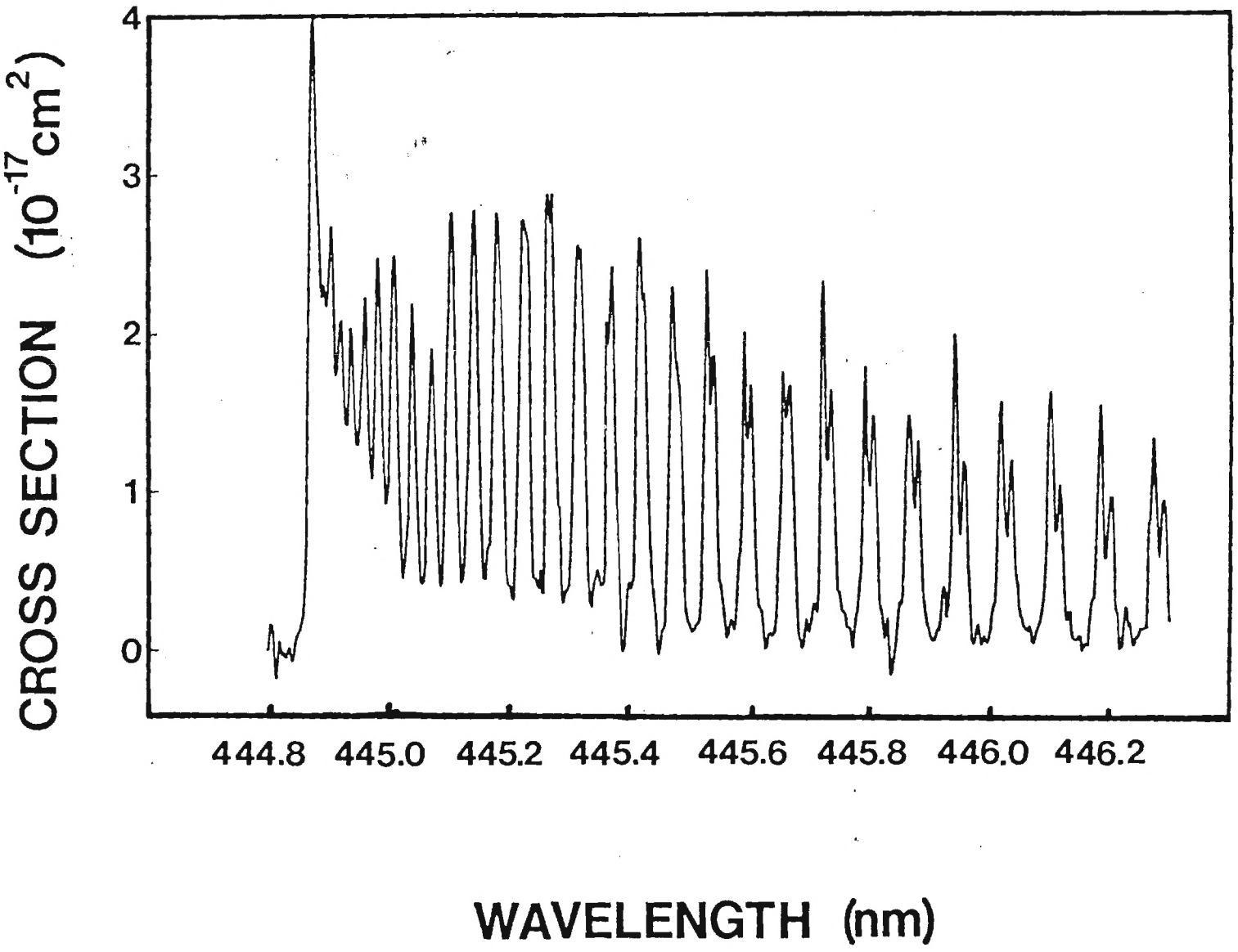
CROSS SECTION (10^-17 cm^2)
4
3
2
1
0
444.8
445.0
445.2
445.4
445.6
445.8
446.0
446.2
WAVELENGTH (nm)

Figure Captions

Fig. 1. Laser flash photolysis/laser-absorption spectroscopy hardware: RC - reaction cell, MPMA - multipass mirror assembly, RD - reference photodiode, SD - signal photodiode , TD - timing diode, T - thermopile, CF - color filters.

Fig. 2. Profile of IO build-up and decay due to the reactions $O(^3P) + I_2$, $I + O_3$, and IO + IO → products.

Fig. 3. Medium resolution plot of the IO absorption cross section versus wavelength for the (5,0),(4,0),(3,0),(2,0),(1,0), and (3,1) bands, resolution .3 nm.

Fig. 4. High resolution plot of IO(2,0) band, .025 nm

High Ozone Events in Atlanta, Georgia in 1983 and 1984

Ronald W. Lindsay
William L. Chameides*

School of Geophysical Sciences
Georgia Institute of Technology
Atlanta, GA 30332

IN PRESS
ENVIRONMENTAL SCIENCE AND
TECHNOLOGY

October 13, 1987

Abstract

Measurements of ozone levels and meteorological parameters were analyzed to determine the relative importance of transport related processes and photochemical production in causing high ozone events in and around the Atlanta metropolitan area. Back trajectories calculated using the Branching Air Trajectory Model indicate that the air associated with high ozone events had often travelled a significant distance within the previous three days: for days with ozone levels above 100 ppbv, half of the calculated trajectories showed that the air had traveled over 600 kilometers, with one half of those coming from the northwest quadrant. Six hour vector averaged winds were used to find that the concentrations of ozone in the air leaving the metropolitan area averaged 20 to 40 ppbv more than that entering the area.

Introduction

The southeastern United States is one of the fastest growing areas of the country. In large part as a result of this growth, major population and industrial centers in the Southeast have begun to experience air quality degradation similar to that which has for many years plagued urban areas in the northern and western United States. This study examines the surface ozone concentrations in and around the Atlanta area in order to determine what proportion of the ozone concentration measured during high concentration days can be attributed to (a) local photochemical production within the metropolitan area, (b) long-range transport of ozone and its precursors from distant sources, and (c) natural sources. We investigate the nature of regional ozone events, the origin and chemical character of air entering the metropolitan area during such events, and the net effect of the metropolitan area on the air as it passes over the city.

The Atlanta area is different from many other cities afflicted with high ozone concentrations in that it is free of confining topographical barriers and is relatively isolated from other large cities. Often during the summer months there is significant instability in the lower atmosphere that helps to ventilate the mixed layer. High ozone events occur when a high pressure system dominates the region and suppresses convection. The summertime winds are usually light, but stagnant air from distant source regions such as the Midwest or Northeast can sometimes be brought into the airshed.

There is ample evidence for the importance of long-range transport in causing regional ozone events in the eastern United States. Vukovich et al. (1) showed that high levels of ozone over the Northeast occur on the back sides of transitory anticyclones, in air that has resided over populated areas for several days. Wight et al. (2) also showed how clean air enters the Midwest as an anticyclone from western Canada and accumulates pollution as it moves slowly across the Northeast, with the worst ozone concentrations found, again, on the back side of the anticyclone. Vukovich and Fishman (3) presented a climatology of summertime ozone levels from rural stations in the eastern U.S. and showed that wide areas with monthly averages above 70 ppbv are not uncommon, compared to levels of 40 to 50 ppbv in the west and near the southern coast. They showed that when the paths of major migratory high-pressure systems remained in the northern portion of the country, the Southeast was largely spared from high ozone concentrations; but when the migratory high-pressure systems passed through the central or southern portion of the country, the centers of high ozone shifted into the south. They drew an important distinction between these migratory anticyclones and the quasi-stationary Bermuda High that is centered off the East Coast in the summer months and dominates the mean pressure analyses, but is not necessarily associated with high ozone events. The climatological study of Zishka and Smith (4) showed that July anticyclones commonly originated in western Canada and traversed the northeastern portion of the United States along the 40th parallel. Rarely were they seen to drop below the 35th parallel, so that the south is largely spared from the migratory anticylcones that Vukovich and Fishman (3) associate with regional high ozone events.

Our study focuses on both the back trajectories of high ozone days and on the analysis of the surface wind observations. We address four key questions: Where has the air of high ozone episodes in Atlanta come from? How do the back trajectories for high ozone days differ from those of low ozone days? What is the ozone concentration of the air entering the city on episode days, and what is it as the air leaves? And what is the typical ozone budget for episode days, i.e. what proportion can be attributed to (a) local production, (b) long-range transport, and (c) natural sources?

Ozone Data

The hourly averaged ozone concentrations from the three urban and suburban monitoring stations in the Atlanta area were obtained from the Georgia Department of Natural Resources for the period of May through November, 1983 and 1984. These stations are South DeKalb Community College, located just southeast of the center of the metropolitan area; Conyers, 25 kilometers to the east of DeKalb; and Dallas, 60 kilometers to the northwest. Figure 1 shows the location of the three stations, the perimeter freeway that encircles much of the metropolitan area, the major freeways that enter the area, and Hartsfield Atlanta International Airport, from which we obtained the surface winds. Suburban communities extend beyond the perimeter, but are in general closer to the perimeter than the two suburban ozone monitoring stations. The stations are well situated to monitor the effect of the metropolitan area on ozone concentrations for the dominant northwest and east winds, but poorly placed for south or north winds.

The maximum daily ozone concentrations between the hours of 9:00 a.m. and 8:00 p.m. were extracted from the time series, excluding days in which the maximum was at the beginning or at the end of a break in the data. As an example of the time series, the daily maxima for the three Atlanta area stations during July and August of 1983 are plotted in Figure 2. We see that there were two extended episodes of high ozone concentrations, one in mid-July and the other in mid-August. These two months contributed 22 of the 32 days in 1983 and 1984 on which the ozone concentrations exceeded the National Ambient Air Quality Standard (NAAQS) of 120 ppbv. 1983 was the worst year for violations of the NAAQS in the seven-year period of 1979 to 1986 for which we have records: over the course of that year, there were 24 days above 120 ppbv. In the fourteen months of the record (428 days) there were 154 days (36%) on which the concentration at one of the three stations was greater than or equal to 80 ppbv, and 70 days (16%) on which it was greater than or equal to 100 ppbv.

BAT model

The Branching Air Trajectory (BAT) model was obtained from the National Climatic Data Center along with 1983 and 1984 radiosonde data for North America. The model is described by Heffter (5). It uses the conventional National Weather Service (NWS) radiosonde network for input data, restricts the tracked air mass to the mixed layer and below 3000 meters, and allows each trajectory to branch into as many as three different layers, thereby reflecting the isolation of the high layers from the surface during the night. Up to 20 different branches are tracked simultaneously. The BAT model was modified to produce back trajectories for one parcel a day,

tracing its progress backwards for three days starting at 1700 EST. Only radisondes within the map area shown in Figures 3-6 were used as input data; any branches that left the map area were dropped. Lost branches were of particular importance to the south, where the boundary of the model area was chosen to be just off the coast since there were no observations south of it. Branches were also dropped if they contained less than 5% of the original mass of the air parcel.

It should be noted that significant uncertainties are associated with back trajectory calculations using conventional meteorological data. For example, Kahl and Samson (6) found that boundary layer trajectories calculated with the current NWS network of radiosondes with twelve-hour resolution have a 50% chance of exceeding horizontal displacement errors of 200 kilometers after 24 hours, 280 kilometers after 48 hours, and 350 kilometers after 72 hours of travel time. However, while the uncertainty of any one trajectory calculation is large, we believe that by determining a large number of back trajectories some insight into the typical past history of air over the Atlanta area during event and non-event days can be obtained.

The maximum daily ozone concentration of the three stations near Atlanta was used to rank the days in decreasing order. The back trajectories for the ten days with the highest ozone concentrations are shown in Figure 3. The three points plotted for each day represent the position of the center of mass of the trajectory after one, two, and three days. All of the trajectories converge, of course, on Atlanta, which is indicated with a circle. In the lower right corner of the figure are the date (YYMMDD), the

maximum ozone concentration (ppbv), and the percent of the mass remaining for each trajectory at the end of each day.

The two worst days are examples of two extreme varieties of trajectories. July 15, 1983 saw ozone concentrations peak at 194 ppbv, and the air showed very little movement over the previous three days. In contrast, July 11, 1983, with 174 ppbv ozone, showed little movement over the previous day but moderately strong motion during the two days before; this movement brought air into the Atlanta area from the population and industrial centers of the Midwest and the Ohio Valley near the beginning of the nineteen-day episode of high ozone levels seen in July.

The episode in July 1983 was one of the worst in several years and is a good illustration of how a mix of transport and stagnation can contribute to such episodes. Figure 4 shows the three-day back trajectories for the first ten consecutive days of a sixteen-day period in mid-July with maximum ozone concentrations above 100 ppbv. Some days, such as the 15th, showed significant movement over the previous three days, while the bulk of the trajectories showed little net motion. Most of the trajectories moved in a southerly or southeasterly direction, reflecting the presence of the center of an anticyclone to the west. The surface weather maps for this period show a persistent high pressure center that moved slowly from the Northeast, stalled west of Atlanta for five days when the highest concentrations were registered, and then drifted to the south and again stalled south of Louisiana. This is in contrast to the findings of Vukovich et al. (1) and Wight et al. (2) that the the strongest pollution episodes in the Northeast occur on the back side, or western side, of anticyclones;

in this case we find that the worst episode occurred on the eastern flank of the system. The relatively uncommon episodes of prolonged high ozone concentrations in Atlanta reflect the rare occurrence of a migratory high pressure center to the west of the Atlanta metropolitan area (4). More commonly the area is dominated in the summer by the Bermuda High, usually found to the east and bringing air into the area from the south. This air from the south tends to be relatively pollution-free as well as moist; the moisture contributes to convective storms that help to ventilate the mixed layer.

In order to compare the typical movement of air on event and non-event days, three-day back trajectories were calculated for all of the days in the three summer months (June, July and August) for both 1983 and 1984, a total of 184 days. The days were divided into quartiles based on their rank in ozone concentration. The first quartile is the 25% of the days with the highest ozone concentrations (110 to 194 ppbv) and the last quartile is the 25% with the lowest concentrations (24 to 64 ppbv). There were 46 points in each quartile. In Figure 5, the position of the center of mass of all branches of each back trajectory is plotted after one day for both the first and the last quartiles. Note that the high ozone days are clustered nearer to Atlanta, reflecting the generally light winds associated with high ozone measurements. The high ozone days also come predominantly from the north and west, although no direction is completely excluded. The low ozone days show much larger travel distances and the air comes predominantly from the south.

Figures 6a, 6b, and 6c show the positions of the center of mass of each back trajectory for all days in which the maximum ozone concentration was greater than 100 ppbv after one, two, and three days. The median distance traveled after one day was 200 kilometers, after two days 400 kilometers, and after three days 600 kilometers. Of the 22 trajectories that had traveled 600 kilometers in three days, 11 had come from the northwest quadrant, 5 from the northeast, 4 from the southwest and 2 from the southeast. This dominance of trajectories originating in the Midwest is apparent in Figure 6c where we see a concentration of points indicating air coming from the Ohio Valley region. The inventories of hydrocarbons and NO_x of both Benkovitz (8) and Clark (9) indicate that this region is in fact a strong source area for these ozone precursors. The studies of Wight et al. (2) and Wolff et al. (7) also show evidence of the Ohio Valley being an important source area for regional high ozone episodes in the entire eastern United States.

The BAT back trajectories indicate that about half of the days with high ozone concentrations were characterized by air that had moved a substantial distance over the three previous days; of those, about half had come from the northwest. Days with low concentrations of ozone are generally characterized by much greater air movement than the high ozone days and the air more often appears to have come from the south. The fact that the air of many high ozone days originated in the Midwest is a strong indication that on occasion long-range transport of ozone and ozone precursors is contributing to the ozone concentrations seen in Atlanta.

Surface Wind and Ozone Relations

Because of the uncertainties in the trajectory calculations and the large distance to the nearest radiosonde station (Athens, Georgia, 100 kilometers to the east), the surface winds from Hartsfield Atlanta International Airport were used to further define the nature of ozone events in the Atlanta area. Figure 7 shows a wind rose of the six-hour vector averaged afternoon (1200 - 1700 EST) surface winds from the airport for the period during which the ozone measurements were made (May - November, 1983 and 1984). There is a predominance of northwest winds with a secondary peak for east winds. Figures 8a and 8b summarize the afternoon winds of days in which the ozone concentrations at Dallas and Conyers exceeded 100 ppbv. We can see that the two suburban stations are directly affected by the urban plume. In Dallas, which is northwest of the city, concentrations were in excess of 100 ppbv mostly for days with calm winds and winds from the east; in Conyers, which is southeast of the city, ozone concentrations were in excess of 100 ppbv predominantly for days with winds from the west and northwest. There were also a number of days with high ozone concentrations in Dallas when winds were from the west and northwest. These days included occasions when the BAT calculations show that the air had come from distant source regions as well as occasions when the air had reentered the city after a period of near calm or after a wind reversal.

Other studies have provided direct measurements of the urban plume downwind of Atlanta. In a 1981 field study for the EPA, Westberg and Lamb (10) found that a well-defined plume was often observed 50 to 75 kilometers downwind from the city center. Ozone levels of 130 to 160 ppbv were commonly observed at levels of 500 to 800 meters above the ground on ten

different afternoon flights. For example, on one day the plume at 40 kilometers from the city center was some 50 kilometers wide with surface winds about 3 m s^{-1} from the north-northwest.

Lying outside the metropolitan area, Dallas and Conyers are well situated to provide a comparison between the incoming and the outgoing air for the predominant northwest and east winds. Figure 9 shows the difference in ozone levels at Conyers and Dallas for each wind direction sector and for three different levels of ozone concentrations: both stations less than 80 ppbv, at least one station greater than 80 ppbv, and at least one station greater than 100 ppbv. At the bottom of the figure are listed the number of observations in each sector, the mean differences, and the standard deviations of the differences. We see that the northwest winds bring ozone levels 20 to 45 ppbv higher at Conyers than at Dallas during episode days (> 100 ppbv) and east winds bring similar differences in the opposite sense. However, on non-episode days (< 80 ppbv) there is little average difference between the two stations for all wind directions.

This change in the ozone concentration with wind direction is further summarized in Table I, where the wind is divided into east and west components and stratified by wind speed. We see that for near-calm winds there is little difference between the two stations. But with winds greater than 2 m s^{-1} and ozone levels above 80 ppbv at one of the two stations, the downwind station is 20 to 40 ppbv higher than the upwind station. Further stratification of the results by wind speed did not reveal any significant trend with wind speed for winds greater than 2m s^{-1}. For all speeds greater than 2 m s^{-1} and ozone levels above 80 ppbv, there is 30 ppbv more ozone measured at Conyers than at Dallas for west winds and

20 ppbv more at Dallas than at Conyers for east winds. These values rise to 38 ppbv and 27 ppbv respectively for days with ozone levels above 100 ppbv. Also of interest are the relatively high values of the ozone concentration at the upwind station: 78 ppbv at Dallas for west winds and 90 ppbv at Conyers for east winds on moderate (> 80 ppbv) days, and 86 ppbv and 81 ppbv respectively on the high concentration (> 100 ppbv) days. These levels indicate that high ozone air is entering the area either (a) from long-range transport of pollution from other urban and industrial centers, (b) from local air already burdened with ozone reentering the city after a reversal in wind direction, and/or (c) from ozone produced rurally in conditions favorable to photochemical production. Progressive vector diagrams of the surface winds indicate that some of the cases in which ozone concentrations at the upwind station were high or actually exceeded those at the downwind station did indeed occur on days following wind reversals. Moreover, such wind reversals are not uncommon.

In order to better characterize the source of the apparent excess ozone entering Atlanta on high ozone days, we have also examined ozone measurements obtained at Leslie, a rural ozone-monitoring station in southwestern Georgia 125 kilometers south of Atlanta. On days when one of the three Atlanta area stations was above 100 ppbv and the winds were out of the west greater than 2 m s^{-1}, the ozone concentration at Leslie averaged 65 ppbv. This compares to the average of 85 ppbv measured at Dallas on similar days, implying that Dallas was some 20 ppbv greater than the rural background level. Moreover, the 65 ppbv measured at Leslie on these days is about 20 ppbv above the two-year mean for this rural station. Thus we find that there was a 20 ppbv enhancement of the ozone

concentration in the rural parts of the region during ozone episodes in Atlanta, and the air entering the Atlanta metropolitan area was another 20 ppbv above this level. The addition of almost 40 ppbv as the air crossed over the city, as discussed above, brought the ozone concentrations in excess of the National Ambient Air Quality Standard (see Table 1) during these episodes.

Conclusions

Both the trajectory analysis and the surface winds indicate that days of high ozone concentrations are often characterized by low winds. Though the wind speeds are not great, rarely exceeding 5 m s^{-1}, back trajectory calculations indicate that there is sometimes significant transport of air over the preceding three days. Half of the trajectories for days over 100 ppbv had moved over 600 kilometers in the three days before; of these, half had come from the northwest quadrant. The movement appears to be bringing high levels of ozone and/or ozone precursors into the region. On those days in which there was more than 100 ppbv ozone in Atlanta and the air had traveled over 600 kilometers from the northwest, we find that the average ozone concentration at the rural station of Leslie was 82 ppbv (n=8) versus 65 ppbv (n=47) for all days over 100 ppbv in Atlanta. This suggests that sometimes the air coming from the northwest is indeed bringing with it enhanced levels of ozone and ozone precursors and affecting a large portion of the state.

An approximate ozone budget for the Atlanta metropolitan area during the summers of 1983 and 1984 is as follows: the rural background level for

all wind directions during episode days (greater than 100 ppbv at one of the Atlanta area stations) is near 65 ppbv, well above the mean rural level of about 45 ppbv due to the photochemical production of ozone from natural sources, from sources in small towns and cities, and from distant large sources; the upwind station measured 15 to 20 ppbv more than the rural background due to the recycling of metropolitan air after previous calm conditions, from wind reversals, or from long-range transport, bringing the concentration up to 80 or 85 ppbv; during the passage over the city, the ozone concentration is further increased by 30 to 40 ppbv, bringing the total to 110 to 125 ppbv. Thus it appears that the one-day production of ozone from the precursors emitted in the metropolitan area is insufficient to raise the ozone concentrations all the way from the rural level (about 65 ppbv on ozone event days) to the NAAQS level of 120 ppbv; instead, the air entering the city must already be elevated in ozone in order for the air in Atlanta and/or leaving Atlanta to exceed the NAAQS for ozone.

The 30 to 40 ppbv increase in the ozone concentration as the air passes over the city is similar to a value cited for Detroit. In a 1981 study of the Detroit area, Kelly et al. (11) looked at the days in the first (highest) quartile of the daily maximum hourly ozone levels measured at sixteen sites. The site with the maximum mean (of the first quartile days, 104 ppbv) was 57 ppbv more than that of mid-morning air at the site with the lowest concentrations (47 ppbv) and this value was attributed to the photochemical production of ozone in the Detroit plume. The mid-morning value was considered representative of the boundary layer air before significant photochemical production could occur. If the first quartile mean daily maximum of the low concentration station (73 ppbv) were

used instead of the mid-morning mean, an increment due to the city of only 31 ppbv would have been found. This lower value would be the additional ozone formed during the day due to the presence of the city and is more comparable to the calculation we have made, both in the way it is done and in the magnitude.

The elevated ozone levels of the air entering the city on high ozone days can result from a variety of causes that may vary considerably from one year to the next, with little or no correlation to the photochemical activity of the city itself. For this reason we do not believe that a reliable indication of photochemical smog production from Atlanta-based sources can be obtained by simply monitoring the number of days per year that O_3 in and around the Atlanta area exceeds the NAAQS. A far more reliable indication may possibly be obtained by monitoring the difference between the ozone level in air leaving Atlanta from that entering Atlanta. In the summers of 1983 and 1984, our study indicated that for high ozone days the air leaving the city had an ozone concentration some 30 to 40 ppbv greater than the air entering the city. We believe this increment is a good indication of the impact of the metropolitan area on air quality. Monitoring the variation of this increment from year to year may provide a useful and accurate means of determining the efficacy of air pollution control efforts within this area.

Acknowledgment

The authors wish to express their gratitude to Drs. Robert H. Collom, Jr., and William Estes of the Georgia Department of Natural Resources for their helpful discussions and for providing us with the ozone data from Georgia.

Table I. Conyers and Dallas Ozone Levels for East and West Winds and Different Wind Speeds

	Ozone < 80 ppbv		Ozone > = 80 ppbv		Ozone > = 100 ppbv	
	West	East	West	East	West	East
Calm: SPD < 2 m s^{-1}						
N	9	10	9	10	5	3
CN	54	62	95	84	105	90
DL	42	61	89	94	104	113
CN - DL	12	1	6	-10	1	-23
SPD ≥ 2 m s^{-1}						
N	101	74	48	32	27	8
CN	50	47	108	69	124	81
DL	44	51	78	89	86	108
CN- DL	6	-3	30	-20	38	-27

(N = number of observations, CN = Conyers, DL = Dallas, SPD = wind speed at Hartsfield Airport, concentrations in ppbv)

Literature Cited

(1) Vukovich, F.M.; Bach, D.W. Jr.; Crissman, B.W.; King, W.J. Atmos. Environ., 1977, 11, 967-983.

(2) Wight, G.D.; Wolff, G.T.; Lioy, P.J.; Meyers, R.E.; Cederwall, R.T. Air Quality Meteorology and Atmospheric Ozone, ASTM STP 653, A.L. Morris and R.C. Barris, eds., American Society for Testing and Materials, Philadelphia, PA, 1978, 445-457.

(3) Vukovich, F.M.; Fishman, J. J. Atmos. Environ., 1986, 12, 2423-2433.

(4) Zishka, K.M.; Smith, P.J. Mon. Wea. Rev., 1980, 108, 387-401.

(5) Heffter, J.L. NOAA Technical Memoranda ERL ARL - 121, 1983, 16 pp.

(6) Kahl, J.D.; Samson, P.J. J. Clim. and Appl. Meteorol., 1987, 25, 1816-1831.

(7) Wolff, G.T.; Kelly, N.A.; Ferman, M.A. Water, Air and Soil Pollution, 1982, 18, 65-81.

(8) Benkovitz, C.M. Atmos. Environ., 1982, 16, 1551-1563.

(9) Clark, T.L. Atmos. Environ., 1980, 14, 961-970.

(10) Westberg, H.; Lamb, B. Unpublished report to EPA from the Laboratory of Atmospheric Research, Washington State University, Pullman, Washington, 1985.

(11) Kelly, N.A.; Ferman, M.A.; and Wolff, G.T. J. Air Pollution Control Ass., 1986, 36, 150-158.

This work was supported in part by funds from the National Science Foundation under Grant # ATM-8600888.

Figure captions

1. Map of the Atlanta metropolitan area showing the locations of the ozone monitoring stations Dallas, South DeKalb, and Conyers, and the National Weather Service observing station at Hartsfield Atlanta International Airport.

2. Maximum daily ozone concentrations for three stations: South DeKalb, Conyers and Dallas, July and August, 1983.

3. Positions of the center of mass of the trajectory branches at the end of one, two and three days for the top 10 days in ozone concentration. The date (YYMMDD), maximum ozone concentration (ppbv), and the remaining mass (%) for each of the three days are listed in the corner.

4. Positions of the center of mass of the trajectory branches at the end of one, two and three days for 10 consecutive days in July 1983 with ozone concentrations above 100 ppbv. The date (YYMMDD), maximum ozone concentration (ppbv), and the remaining mass (%) for each of the three days are listed in the corner.

5. Positions of the center of mass of the trajectory branches for the first and last quartiles of ozone concentration at the end of the first day.

6. (a-c) Positions of the center of mass of the trajectory branches for all days with ozone concentrations greater than 100 ppbv after one, two, and three days.

7. Windrose of afternoon (12-17 EST) vector averaged winds for 1983 and 1984, 8 months each year.

8. a) Windrose of afternoon (12-17 EST) winds for days with ozone concentrations greater than 100 ppbv at Dallas.
   b) Windrose of afternoon (12-17 EST) winds for days with ozone concentrations greater than 100 ppbv at Conyers.

9. Bar graph of the mean Conyers-Dallas ozone concentration difference for each wind direction sector and for the maximum ozone level of the two stations < 80, > 80, and > 100 ppbv. The number of observations, the mean difference, and the standard deviation of the difference are given for each direction and concentration class.

Atlanta Metropolitan Area

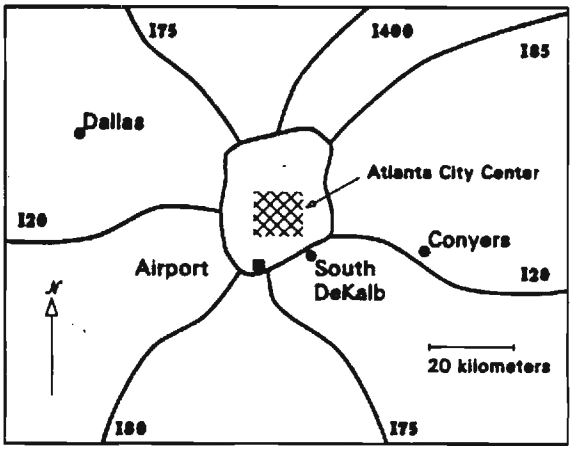

Map of the Atlanta metropolitan area showing the locations of the ozone monitoring stations Dallas, South DeKalb, and Conyers, and the National Weather Service observing station at Hartsfield Atlanta International Airport.

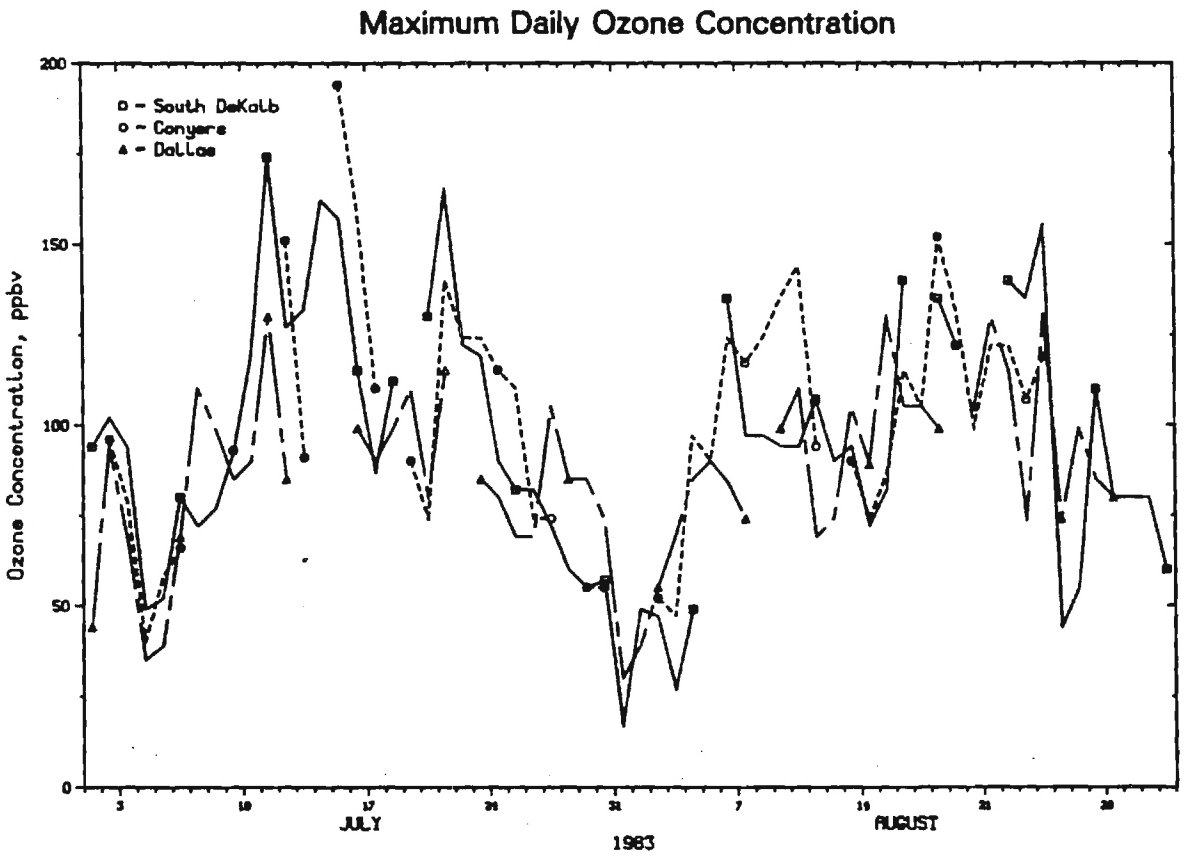

Maximum daily ozone concentrations for three stations: South DeKalb, Conyers and Dallas, July and August, 1983.

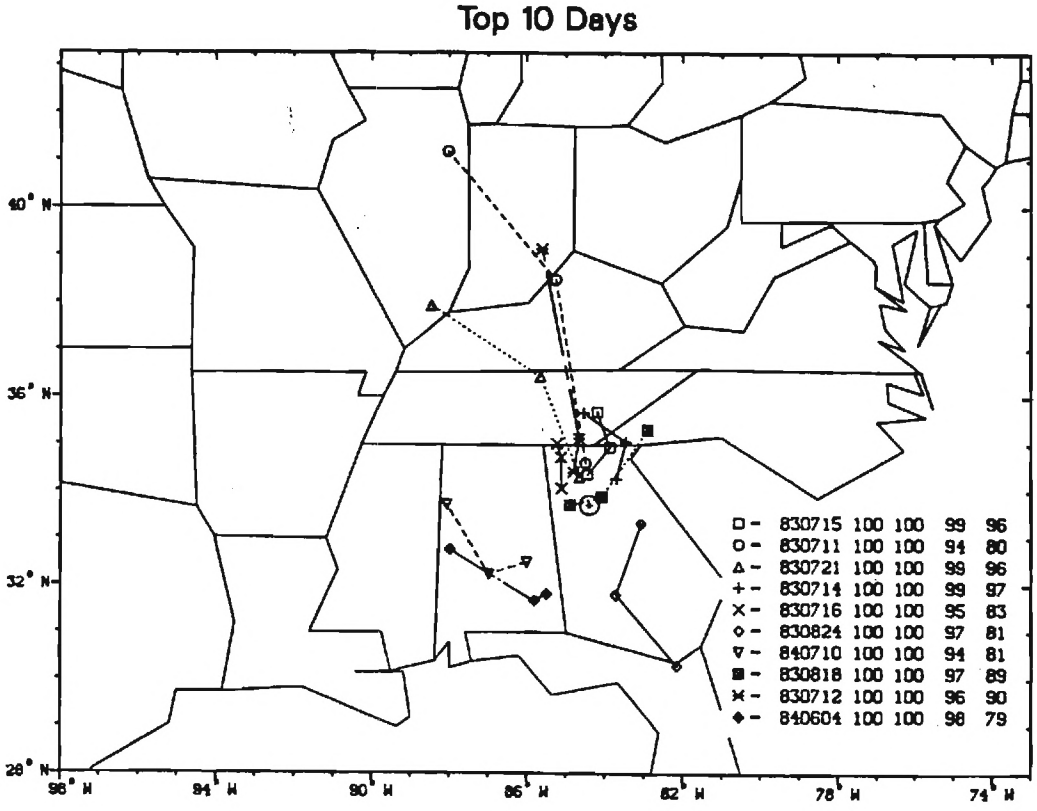

3. Positions of the center of mass of the trajectory branches at the end of one, two and three days for the top 10 days in ozone concentration. The date (YYMMDD), maximum ozone concentration (ppbv), and the remaining mass (%) for each of the three days are listed in the corner.

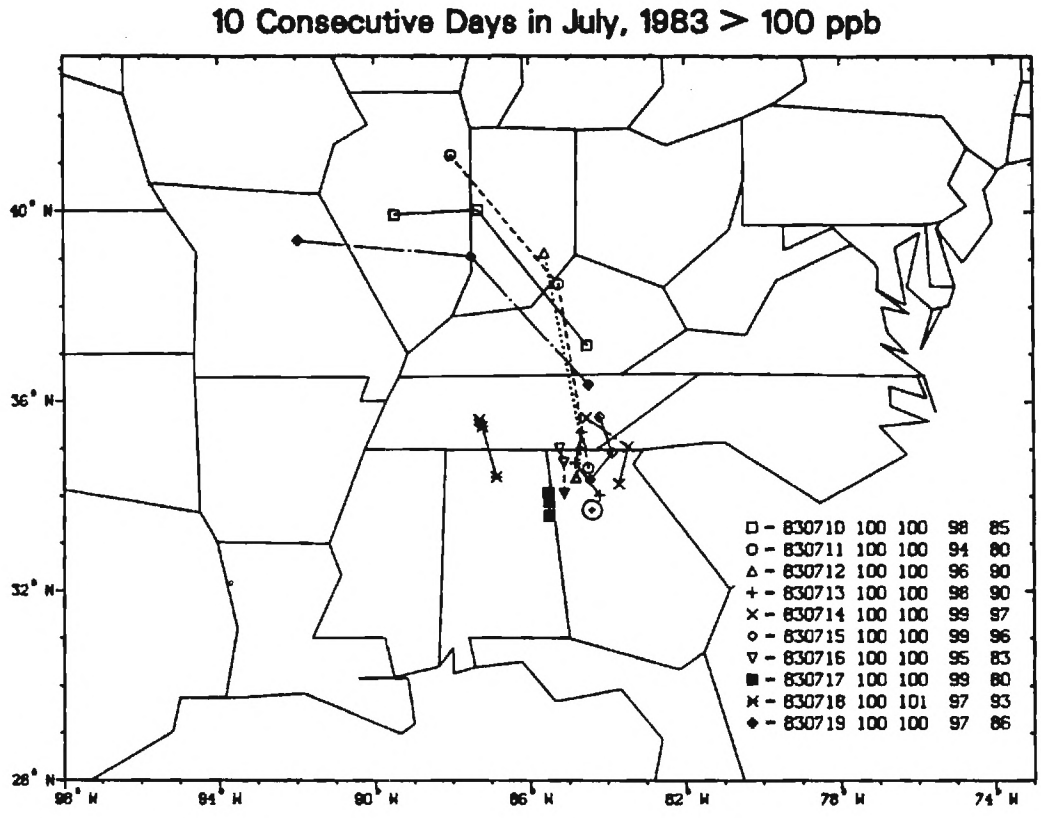

4. Positions of the center of mass of the trajectory branches at the end of one, two and three days for 10 consecutive days in July 1983 with ozone concentrations above 100 ppbv. The date (YYMMDD), maximum ozone concentration (ppbv), and the remaining mass (%) for each of the three days are listed in the corner.

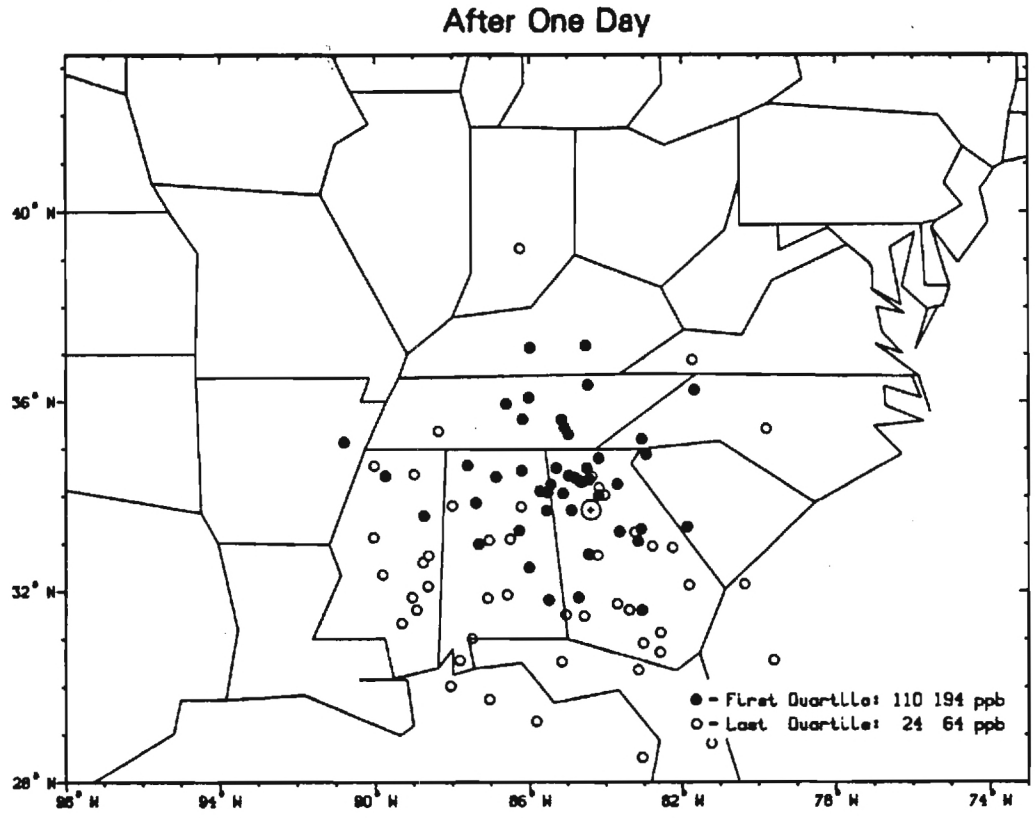

5. Positions of the center of mass of the trajectory branches for the first and last quartiles of ozone concentration at the end of the first day.

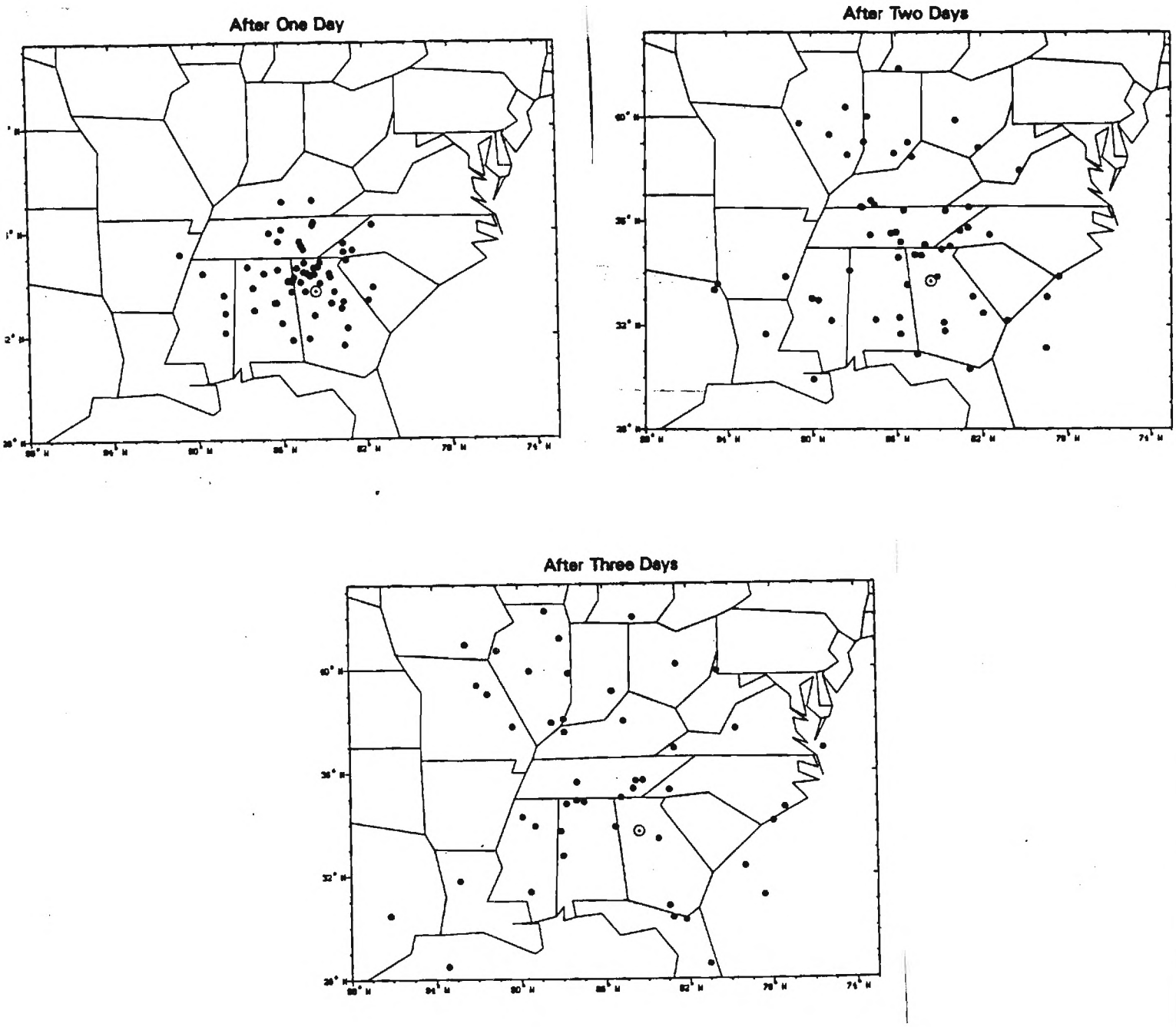

6. (a-c) Positions of the center of mass of the trajectory branches for all days with ozone concentrations greater than 100 ppbv after one, two, and three days.

Atlanta Afternoon Winds

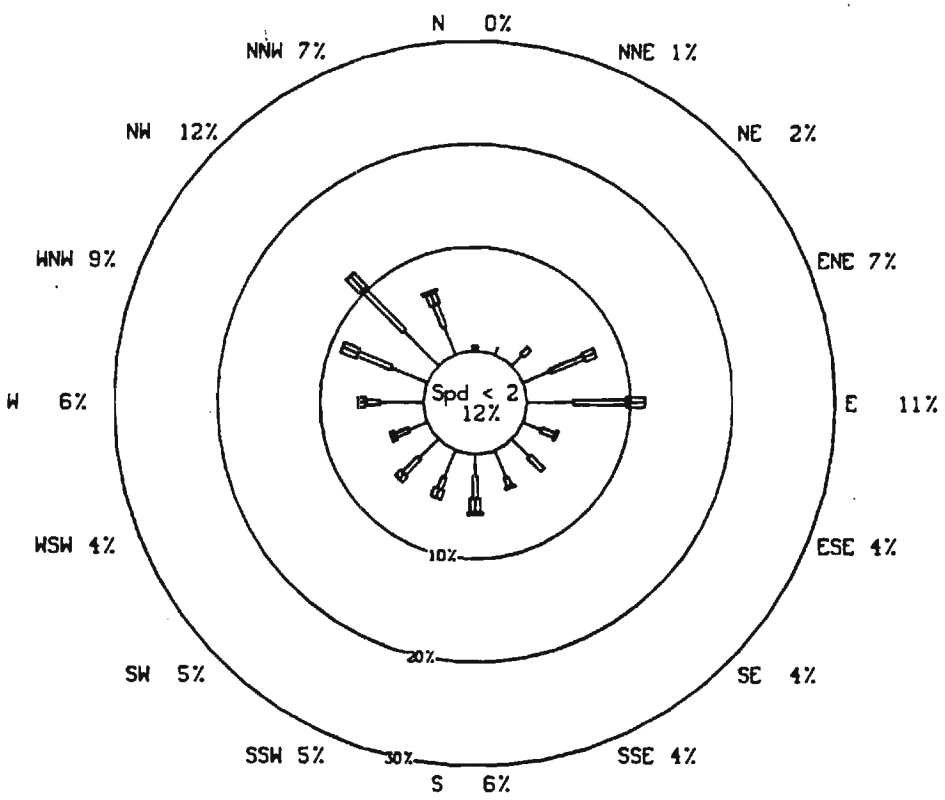

Start date: 83/ 5/ 1
End date: 84/11/30

Number of points = 428

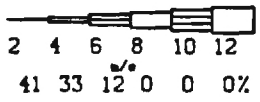

7. Windrose of afternoon (12-17 EST) vector averaged winds for 1983 and 1984, 8 months each year.

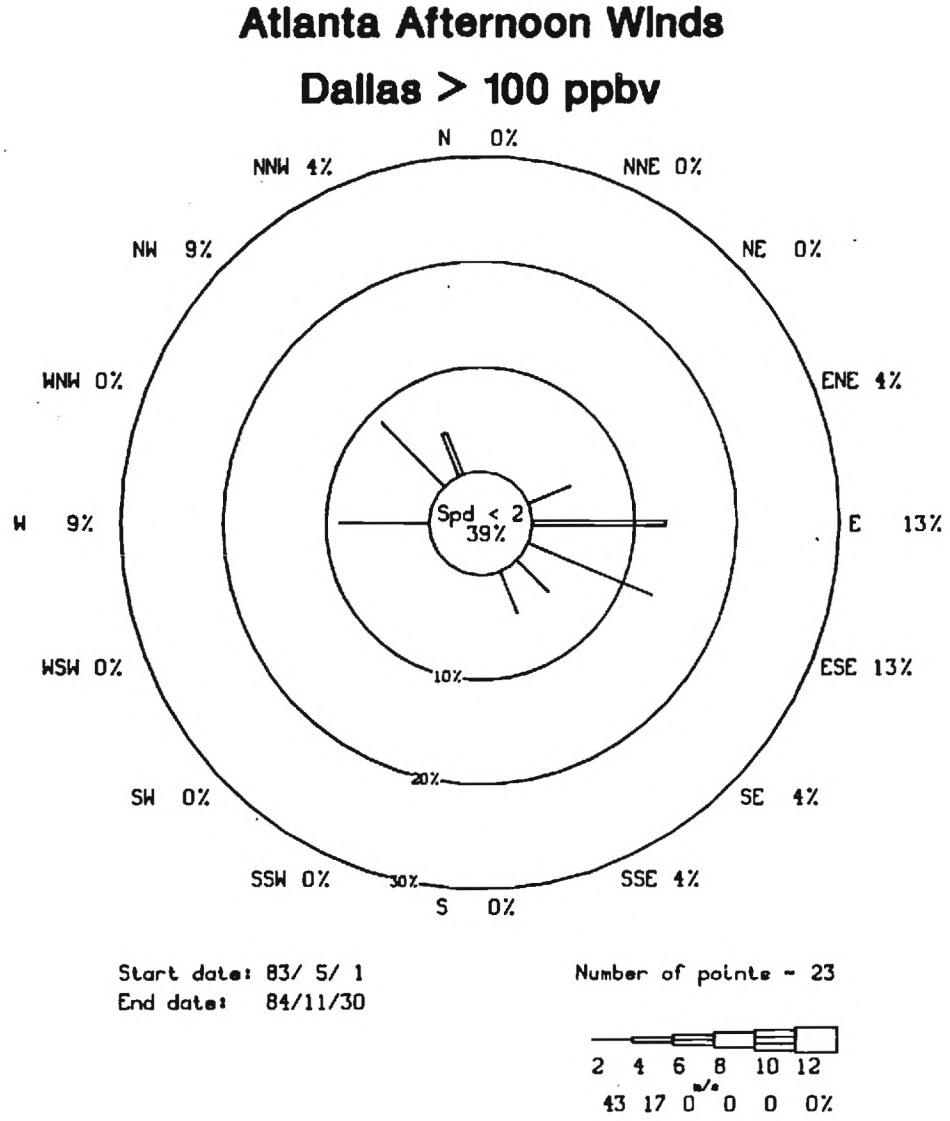

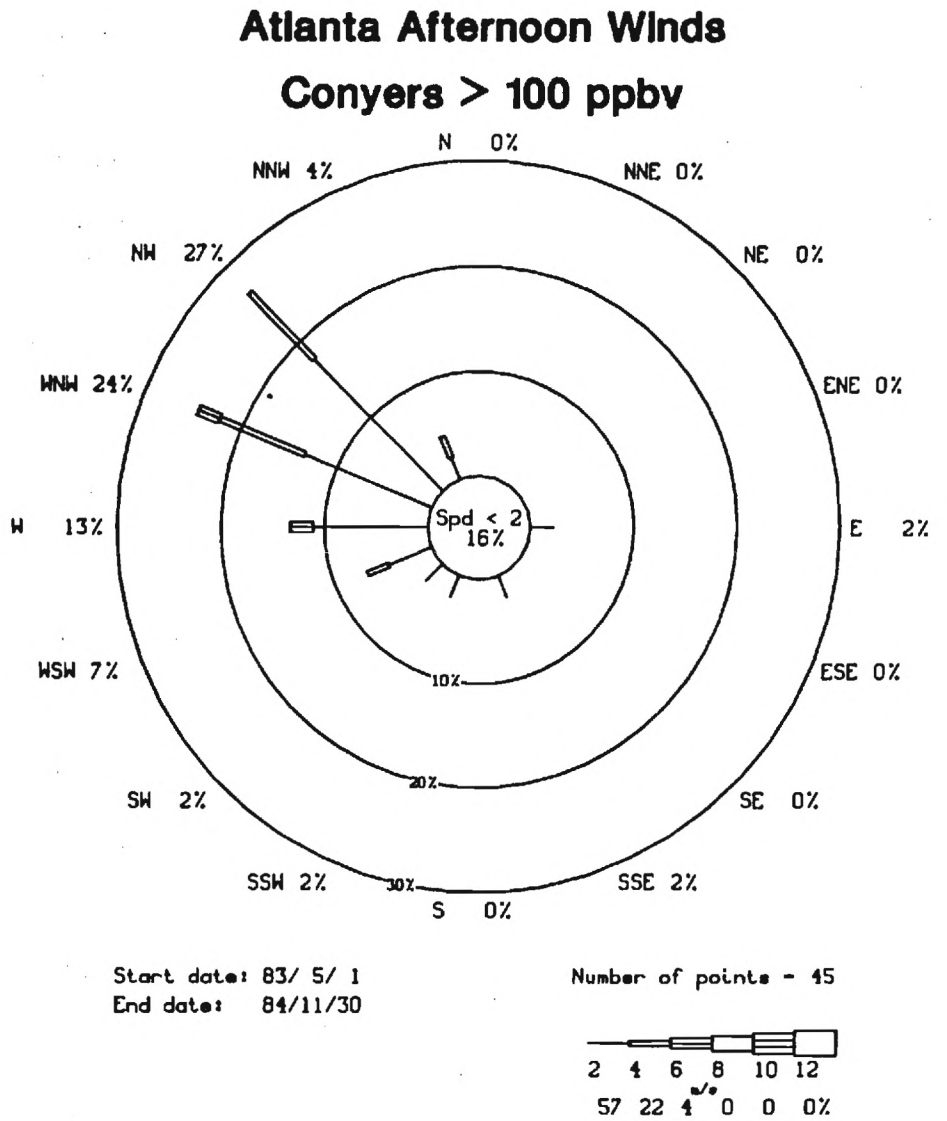

8. a) Windrose of afternoon (12-17 EST) winds for days with ozone concentrations greater than 100 ppbv at Dallas.
b) Windrose of afternoon (12-17 EST) winds for days with ozone concentrations greater than 100 ppbv at Conyers.

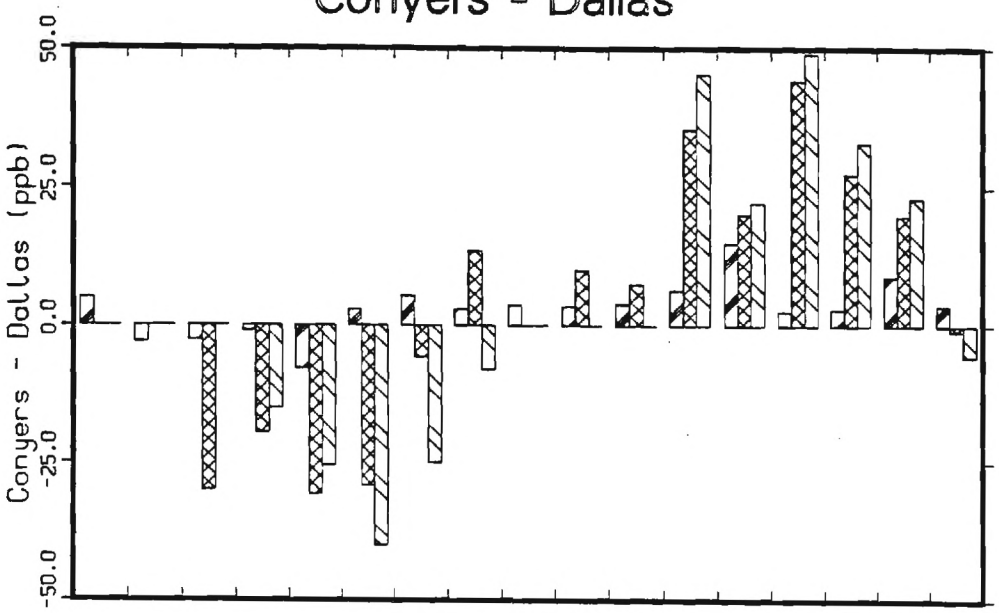

	N	NNE	NE	ENE	E	ESE	SE	SSE	S	SSW	SW	WSW	W	WNW	NW	NNW	CALM
Maximum Ozone < 80 ppb																	
N:	1	1	7	13	22	6	11	12	12	11	17	7	15	15	20	18	21
M:	5	-3	-2	-1	-7	2	5	2	3	3	3	6	14	2	2	8	3
σ:	0	0	7	6	10	9	10	7	8	10	8	13	11	13	12	9	12
Maximum Ozone >= 80 ppb																	
N:	0	0	1	12	8	5	4	2	3	1	2	5	9	11	17	5	22
M:	0	0	-30	-19	-30	-29	-5	13	0	10	7	35	20	44	27	19	0
σ:	0	0	0	13	12	17	26	30	17	0	31	20	15	18	22	31	19
Maximum Ozone >= 100 ppb																	
N:	0	0	0	1	2	3	1	1	0	0	0	3	5	8	10	2	9
M:	0	0	0	-15	-25	-40	-25	-8	0	0	0	45	22	49	32	23	-5
σ:	0	0	0	0	7	10	0	0	0	0	0	21	18	19	23	60	21

9. Bar graph of the mean Conyers-Dallas ozone concentration difference for each wind direction sector and for the maximum ozone level of the two stations < 80, > 80, and > 100 ppbv. The number of observations, the mean difference, and the standard deviation of the difference is given for each direction and concentration class.

Ozone Precursors and Ozone Photochemistry Over the Eastern North Pacific Ocean During the Spring of 1984 Based on the NASA/CITE 1 Airborne Observations

W.L. Chameides, and D.D. Davis

School of Geophysical Sciences

Georgia Institute of Technology

Atlanta, GA 30332

In review at the

Journal of Geophysical Research

December 14, 1987

ABSTRACT: Simultaneous, high resolution measurements of O_3, NO, CO, dew point temperature, and UV-flux obtained during the NASA GTE/CITE 1 spring, 1984 airborne field exercise over the eastern North Pacific Ocean are analyzed. Mid-tropospheric CO, O_3, and NO mixing ratios averaged about 120 ppbv, 50 ppbv, and 10 pptv, respectively. The CO and O_3 concentrations are comparable to those encountered over the North Pacific Ocean during the GAMETAG flights of 1977 and 1978, but are significantly higher than those encountered over the North Pacific Ocean during the fall, 1983 GTE/CITE 1 flights. By contrast, the average NO concentration from the spring flights is a factor of 1.5 times lower than that observed during the fall GTE/CITE 1 flights. Modeling calculations imply that, from the surface to about 8 km, photochemical reactions probably supplied a small, net sink of ozone to the region overlying the eastern North Pacific Ocean during the sampling period. Statistical analysis of the high resolution data indicates the existence of two ozone sources: one related to the downward transport of ozone-rich air from the upper troposphere and stratosphere and the other to the transport of ozone-rich air from the continents. However the results of the statistical analysis are obscured by the fact that simultaneous, high resolution NO measurements made by two independently operated chemiluminescent instruments were weakly correlated.

Introduction

In the fall of 1983 and spring of 1984, two field sampling expeditions were carried out over the North Pacific Ocean as part of the first phase of the Chemical Instrumentation Test and Evaluation activities of the National Aeronautics and Space Administration's Global Tropospheric Experiment (i.e. GTE/CITE 1) [see McNeal, 1987]. The operational overview for these flights and the results of the fall, 1983 operation have been previously presented in a Special Section of the Journal of Geophysical Research [see Beck et al., 1987; Danielsen et al., 1987a, b; Hoell et al., 1987a, b; Davis et al., 1987a; Ridley et al., 1987; Davis et al., 1987b; Sachse et al., 1987; Fishman et al., 1987; Condon et al., 1987; Browell et al., 1987; Hipskind et al., 1987; and Chameides et al., 1987 a,b]. In this work an analysis is presented of the data obtained during the Spring, 1984 campaign. Similar to the study of Chameides et al., [1987a] which was based on the data from the 1983 flights, our analysis will focus on the observed concentrations and variability of ozone and its precursors over the North Pacific Ocean. Through a combination of statistical and photochemical modeling calculations we will attempt to identify the primary processes controlling the concentrations of ozone and its precursors over this region of the globe. By comparing the present results with those of Chameides et al., [1987a] we will attempt to infer how the processes affecting ozone and its precursors vary from the fall to the spring. An additional aspect of the analysis of the 1984 data is that it makes use of two independent sets of NO measurements recorded simultaneously by two different chemiluminescent instruments. The impact of these two different NO data sets on our calculations will be discussed.

Database

Our focus for the present study is the chemistry of the atmosphere overlying the

North Pacific Ocean and thus we analyze here the data obtained during Flights 4, 5, 6, 9, and 10 of the spring, 1984 campaign; each of these flights originated from Moffett Field, California and involved extensive air sampling over the eastern North Pacific Ocean before returning to Moffett Field at the termination of the flight. The tracks for each of the flights included in the present study are illustrated in Figure 1 and pertinent data for each of the flights are summarized in Table 1. Collectively the flight tracks covered an area ranging from approximately 24 to 40°N latitude and 122 to 135°W longitude. However, in order to minimize the influence of continental sources from North America upon our results any data collected north of 35°N and east of 124°W was excluded from the analysis.

Note in Table 1 that the data from Flights 4, 5, 6, and 9 were obtained from essentially constant-altitude tracks in the middle free troposphere. The data from Flight 10, on the other hand, includes a combination of constant-altitude tracks and vertical ascents and descents with altitude ranging from the boundary layer to the middle free troposphere; this data has been separated in Table 1 into three groups corresponding to the altitude regime below 2 km, from 2 to 4 km, and above 4 km. Furthermore note that while Flights 4 and 5 were carried out during the night and as a result NO levels were at or below the detection limit of the NO instruments. Flights 6, 9, and 10 were carried out during midday, with solar zenith angles ranging from about 8 to 34°.

Our analysis makes use of measurements of temperature, T, dew point, T_d, CO mixing ratio, X_{CO}, NO mixing ratio, X_{NO}, O_3 mixing ratio, X_{O3}, and solar uv-flux. These measurements were made aboard the NASA Convair 990 aircraft, as described by Beck et al. [1987] and the references cited therein. Temperature and dew point measurements were recorded by NASA personnel using standard instrumentation; temperature from a platinum resistance sensor and dew point from two dew-point hygrometers. The ozone measurements were recorded by Gregory et al., [1984] using an ethylene chemiluminescence instrument with a UV absorption instrument (Dasibi) as a

backup. The CO measurements used here were those obtained by Sachse et al., [1987] using an IR tunable-diode-laser based differential absorption technique. The nitric oxide measurements were made independently by Ridley et al., [1987] and Torres et al., [1985] using a chemiluminescence technique involving the reaction of ambient NO with O_3. Measurements of the downwelling UV-flux were made by NASA personnel and were also included in our analysis.

As described by Beck et al., [1987], all the data from the spring, 1984 flights have been archived on magnetic tape; a copy of the archived data was obtained from the NASA GTE Project Office and used in the analysis described here. However, it should be noted that through private communication with the individual investigators of the spring campaign it was learned that a number of individual data points in the archive were erroneous; for the most part these erroneous data points could be attributed to a failure to delete calibration readings from the final data archive. The erroneous data points were appropriately corrected or deleted before the analysis was carried out. In general data for all of the above parameters were recorded with a time resolution of one to two minutes; these data points will be referred to as the high resolution data while time averages of the observations will be referred to as the low resolution data. For the purposes of carrying out our statistical and diagnostic analyses on the high resolution data, which require a set of simultaneous values for each of the five parameters, all data recorded at times within 30 seconds of each other were assumed to be simultaneous.

A discussion of the precision and accuracy of each of the above measurements and the general impact of uncertainties in these measurements on our analysis may be found in Chameides et al., [1987a] and the references cited therein. However, some specific points with regard to the data for T_d, X_{NO}, and UV-flux should be noted. In their analysis of the fall, 1983 GTE/CITE 1 measurements, Chameides et al., [1987a] encountered problems with the data for T_d and the UV-flux. In the case of T_d, these authors found frequent intervals when the recorded dew-point temperatures for clear

air conditions were significantly in excess of those recorded for the static temperatures, an indication of instrument failure on the part of the dew-point hygrometers. Further, the problem was found to be most severe at altitudes above 8 km. Fortunately as a result of modifications made to the dew-point instruments following the fall, 1983 flights and perhaps also because of the lower altitudes flown during the spring campaign, a similar problem did not arise in the dew-point data from the spring, 1984 campaign. Except for a very brief period during Flight 4, the recorded values for T_d were always well below those to T; the suspect T_d data points from Flight 4 were excluded from our analysis.

Since a portion of our analysis involves photochemical-modeling calculations, knowledge of the solar flux is needed to infer the photolysis rates of species such as O_3 and NO_2. In a similar analysis of the fall, 1983 measurements, Chameides et al., [1987] elected to not use the UV-flux data recorded during the flights to aid in the determination of the photolysis rates because of apparent problems with either the measurements themselves or the data reduction and analysis of these measurements. (It was found, for example, that in several instances the reported downwelling flux was greater than the incident flux from the sun that reaches the top of the earth's atmosphere). However, these problems were not encountered in the UV-flux data from the spring campaign and as a result we were able to use these data in the present analysis. A description of how the UV-flux data were incorporated into our photochemical modelling calculations will be presented later.

As noted earlier, NO concentrations were measured by two independently operated chemiluminescent instruments; one from the Wallops Flight Facility (WFF) [Torres, 1985] and the other from the National Oceanic and Atmospheric Administrative and the National Center for Atmospheric Research (NOCAR) [Ridley et al., 1987]. For the most part data from the NOCAR instrument was recorded at one minute intervals while the data from the WFF instrument was recorded at two minute intervals. On occasion, especially in regions characterized by NO levels of 10 pptv or less, small, negative

values were recorded for some of the individual, high resolution NO data points. Consistent with the practice of the investigators using these instruments, the negative values were included in our statistical analysis as they were recorded. However, for the diagnostic photochemical modeling calculations, where negative concentrations can not be used, all negative, high resolution NO data points were arbitrarily set equal to a value of 0.1 pptv; at this level NO has a negligible impact upon the model calculations.

It is important to note that while the averaged or low resolution NO mixing ratios obtained by the two NO instruments were in reasonably good agreement (the Pearson-r correlation coefficient between the two sets of averaged NO observations listed in Table 1 is 0.54), the agreement between the two high resolution data sets was weak. During Flights 6, 9, and 10 there were 124 overlapping NO measurements in which the WFF-measured NO concentration was obtained within 30 seconds of a measurement by the NOCAR instrument. The Pearson-r correlation coefficient between the two sets of NO measurements for these 124 cases was calculated to be only 0.23. The fact that the two NO data sets are better correlated in low resolution that in high resolution could be indicative of the presence of significant NO variability on time scales of 30 seconds or less. Alternatively, it could be due to poor precision in one or both of the instruments. In the later regard it is noteworthy that the NO levels encountered during the 1984 flights were quite low and were often below the stated precision of the instruments of about ±6 pptv for a 60 s measurement by the WFF instrument and ± 8 pptv for a 10 s measurement by the NOCAR instrument [Hoell et al., 1987a]. (For a more detailed discussion of the comparability of the WFF and NOCAR NO measurements made during the GTE/CITE 1 flights the reader is referred to Hoell et al., [1987a], where a complete statistical intercomparison of the two data sets can be found. While our findings are qualitatively similar to those of Hoell et al., they are not identical. The differences arise primarily from the fact that while the Hoell et al., intercomparison was limited to only those periods during the

flights when the pressure, temperature, and humidity were relatively constant, our analysis includes all periods regardless of the conditions encountered at the time of the measurements.) Because of the weak correlation between the NOCAR and WFF high resolution NO measurements for the 1984 flights, these data sets were not combined into a single data set for the analysis carried out in this work; instead, separate analyses for each NO data set have been performed and the results of both analyses are presented.

Meteorological Conditions

An inspection of weather maps from the National Weather Service and satellite photographs from the National Oceanic and Atmospheric Administration reveals that a steep ridge of high pressure was stalled off the west coast of the United States during the period of Flights 4, 5, and 6 (i.e., April 26 - 30, 1984). As a result of this pressure ridge, the jet stream tended to flow from the northwest to the southeast across the northern part of the GTE/CITE 1 sampling region during these flights and gave rise to strong northwesterly upper level winds ranging from 10 to 50 m s^{-1}. For this reason all of the data points obtained during Flights 4, 5, and 6 had winds out of the northwest quadrant (see Table 1). The presence of this high pressure ridge and its associated northwesterly winds suggests that the air sampled during this period of the spring campaign was most likely of a remote marine origin and not from the North American continent.

Quite different meteorological conditions were encountered during Flights 9 and 10. By May 7, 1984, the day of Flight 9, the high pressure ridge off the coast of the United States had largely dissipated and the region was coming under the influence of an intense low pressure system located to the southwest of the Gulf of Alaska; as a result of the position of this low pressure system, the jetstream was located well to the north of the GTE/CITE 1 sampling region during Flight 9. For

this reason the winds during Flight 9 were light, averaging only about 5 m/s, and variable; note in Table 1 that winds from all four quadrants were encountered during this flight.

By May 9, 1984, the day of Flight 10, the low pressure system had moved to the east and south and was now located over the northwestern United States. In conjunction with the movement of the low, the jet stream over the eastern North Pacific had also moved southward and was back in the general vicinity of the GTE/CITE 1 sampling region. In addition, a southward moving cold front associated with the low pressure system had crossed through the sampling region on May 8 and was located just to the south of the flight track on May 9. Given the position of the jet stream, it is not surprising that the upper level winds encountered during Flight 10 were all out of the northwest and southwest quadrants. Note in Table 1, however, that in the boundary layer a small number of datapoints were obtained with winds out of the east. Because the flight track on May 9 was located to the north of the cold front, it is possible that some of the lower level air sampled during this flight had its origin from the North American continent, having been advected first westward and then southward by the low pressure system. In fact, as will be discussed below, inspection of the CO data from Flight 10 does suggest that the boundary layer air had recently been under the influence of continental sources.

T_d, X_{CO}, X_{NO}, and X_{O3} Measurements

Averaged values for T_d, X_{CO}, X_{NO}, and X_{O3} from Flights 4, 5, 6, 9, and 10 are indicated in Table 1. Above 2 km, the CO and O_3 averages show very little variability from flight to flight, with X_{CO} averages varying from 112 to 126 ppbv and average X_{O3} ranging from 32 to 55 ppbv. In contrast to CO and O_3, large flight-to-flight variations were reported for the average NO concentrations above 2 km with X_{NO} ranging from 3 to 20 ppbv.

An intriguing set of measurements from the lower troposphere and boundary layer were obtained during Flight 10. In Figure 2 time series plots from the flight are presented for X_{CO}, X_{03}, X_{NO}, T_d, T, and altitude, z. From the plot of altitude vs time it can be seen that the flight involved a series of ascents and descents. After a period of level flight at 6 km, the aircraft descended in two stages to 2.5 km and then to 660m. This was followed by an ascent to 2.5 km, another brief descent into the marine boundary layer, and a final ascent back to the middle free troposphere before the flight terminated at Moffett Field. The chemical observations made during these descents and ascents, which are plotted in Figure 2, reveal the presence of a very complex vertical structure in the region between the surface and 2.5 km; this complex structure may have been associated with the aforementioned frontal activity in the region just prior to the flight. Immediately below 2.5 km there appears to have been a thin layer of dry air with extremely high levels of CO, 0_3, and NO; the CO and NO levels observed during the beginning of the second descent of about 165 ppbv and 25 pptv, respectively, were the highest of the entire data set and the peak 0_3 level observed during the first descent of about 70 ppbv was the highest observed during the flight. Below this thin dry layer, the air was found to be quite moist with somewhat lower levels of CO and 0_3 and NO concentrations well below 10 pptv. The temperature structure below 2.5 km was also unusual; the lapse rate was quite small and even negative at times indicating that the layer was statically stable with little or no vertical mixing.

Given the high levels of CO and 0_3 observed below 2.5 km, as well as the meteorological conditions during the flight, it seems quite likely that a significant portion of the air sampled at this altitude during Flight 10 was contaminated with freshly polluted air recently transported from the North American continent; since the air in this region was statically stable, it could have been transported a long distance without losing its chemical character. The anomalous nature of the data obtained below 2.5 km during Flight 10 and the likelihood that this air was not

typical of the boundary layer over the eastern North Pacific Ocean should be borne in mind during the discussions that follow.

In Table 2 the averaged concentrations in CO, O_3, and NO observed over the North Pacific Ocean during the spring campaign for altitudes ranging from 4 to 8 km are compared to previous CO, O_3, and NO measurements made in this region; these measurements include those obtained from the fall, 1983 GTE/CITE 1 operation as well as the GAMETAG flights of the summer of 1977 and spring of 1978 [Davis, 1980]. Note in Table 2 that in spite of the fact that the spring GTE/CITE 1 flights were limited to the eastern North Pacific Ocean (close to the North American continent), the average CO and O_3 levels observed during these flights are remarkably similar to the averaged concentrations observed for these species during the spring and summer GAMETAG flights which covered a considerably more remote portion of the North Pacific Ocean. The similarity between these data sets provides further support to our earlier conclusion based on an analysis of meteorological conditions that, except for the boundary layer measurements made during Flight 10, the air sampled during the spring, 1984 GTE/CITE 1 operation was largely of a remote, marine origin and not strongly influenced by direct injections of polluted air from the North American continent.

Interestingly, while the O_3 and CO levels observed during the spring, 1984 GTE/CITE 1 flights were consistent with those observed during the summer and spring GAMETAG flights, they were significantly different from the averaged levels observed during the fall, 1983 GTE/CITE 1 flights. As indicated in Table 2, CO levels during the fall averaged about 40% lower than in the spring, while O_3 levels were almost a factor of 2 lower in the fall. Because both CO and O_3 have been found to exhibit concentration minima in the fall in many regions [cf., Herring and Borden, 1967; Chatfield and Harrison, 1976; Dianov-Klokov et al., 1976; Seiler and Fishman, 1981], it is is tempting to ascribe the difference in the fall and spring observations to a seasonal variation over the North Pacific Ocean. However, much more extensive

sampling over the North Pacific Ocean will be needed before an accurate picture of the seasonal cycle of CO and O_3 can be established for this region. Finally, note that while the CO and O_3 concentrations observed during the spring were significantly higher than those observed during the fall, the NO levels observed during the spring were systematically higher than those observed during the fall by nearly a factor of 1.5. This result suggests that processes other than those which control the levels of CO and O_3 may be important in determining the levels of NO in the remote troposphere; one such process could be the production of NO by lightning.

Statistical Analysis: Similar to the analysis of the fall GTE/CITE 1 data by Chameides et al., [1987a], we have carried out bivariate and multivariate analyses of the high resolution data gathered from the spring, 1984 campaign. (A description of multivariate or factor analysis can be found in Chameides et al., [1987a] and the references cited therein.) In these analyses the statistical correlations between ozone and three other tracers were examined; the three tracers were NO, associated with descending air from the stratosphere or upper troposphere or air that had recently detrained from electrified clouds, CO, a tracer indicative of polluted air masses, and H_2O, associated with boundary layer and lower tropospheric air.

The results of the bivariate analysis are summarized in Table 3. The correlations between the variables were all found to be relatively weak. While O_3 and CO as well O_3 and NO tended to be positively correlated, O_3 and T_d and NO and T_d exhibited weak negative correlations. It is also interesting to note that the correlation coefficients calculated for NO using the WFF data were generally found to be smaller than those calculated using the NOCAR data. (Recall that while the averaged or low-resolution observations from the two NO instruments were in reasonable good agreement, the data were weakly correlated at high resolution. It is this poor agreement at high resolution that leads to the difference in the Pearson-r correlation coefficients calculated for NO from the two instruments.)

The results of the multivariate analysis are listed in Table 4. In this table results are presented for analyses using the NOCAR NO measurements as well as the NO measurements from the WFF instrument; in both cases the analyses were limited to the data obtained above 4 km to avoid the anomalous set of low altitude observations from Flight 10. In the case of the analysis using the NOCAR data (Table 4a), we find that over 75% of the total variance in the four variables can be explained by two factors; Factor 1 explains about 43% of the variance and Factor 2 about 33%. Two factors of roughly equal weighting were also identified in the multivariate analysis using the WFF NO data (see Table 4b), although in this case only about 60% of the total variance in the four variables and only 50% of the variance in NO could be explained by these factors. Given the fact that the variance in the four variables appears to be controlled by two competing processes of approximately equal importance, it is not surprising that the Pearson-r correlation coefficients between the individual variables were calculated to be so small; the effect of two competing but approximately equal processes could be to limit the linear correlations between any two variables.

Turning first to the results of the multivariate analysis using the NOCAR NO data, we find that the first factor has significant positive loading for NO and O_3, a negative loading for T_d, and no significant loading for CO. The second factor, on the other hand, has significant positive loadings for CO and O_3, a weak positive loading for T_d, and no significant loading for NO. These results suggest that during the period of the GTE/CITE 1 spring operation, ozone over the eastern North Pacific Ocean was primarily influenced by two sources. One source was associated with high levels of NO and low levels of H_2O and most likely arose from the downward transport of air from the stratosphere and upper troposphere. The second source was related to high levels of CO and thus most probably to pollution from the continents. The fact that high levels of NO were not correlated with Factor 2, suggests that the air associated with this source was aged, rather than newly formed, polluted air whose NO

and NO_2 had already been converted to less chemically active species, such as nitric acid or PAN, or had been removed before entering the sampling region.

It is interesting to note that the above conclusions are quite similar to those obtained from the statistical analysis of the data gathered from the fall, 1983 GTE/CITE 1 field operation [Chameides et al., 1987a], with one exception. While the analysis of the fall data indicated that ozone production was dominated by the source associated with high NO and low H_2O levels and that the source associated with pollution was only of secondary importance, the present analysis of the spring data indicates that the two sources were of roughly equal importance. This difference could be related to the fact that the total quantity of data from the 1984 Pacific spring flights was much smaller than that from the 1983 CITE 1 mission and thus the representatives of the former data set may be questioned. Alternatively the difference may be due to the fact that the geographical region sampled during the spring operation was limited to the eastern North Pacific Ocean, while the data analyzed from the fall operation was primarily obtained from the central North Pacific Ocean. Thus the greater importance of the pollution-related ozone source inferred for the spring data set could simply reflect the fact that the region sampled during the spring was considerably closer to the North American continent and was therefore more susceptible to injections of polluted air from the western United States. On the other hand the comparability between mid-tropospheric CO and O_3 levels observed during the spring flights and those observed during the GAMETAG flights, which also covered a more remote region of the North Pacific Ocean, implies that such injections were probably not common during the spring field operation and thus argues against this explanation. Finally, it is possible that the difference in the statistical results was caused by a seasonal variation in the ozone budget with ozone sources related to anthropogenic activities having generally a greater impact over the entire North Pacific Ocean in the spring than in the fall. It is interesting to note in this regard that such a possibility is consistent with the

model calculations of Liu et al., [1987]. On the basis of these calculations, it was argued that, because of the lower levels of free radicals in the winter and early spring, pollutants are transported over greater distances and, as a result, photochemical production of ozone from anthropogenic precursors has its greatest global impact in the late winter and early spring.

Significantly different conclusions are implied by the multivariate analysis using the WFF NO data and summarized in Table 4b. While two factors were identified from this analysis, only Factor 1 has significant loadings for O_3. In addition to O_3, this factor has positive loadings for both CO and NO. Since the WFF NO data is not significantly anti-correlated with T_d, as was the NOCAR NO data, the first factor does not have a significant negative loading for T_d. Since the WFF NO data is not negatively correlated with CO, as was the NOCAR NO data, only a single factor with positive loadings for both CO and NO was needed to explain most of the O_3 variance. Finally because the Pearson-r correlation coefficients involving the WFF NO data were all so small, only a relatively small fraction (e.g., 50%) of the total variance in WFF NO could be explained by factors correlated to variations in the other three variables.

Thus while the multivariate analysis of the spring, 1984 GTE/CITE 1 data using the NOCAR NO measurements as well as the Chameides et al., [1987a] analysis of the fall, 1983 GTE/CITE 1 data (which was based on NO measurements using a two-photo-laser-induced-fluorescence technique [Bradshaw et al., 1985]) implied the existence of two ozone sources, only a single ozone source is implied by the analysis using the WFF NO data. This single source is most likely associated with pollution in view of the positive CO loadings shown in Table 4b. In addition it should be noted that the analysis using the WFF NO data also implies a different kind of source for NO. While the analysis of the spring data using the NOCAR NO measurements and the analysis of the fall data indicated that NO was anti-correlated with both T_d and CO implying the existence of a remote, upper tropospheric and/or stratospheric NO source, the

analysis using the WFF NO data implies a more disperse NO source not correlated or anti-correlated with either CO or T_d. In order to avoid similar discrepancies in the future it would appear that the accuracy and precision of high resolution NO measurements in the remote troposphere needs to be more reliably established.

Ozone Photochemistry

In this section we discuss the results of diagnostic modelling calculations in which the data gathered during the spring GTE/CITE 1 mission were used to determine the net rate of ozone production by photochemical reactions over the eastern North Pacific Ocean. Values for $P(O_3)$, the ozone photochemical tendency or net rate of ozone photochemical production, were calculated for each time interval in which simultaneous measurements of T_d, X_{CO}, X_{NO}, and X_{O3} were recorded during each of the spring flights. The calculations were carried out using a photochemical box model similar to that of Chameides et al., [1987a]. In these calculations, the levels of O_3, NO, H_2O, CH_4, and H_2 as well as temperature and pressure were specified and the concentrations of short-lived species involved in ozone photochemistry were then calculated assuming photochemical equilibrium using standard numerical techniques. The net rate of ozone photochemical production was determined from these specified and calculated concentrations using Equation (1) of Chameides et al., [1987a]. In the model, real time values for X_{O3}, X_{NO}, X_{CO}, T_d, T, and pressure were taken from the observations recorded during the flights; however, note that in the case of NO only the data from the NOCAR instrument was used. The mixing ratios for CH_4 and H_2 were assumed to be 1.65 ppbv and 0.55 ppbv, respectively [Rasmussen and Khalil, 1981].

As described in Chameides et al., [1987a], the model uses a standard gas-phase chemical mechanism using rate constants taken from the recent review of DeMore et al., [1985]. Reactions involving non-methane hydrocarbons were not included in the

calculations; with the exception of the low altitude data points from Flight 10 which appear to have been influenced by anthropogenic sources, it is not likely that non-methane hydrocarbons had a significant effect on the ozone chemistry of the air studied in this work (cf., Liu et al., 1983]. The J-values for the photolytic processes in the chemical mechanism were calculated for each time interval using a two-stream approximation to determine the solar flux as a function of altitude, solar zenith angle and wavelength [cf., Dickerson et al., 1979]. The measurements made during the flights of the downwelling solar flux density (through a flat horizontal plane) in conjunction with TOMS satellite data [W. Evans, private communication, 1987] were used to estimate the column of ozone and the amount of cloud cover overlying the aircraft at the time of the observations. The sensitivity of the model-calculated ozone production rates to uncertainties in the J-values has already been addressed by Chameides et al., [1987a]; generally a factor of 2 decrease in all the photolysis rates was found to result in a 30 - 50% decrease in the magnitude of $P(O_3)$.

The mean values calculated for $P(O_3)$ for each flight are listed in Table 1 as a function of wind direction and altitude interval; a positive value in $P(O_3)$ indicates that photochemical processes supply a net source of ozone, while a negative $P(O_3)$ indicates that photochemistry acts as a net sink for ozone. Except for a small subset of the data during Flight 9, when the winds were out of the northwest and the NOCAR instrument recorded relatively high NO levels, we find that on average photochemical processes represented a small net sink for ozone over the sampling region during the spring, 1984 flight operation. The dependence of $P(O_3)$ on NO, H_2O, CO and O_3 levels revealed in Table 5 is quite similar to that found by Chameides et al., [1987a]. The sign of $P(O_3)$ tends to be determined by the NO level, with levels of NO below about 10-15 pptv leading to a negative $P(O_3)$ and higher NO concentrations causing $P(O_3)$ to be positive. The levels of H_2O and CO influence the absolute magnitude of $P(O_3)$; as the levels of these species increase, $P(O_3)$ will generally

tend to become either more positive or more negative depending upon the NO level. Finally increases in O_3 tend to cause $P(O_3)$ to become less positive and more negative. Thus in Table 5 we find that the most negative values in $P(O_3)$ occur for those intervals with the lowest NO concentrations. Further note in Table 5 that since the average NO mixing ratios were generally below 15 pptv, increases in the concentrations of the other species tended to lead to more negative values in $P(O_3)$.

An indication of the variations in $P(O_3)$ as a function of altitude can be obtained from Figure 2 where a time series plot of the calculated values for $P(O_3)$ implied by the observations made during Flight 10 is presented along with the other time series plots. The general tendency for $P(O_3)$ to become more negative with decreasing altitude is qualitatively consistent with the calculation of Chameides et al., [1987a] based on the data from the fall, 1983 GTE/CITE 1 flights. However, note that this tendency is not followed in the thin layer of air below 2.5 km where high levels of NO result in relatively large, positive values for $P(O_3)$.

While the results listed in Table 1 and illustrated in Figure 2 give an indication of the photochemistry of ozone implied by the observations during the spring operation, they do not quantitatively reflect the average ozone photochemical tendency in the region as the calculations were carried out for only a narrow range of zenith angles at midday. To obtain a more quantitative estimate of the ozone photochemical budget, a time-dependent photochemical box model (see Chameides et al., [1987a] and the references cited therein) was used to calculate the average value of $P(O_3)$ over a diurnal cycle in the altitude interval between 4 and 8 km, where most of the data was collected. The model was constrained to yield values for T, T_d, X_{CO}, X_{O3}, and X_{NO} (at noon) equal to those in Table 2 for the spring flights. The resulting calculations indicate that in this region of the atmosphere the photochemistry is close to being in balance; photochemical reactions were calculated to produce ozone at a 24-hour averaged rate of about 1.2×10^5 molecules cm^{-3} s^{-1} and consume ozone at an average rate of about 1.6×10^5 molecules cm^{-3} s^{-1}, resulting in

a net 24-hour average ozone photochemical tendency of -4×10^4 molecules cm^{-3} s^{-1}. If this average rate were uniform throughout the 4 km column between 4 and 8 km, it would correspond to a middle-free-tropospheric column destruction rate of about 1.6×10^{10} molecules cm^{-2} s^{-1}; by comparison note that the estimated rates of ozone injection from the stratosphere and deposition on the ocean surface are about $(5 - 10) \times 10^{10}$ and 2.5×10^{10} molecules cm^{-2} s^{-1}, respectively.

Another interesting comparison is that between the 24-hour ozone photochemical tendency calculated here of -4×10^4 molecules cm^{-3} s^{-1} and the equivalent value of $+6 \times 10^4$ molecules cm^{-3} s^{-1} calculated by Chameides et al., [1987a] for the same altitude interval based on the data collected over the eastern and central North Pacific Ocean during the fall, 1983 GTE/CITE 1 field operation. While this comparison would appear to imply that the spring photochemistry was quite distinct from that of the fall with photochemical reactions supplying a net sink rather than a source of ozone to the middle free troposphere, some caution should be exercised in interpreting this result since the photochemistry is so close to being in balance and relatively large variations are associated with the mean NO, O_3, and CO concentrations used in the model. In fact if the (midday) NO concentration used in the spring calculations was increased by 7 pptv (its 1-σ standard deviation, as shown in Table 2) and CO and O_3 were similarly decreased by their 1-σ standard deviations, the resulting 24-hour net ozone photochemical tendency would be essentially the same as that calculated for the fall. Finally as noted earlier one must keep in mind the more limited data set available from the spring, 1984 operation relative to the fall, 1983 flights and that the geographical regions sampled during these two flight operations were not identical.

Conclusion

During a series of flights over the eastern North Pacific Ocean in the spring of

1984, CO, O_3, and NO mixing ratios in the middle free troposphere were found to average about 120 ppbv, 50 ppbv, and 10 pptv, respectively. Photochemical modeling calculations indicate that during this period photochemical processes tended to supply a net sink to the atmosphere overlying the eastern North Pacific Ocean in the altitude regime between the surface and about 8 km; however small areas were found where enhanced levels of NO resulted in a net production of ozone by photochemistry.

The statistical analysis of the data was obscured somewhat by the fact that simultaneous, high resolution NO measurements made by two independent chemiluminescent instruments were weakly correlated. Similar to a previous study of the fall, 1983 GTE/CITE 1 data, an analysis of the spring data using NO measurements from the NOCAR instrument suggested that ozone was influenced by two main sources - one associated with downward transport of air from the upper troposphere or stratosphere and the other associated with transport of ozone from continental source areas. On the other hand, only one source of ozone, probably associated with polluted air masses, was suggested by the analysis using the WFF NO data. This discrepancy underscores the continued need to establish the accuracy and precision of current, state-of-the-art NO measurements techniques in remote locations where NO levels are relatively low.

A comparison of the results of the present work with previous studies of the chemistry of the North Pacific Ocean indicates some interesting trends. In the case of CO and O_3, the concentrations observed during the spring, 1984 flights were quite similar to those observed previously in the region during the GAMETAG flights of the summer of 1977 and the spring of 1979 but were substantially higher than the average levels observed during the fall, 1983 GTE/CITE 1 flights over the North Pacific Ocean. By contrast, the average NO level observed during the spring, 1984 flights was nearly a factor of 1.5 times lower than the average NO concentration measured during the fall, 1983 GTE/CITE 1 flights. The results of the statistical analysis suggest that the source of ozone to the region arising from the transport of polluted

air from continental regions was somewhat stronger during the springtime mission than during the fall mission. Finally, the photochemical modeling calculations suggested that chemical processes in the middle free troposphere tended to supply a net sink of ozone in the spring, while in the fall they tended to supply a net source. While these variations are suggestive of a seasonal variation, considerably more observations will be needed before a comprehensive picture of the seasonal cycle in CO, O_3, and NO and their sources and sinks over the North Pacific Ocean can be established.

Acknowledgments

This work was supported in part by funds from the National Aeronautics and Space Administration (NASA) under grants NAG-1-385 and NAG-1-50 and from the National Science Foundation under grants ATM-8208828 and ATM-8600888. The authors also express their appreciation to several individuals as well as well as groups for their contributions of services and data used in the completion of this paper. Among these are: Mr. Ron Lindsay of Georgia Tech who provided much of the effort required to read and reformat the NASA/GTE/CITE 1 archived data tape for our calculations. We are indebted to J. Drewry of the NASA/GTE program office for making available the archived GTE/CITE 1 (Spring 1984) data tape. Finally, we would like to express our thanks to the many principal investigators of CITE 1 who contributed their measurements to the NASA/GTE office for archiving. These include: G. Gregory (NASA Langley), O_3; G. Sachse (NASA Langley), CO; S. Beck (NASA Langley), Dew-Point; A. Torres (NASA Wallops Island Flight Facility), NO; B. Ridley (NCAR) and M.A. Carroll (NOAA Boulder), NO.

References

Beck, S. M., R. J. Bendural, D. S. McDougal, J. M. Hoell, Jr., G. L. Gregory, H. J. Curfman, Jr., D. D. Davis, J. Bradshaw, M. O. Rodgers, C. C. Wang, L. I. Davis, M. C. Campbell, A. L. Torres, M. A. Carroll, B. A. Ridley, G. W. Sachse, G. F. Hill, E. P. Condon, and R. A. Rasmussen, Operational overview of NASA/GTE/CITE 1 airborne instrument intercomparisons: Carbon monoxide, nitric oxide and hydroxyl instrumentation, J. Geophys. Res., 92, 1977-1985, 1987.

Bradshaw, J. D., M. O. Rodgers, S. T. Sandholm, S. KeSheng, and D. D. Davis, A two-photon laser-induced fluorescence field instrument for ground-based and airborne measurements of atmospheric NO, J. Geophys. Res., 90, 12861-12874, 1985.

Browell, E. V., E. F. Danielsen, S. Ismail, G. L. Gregory, and S. M. Beck, Tropopause fold structure determined from airborne Lidar and in situ measurements, J. Geophys. Res., 92, 2112-2120, 1987.

Chameides, W. L., D. D. Davis, M. O. Rodgers, J. Bradshaw, S. Sandholm, G. Sachse, G. Hill, G. Gregory, and R. A. Rasmussen, Net ozone photochemical production over the eastern and central North Pacific as inferred from GTE/CITE 1 observations during fall 1987, J. Geophys. Res., 92, 2131-2152, 1987a.

Chameides, W. L., D. D. Davis, J. Bradshaw, M. O. Rodgers, S. Sandholm, and D. B. Bai, An estimate of the NO_x production rate in electrified clouds based on NO observations from the GTE/CITE 1 fall 1983 field operation, J. Geophys. Res., 92, 2153-3156, 1987b.

Chatfield, R., and H. Harrison, Tropospheric ozone II: Variation along a meriodional band, J. Geophys. Res., 1976.

Condon, E. P., E. F. Danielsen, G. W. Sachse and G. F. Hill, Carbon monoxide measurements over the Eastern Pacific during GTE/CITE 1, J. Geophys. Res., 1987.

Danielsen, E. F., S. E. Gaines, R. S. Hipskind, G. L. Gregory, G. W. Sachse, and G. F. Hill, Meteorological context for fall experiments including distributions of water vapor, ozone and carbon monoxide, J. Geophys. Res., 92, 1986-1994, 1987a.

Danielsen, E. F., R. S. Hipskind, S. E. Gaines, G. W. Sachse, G. L. Gregory, and G. F. Hill, Three-dimensional analysis of potential vorticity associated with tropopause folds and observed variations of ozone and carbon monoxide, J. Geophys. Res., 92, 2103-2111, 1987b.

Davis, D. D., Project GAMETAG: An overview, J. Geophys. Res. 85, 7285-7292, 1985.

Davis, D. D., J. Bradshaw, M. O. Rodgers, S. T. Sandholm, and S. KeSheng, Free tropospheric and boundary layer measurements of NO over the central and eastern North Pacific Ocean, J. Geophys. Res., 2049-2070, 1987b.

Davis, L. I., J. V. James, C. C. Wang, C. Guo, P. T. Morris, and J. Fishman, OH measurements near the intertropical convergence zone in the Pacific, J. Geophys. Res., 92, 2020-2024, 1987a.

DeMore, W. B., J. J. Margitan, M. J. Molina, R. T. Watson, D. M. Golden, R. F. Hampson, M. J. Kurylo, C. J. Howard, and A. R. Ravishankara, Chemical Kinetics and Photochemical Data for Use in Stratospheric Modeling. Evaluation Number 7, JPL Publication 85-37, Jet Propulsion Laboratory, California Institute of Technology, 217 pp, 1985.

Dianov-Klokov, V. I., E. V. Fokeeva, and L. N. Yurganov, The investigation of the abundance of atmospheric carbon monoxide, Izv. Acad. Sci., USSR, Atmos. Oceanic Phys., English Translation, 14, 366-377, 1978.

Dickerson, R. R., D. H. Stedman, W. L. Chameides, P. J. Crutzen, and J. Fishman, Actinometric measurements and theoretical calcuations of $j(O_3)$, the rate of photolysis of ozone to $O(^1D)$, Geophys. Res. Lett., 6, 833-836, 1979.

Fishman, J., G. L. Gregory, G. W. Sachse, S. M. Beck, and G. F. Hill, Vertical profiles of ozone, carbon monoxide, and dew-point temperature obtained during GTE/CITE 1, October-November 1983, J. Geophys. Res., 92, 2093-2094, 1987.

Gregory, G. L., S. M. Beck, and J. A. Williams, Measurements of free tropospheric ozone: An aircraft survey from 44° north to 46° south latitude, J. Geophys. Res., 9642-9648, 1984.

Heidt, L. E., J. P. Krasnec, R. A. Lueb, W. H. Pollock, B. E. Henry, and P.J. Crutzen, Latitudinal distributions of CO and CH_4 over the Pacific, J. Geophys. Res., 85, 7329-7336, 1980.

Hering, W. S., and T. R. Borden, Ozonesonde observations over North American, V.4., AFCRL-64-30 (IV), 1967. We have 1964 in text, which is correct?

Hipskind, R. S., G. L. Gregory, G. W. Sachse, G. F. Hill, and E. F. Danielsen, Correlations between ozone and carbon monoxide in the lower stratosphere, folded tropopause, and maritime troposphere, J. Geophys. Res., 92, 2121-2130, 1987.

Hoell, J. M., Jr., G. L. Gregory, D. S. McDougal, A. L. Torres, D. D. Davis, J. Bradshaw, M. O. Rodgers, B. A. Ridley, and M. A. Carroll, Airborne intercomparison of nitric oxide measurement techniques, J. Geophys. Res., 92, 1995-2008, 1987a

Hoell, J. M., Jr., G. L. Gregory, D. S. McDougal, G. W. Sachse, G. F. Hill, E. P. Condon, and R. A. Rasmussen, Airborne intercomparison of carbon monoxide measurement techniques, J. Geophys. Res., 92, 2009-2019, 1987b.

Liu, S. C., M. McFarland, D. Kley, O. Zafiriou, and B. Huebert, Tropospheric NO_x and O_3 budgets in the equatorial Pacific, J. Geophys. Res., 88, 1360-1983.

Liu, S. C., M. Trainer, F. C. Fehsenfeld, D. D. Parrish, E. J. Williams, D. W. Fahey, G. Hubler, and P. C. Murphy, Ozone production in the rural troposphere and the implications for regional and global distributions, J. Geophys. Res., 92, 4191-4207, 1987

McNeal, R. J., Preface to special section on Global Tropospheric Experiment/Chemical Instrumentation Test and Evaluation Results, J. Geophys. Res., 92, 1976, 1987.

Rasmussen, R. A., and M. A. K. Khalil, Atmospheric methane (CH_4): Trends and seasonal cycles, J. Geophys. Res., 86, 9826-9832, 1981.

Ridley, B. A., M. A. Carroll, and G. L. Gregory, Measurements of nitric oxide in the boundary layer and free troposphere over the Pacific Ocean, J. Geophys. Res., 92, 2025-2048, 1987.

Routhier, F., R. Dennett, D. D. Davis, E. Danielsen, A. Wartburg, P. Haagenson, and A. C. Delaney, Free tropospheric and boundary layer airborne measurements of ozone over the latitude range of 58°S to 70°N, J. Geophys. Res., 85, 7307-7321, 1980.

Sachse, G. W., G. F. Hill, L. O. Wade, and M. G. Perry, Fast-response, high-precision, carbon monoxide sensor using a tunable diode laser absorption technique, J. Geophys. Res., 92, 2071-2082, 1987.

Seiler, W., and J. Fishman, The distribution of carbon monoxide and ozone in the free troposphere, J. Geophys. Res., 86, 7255-7265, 1981.

Torres, A., Nitric oxide measurements at a nonurban eastern United States site: Wallops Instrument Results from July 1983 GTE/CITE Mission, J. Geophys. Res., 90, 12875-12880, 1985.

Flight # and date	Wind Direction	Number	%	z km	Zenith Angle	T_d	CO ppbv	NO(NOCAR) pptv	NO(WFF) pptv	O_3, ppbv	$P(O_3)$, 105 mole cm^{-3} s^{-1}
4-4/26/84	NW	223	100%	5.4-6.0	a	-33	122	a	a	49	-
5-4/28/84	NW	213	100%	7.4-7.6	a	-33	126	a	a	54	-
6-4/30/84	NW	223	100%	6.2-6.4	10-35	-26	122	10	14	55	- 4.3
9-5/7/84	NW	50	22%	6.4-6.7	15-22	-36	111	20	12	35	+ 1.9
	SW	37	16%	6.4-6.7	9-33	-33	110	12	4	44	- 0.7
	NE	78	35%	6.4-6.7	8-33	-32	112	8	9	32	- 1.1
	SE	61	27%	6.4-6.7	8-17	-31	102	13	11	40	- 0.6
10-5/9/84 (z > 4km)	NW	50	47%	4.0-6.4	20-34	-11	110	5	4	33	-12
	SW	56	53%	4.8-6.4	23-35	-33	118	9	10	44	- 1.8
10-5/9/84 (2 < z < 4km)	NW	68	100%	2.0-4.0	19-34	- 3	116	3	8	37	-24
10-5/9/84 (z < 2km)	NW	39	81%	0.6-2.0	20-34	+ 2	161	4	5	52	-38
	SW	15	11%	0.6-2.0	19-20	+ 2	159	4	5	56	-49
	NE	5	4%	0.7-1.3	19-34	+ 1	161	5	10	50	-46
	SE	5	4%	0.7	20	+ 6	161	4	5	51	-50

*All data obtained from the NASA Data Archive for the GTE/CITE 1 spring, 1984 field operation.

Number = number of one minute time intervals having winds from the indicated quadrant during a given flight for which high resolution measurements were recorded for at least one of the five chemical parameters.

% = Percentage of data points having winds from the indicated quadrant.

T_d = Mean T_d

CO = Mean X_{CO}

NO(NOCAR) = Mean X_{NO} obtained from the NOCAR/NOAA chemiluminescent instrument.

NO(WFF) = Mean X_{NO} obtained from the Wallops Flight Facility chemiluminescent instrument.

O_3 = Mean X_{03}

$P(O_3)$ = Mean net calculated rate of photochemical production (see text).

Flights 4 and 5 were carried out at night and as a result NO was at or below the detection limit of the NO instruments.

Table 2. Averaged CO, O_3, and NO Concentrations Over the North Pacific Ocean in the Middle Free Troposphere (i.e. $4 \leq z \leq 8$ km) Obtained From the GTE/CITE 1 and GAMETAG Flights

Flight Operation	Geographical Region	X_{CO}, ppbv	X_{O3}, ppbv	X_{NO}, pptv
Summer, 1977 GAMETAG	15°N to 34°N 170° to 123°W	ND	53 ± 11[a]	ND
Spring, 1978 GAMETAG	15°N to 34°N 170°W to 128°W	124 ± 29[b]	50 ± 9	ND
Fall, 1983 GTE/CITE 1	15°N to 35°N 164°W to 124°W	84 ± 15[c]	25 ± 7[c]	15 ± 8[c]
Spring, 1984 GTE/CITE 1	24°N to 38°N 124°W to 135°W	118 ± 11	48 ± 15	10 ± 6[d] 11 ± 7[e]

Uncertainties cited represent the standard deviation calculated from all data collected within the deisgnated geographical region.
ND = No data
a. Routhier et al., 1980
b. Heidt et al., 1980
c. As reported by Chameides [1987a]
d. NO measurement made by NOCAR chemiluminescent instrument
e. NO measurement made by WFF chemiluminescent instrument

Table 3. Pearson-r Correlation Coefficients Between O_3, CO, T_d, and NO

Correlation Coefficient[a]	z = ≧ 4 km	All data
$r(O_3, CO)$	+0.30	+0.31
$r(O_3, T_d)$	-0.42	-0.29
$r(CO, T_d$	-0.13	+0.25
$r(O_3, NO)$	+0.51[b] +0.23[c]	+0.49[b] +0.22[c]
r(NO, CO)	-0.15[b] +0.12[c]	-0.23[b] 0.05[c]
$r(NO, T_d)$	-0.45[b] -0.05[c]	-0.59[b] -0.18[c]

[a] The value r(a, b) indicates the Pearson-r correlation coefficient between parameters a and b.

[b] NOCAR data used for NO.

[c] WFF data used for NO.

Table 4. Factor Loadings for O_3, CO, T_d, and NO Obtained from Multivariate Analysis of Data for $z \geq 4$ km.*

	Variable	Factor 1	Factor 1
A.	Using NOCAR NO data		
	O_3	0.61	0.66
	CO	-	0.84
	T_d	-0.72	+0.35
	NO	0.90	-
B.	Using WFF NO data		
	O_3	0.84	-
	CO	0.59	0.53
	T_d	-	0.87
	NO	0.71	-

*Factor loadings less than 0.25 are not considered to be significant and have been replaced by dashes.

Figure Captions

Figure 1 Tracks for flights from GTE/CITE 1 spring, 1984 field exercise which were included in our analysis.

Figure 2 Time series plots from Flight 10 of altitude, temperature, dew point temperature, carbon monoxide mixing ratio, NO mixing ratio for the NOCAR and WFF instruments, O_3 mixing ratio, and the model-calculated ozone photochemical tendency. Axes on the left are for the solid lines and axes on the right are for the dashed lines.

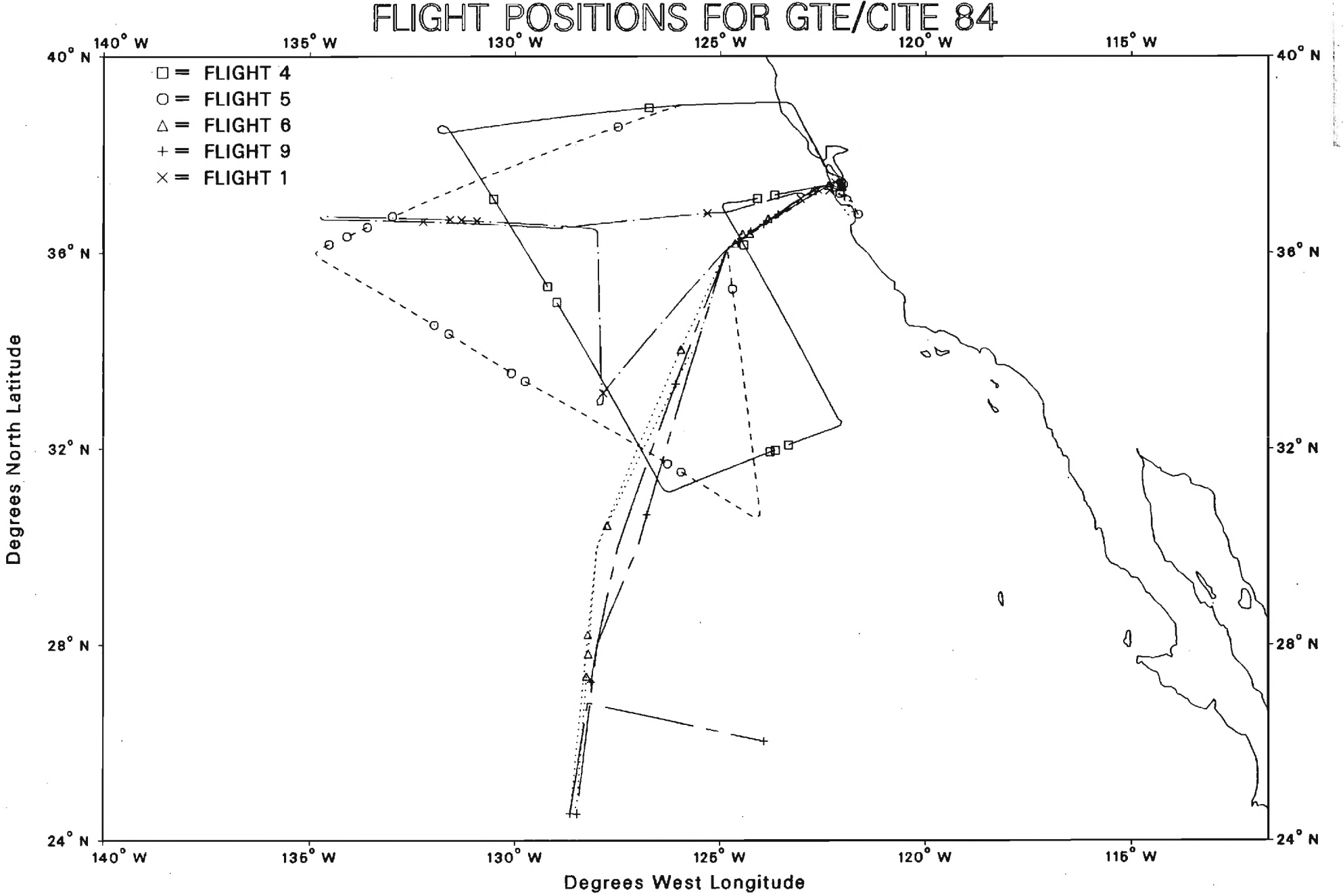

Figure 1 Tracks for flights from GTE/CITE 1 spring, 1984 field exercise which were included in our analysis.

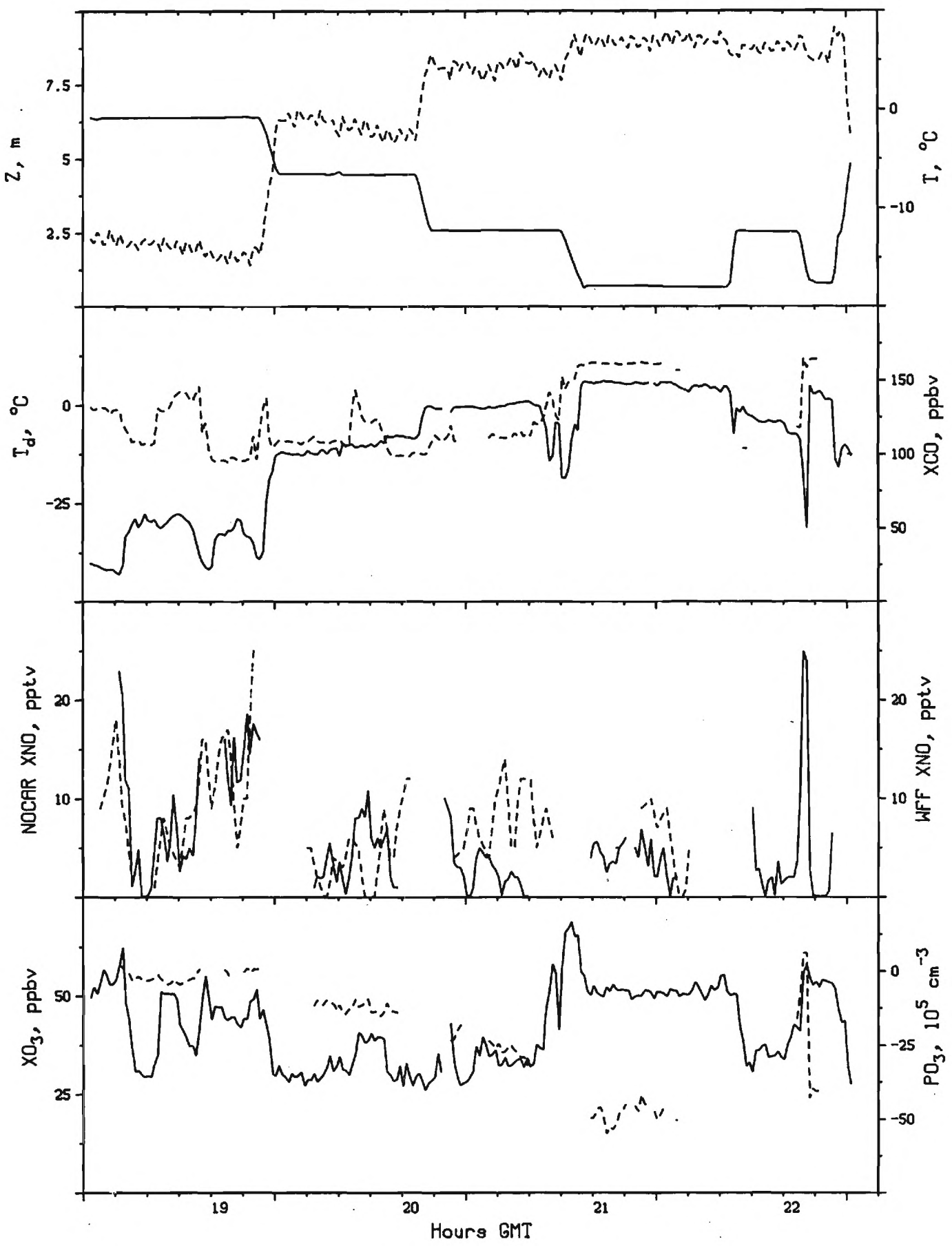

Figure 2 Time series plots from Flight 10 of altitude, temperature, dew point temperature, carbon monoxide mixing ratio, NO mixing ratio for the NOCAR and WFF instruments, O_3 mixing ratio, and the model-calculated ozone photochemical tendency. Axes on the left are for the solid lines and axes on the right are for the dashed lines.

Biomedical Research Support

Shared Instrumentation Grant Program

Division of Research Resources

Final Progress Report

Grant No:	1 S10 RRO4001-01
Principal Investigator:	Robert Amadeo Pierotti, Director School of Chemistry Georgia Institute of Technology Atlanta, GA 30332
Funding Period:	16 May 1988 – 15 May 1989
Instrument:	Nicolet 60SXR Fourier Transform Infrared Spectrometer
Total Purchase Cost:	$139,208.00 (spectrometer and accessories, including plotter and laser printer, $137,208; a compressed air purification system with accompanying installion costs amounted to $2000)
Total DRR Award:	$133,000.00
Other Sources of Funding:	Georgia Institute of Technology ($6,208)

Narrative

The School of Chemistry has purchased a Nicolet Analytical Instruments 60SXR Fourier transform infrared spectrometer equipped for data acquisition over the spectral range 13,000 cm^{-1} to 25 cm^{-1}. To achieve this spectral range requires three detectors, four beam splitters, and two sources. In addition, the instrument is outfitted with an automated beam splitter changer, a time resolve package for rapid kinetics, and a microbeam acessory with microprocessor controlled translational stage stage. Spectral output is to a Zeta 8-pen plotter. Accessories include an ATR stage and diffuse reflectance accessory. Software for interfacing with, and spectral manipulation on, the School's Digital Electronics VAX computer was also obtained. Spectral output from the VAX is to a QMS laser printer. The instrument has been operational since October 1988.

In the proposal it was stated that Dr. Robert Jones, who was a research scientist in the School of Chemistry's Centralized Instrumentation Facility at the time, would have responsibility for the maintenance and operation of the instrument and for the training of operators. Dr. Jones left Georgia Tech before delivery of the instrument. Dr. Robert Braga, also a research scientist in the School, has assumed responsibility for maintenance and training of operators. Scheduling is by prior sign-up on a first-come basis. Useage records are maintained via an electronic log-book maintained by the instrument software (routine written by Dr. Braga). Repairs, when needed, will be handled by our electronics shop, which has five, full-time technicians including an electrical engineer who is an expert in digital electronics.

The FTIR spectrometer is being, or will be, used in connection with NIH funded projects concerned with the mechanism of binding of molecular oxygen by metalloporphrins, in the design of new antihypertensive agents, in the development of inhibitors for blood coagulation

proterases and elastase, studies of lenses and lens' proteins, particularly as related to the mechanism of cataract formation and in studies of the mechanism of biooxidation of arylalkyl hydrocarbons. The intrument also serves a number of other projects within the School and instrument time has been made available to researchers from Atlanta University.